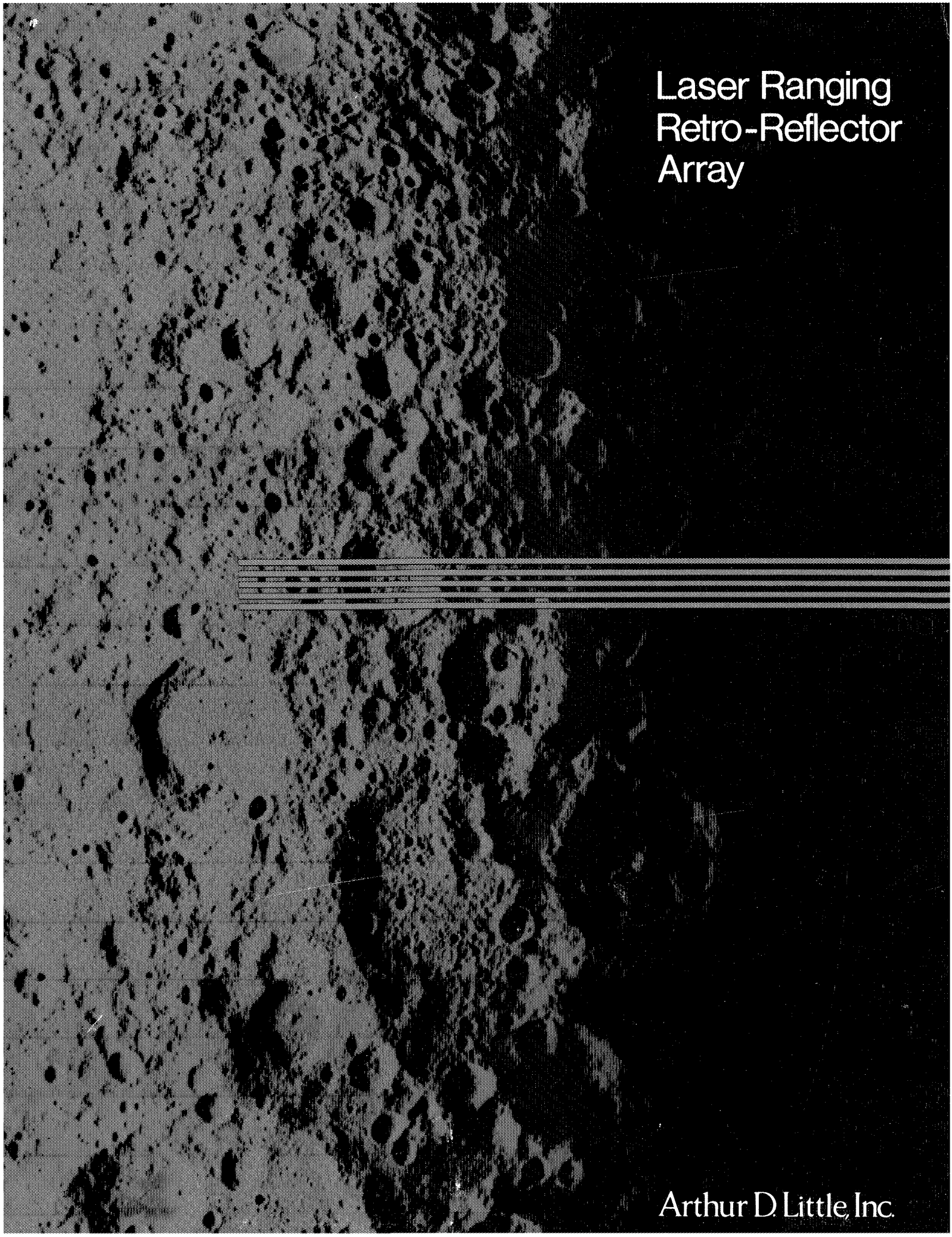

# Laser Ranging Retro-Reflector Array

Arthur D. Little, Inc.

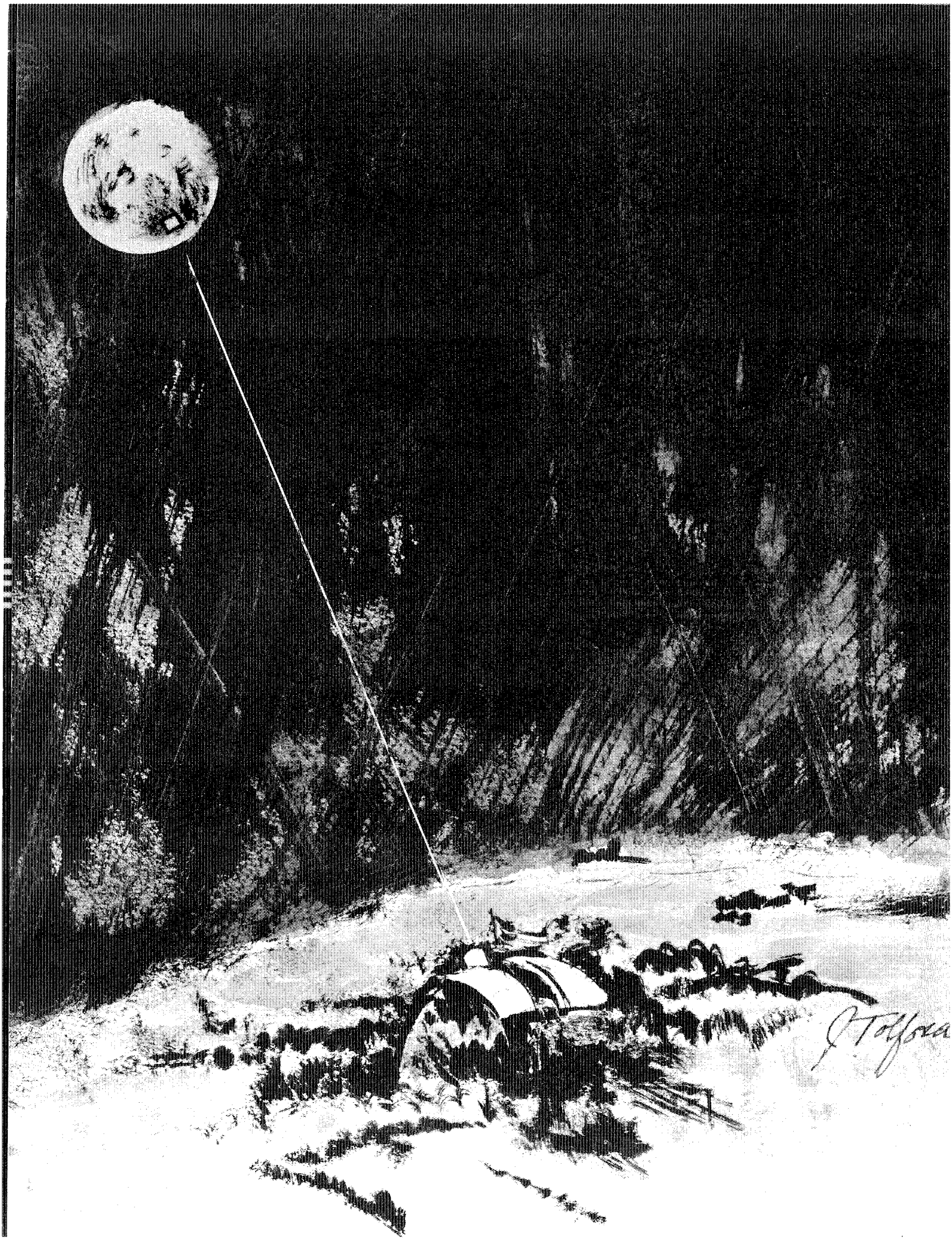

# LASER RANGING RETRO-REFLECTOR ARRAY FOR THE EARLY APOLLO SCIENTIFIC EXPERIMENTS PACKAGE

Final Report to
Aerospace Systems Division
The Bendix Corporation
Ann Arbor, Michigan

June 30, 1969

Arthur D. Little, Inc.

## ACKNOWLEDGEMENTS

The guidance of the Investigator Group, particularly the Principal Investigator, Professor C.O. Alley of the University of Maryland and his associates, Professor D.G. Currie and Mr. H. Kriemelmeyer of the University of Maryland and Professor J. Faller of Wesleyan, was invaluable in assuring that the LRRR Array would meet the scientific objectives of the experiment. The assistance and support of the staff of Bendix Aerospace Systems Division, particularly C. Weatherred, J. Brueger, R. Wolford, G. Mueller, P. Waterman, J.McNaughton, R. Stegler, K. More, C. Lindner, M. O'Mara, L. Deck, D. Dewhirst, and S. Craig, in speedily resolving all interface problems contributed to prompt delivery of the arrays and ensured successful integration with EASEP. The cooperation and assistance of Perkin Elmer Corporation extended by G. Watt, S. Driver, H. Dieselman, and M. Sibiskie was most helpful in the evolution of the retro-reflector tab design and enabled us to meet the schedule for the installation of the retro-reflectors in the array. The consulting and computational support of Itek Corporation, particularly that from J. Zimmerman, O. Latham, W. Britton, A. Raab, and S. Lehrman, was invaluable in establishing cleanliness procedures, evolving a successful retro-reflector mount design, and calculating optical performance. The efforts of Mr. R. Estabrook of Estabrook Engineering Company (Rowley, Massachusetts) and Mr. M. Bent of Benver Tool and Die Company (Lynn, Massachusetts) in supplying accurately machined aluminum panels, and the efforts of Mr. P. Clow of Heuronic Associates (Sudbury, Massachusetts) in producing Teflon mounting rings to meet our specific requirements materially contributed to the successful fabrication of the arrays. The assistance of Mr. P. Marshall, H. Hamilton, and J. Boeggeman of Marshall Research & Development Company (Burlington, Massachusetts) in scheduling and implementing mechanical testing of the arrays is gratefully acknowledged.

The concientious efforts of over 80 of the Arthur D. Little, Inc., staff who participated in the analyses, design, fabrication, assembly, and tests of the LRRR Arrays were essential to meeting the program objectives.

## PREFACE

The Laser Ranging Retro-Reflector (LRRR) Experiment, which will make possible distance measurements from the earth to the moon with an accuracy of 6 inches, was conceived, and its basic design established, by an Investigator Group of scientists from several institutions. The Principal Investigator is Professor C.O. Alley at the University of Maryland. The LRRR Experiment was originally suggested in a letter to the Journal of Geophysical Research in 1965. A complete discussion of the experiment technique, including design considerations for the LRRR Array, was presented in a University of Maryland proposal submitted to NASA in December of 1965. Under a NASA grant, retro-reflectors were successfully tested for their optical performance in a simulated lunar environment during the Summer of 1966. The placing of a retro-reflector package on the moon was approved by NASA in 1967, as an official Apollo experiment, and the decision to include it on Apollo 11, as part of the Early Apollo Scientific Experiment Package (EASEP), was made in the Fall of 1968.

The association of Arthur D. Little, Inc., (ADL) with the Investigator Group and Bendix Aerospace Systems Division on the LRRR Experiment dates back to early 1967. Under contract to the University of Maryland during the Spring of 1967, we conducted preliminary thermal analyses and mechanical design of the LRRR Array for the Apollo Lunar Scientific Experiment Package (ALSEP) Program. Our final report contained predictions of retro-reflector temperature gradients and included a preliminary design concept incorporating both thermal control and structural protection. From mid-1967 to mid-1968, we participated in an investigation of retro-reflector vendors, and liaison with the investigator group. In June 1968, ADL was awarded a contract by the University of Maryland to define the thermal performance of various thermal control designs for LRRR Arrays. Following this work, we began, under contract to Bendix Aerospace Systems Division, the design and fabrication of LRRR Arrays for the EASEP Program.

## TABLE OF CONTENTS

TABLE OF CONTENTS (Continued)

TABLE OF CONTENTS (Continued)

## LIST OF FIGURES

## LIST OF FIGURES (Continued)

## LIST OF TABLES

## SUMMARY

### PURPOSE AND SCOPE

The Laser Ranging Retro-Reflector (LRRR) Experiment is one of the two experiments constituting the Early Apollo Scientific Experiments Package (EASEP) which will be deployed on the first manned lunar landing. The LRRR experiment will use a moon-based array of 100 retro-reflectors and an earth-based laser telescope to obtain measurements of earth-to-moon distances with an accuracy of six inches.

Under contract to the Bendix Aerospace Systems Division of the Bendix Corporation, Arthur D. Little, Inc., has designed, developed, fabricated, assembled, tested, and delivered the LRRR array in accordance with the stringent time schedule of the EASEP program. This report describes the LRRR array program under sub-contract SC 511 of contract NAS 9-5829.

### RESULTS

The array was designed to support and align the retro-reflectors, to protect them from the mechanical environment of the Apollo flight, and to provide thermal control in the lunar environment. To provide a strong structure, consistent with short development time, the array panel was machined from aluminum. To minimize temperature gradients, the retro-reflectors were recessed in cylindrical cavities in the panel structure. The retro-reflectors were supported within these cavities with temperature-compensated Teflon ring mounts – which minimized heat conduction and yet provided sufficient support to hold the retro-reflectors securely when exposed to the various mission environments. In the course of this work, a comprehensive thermal and optical computer program was prepared, both to guide the design and to define the optical performance of the final array.

We built and tested three arrays – an engineering test model, a qualification model, and a flight model. Testing included vibration, shock, optical alignment, and thermal distortion tests of the engineering test model, and vibration and optical alignment tests on the qualification and flight models. The qualification and flight models were built and tested to meet space flight hardware quality assurance requirements.

Qualification and flight models, meeting all performance requirements, were delivered in accordance with the EASEP program schedule.

# I. INTRODUCTION

The Early Apollo Scientific Experiments Payload (EASEP) was conceived in mid-1968 to provide valuable scientific information with minimal astronaut deployment in the initial landing on the moon. Two experiments were selected for EASEP: the Passive Seismic Experiment and the Laser Ranging Retro-Reflector (LRRR) Experiment.

## A. LRRR EXPERIMENT OBJECTIVE

The objective of the LRRR Experiment is to obtain precise earth-moon distances by measuring the time required for a laser pulse to make a round trip between a moon-based retro-reflector array (Figure 1) and an earth-based laser telescope installation. By measuring a laser pulse round-trip travel time (about 2.5 seconds) to within a few nanoseconds, it will be possible to determine earth-moon distances within 6 inches (15 centimeters). The precise monitoring of earth-moon distance will result in greatly improved understanding of the physics of the earth and the moon. For example, such measurements will determine whether the Newtonian gravitational constant may be decreasing in time; they will also result in a much better definition of the oscillation of the earth and its axis known as Chandler's Wobble, which may be associated with major earthquakes. Many important observations can be obtained within six months; others will require up to ten years of operation.

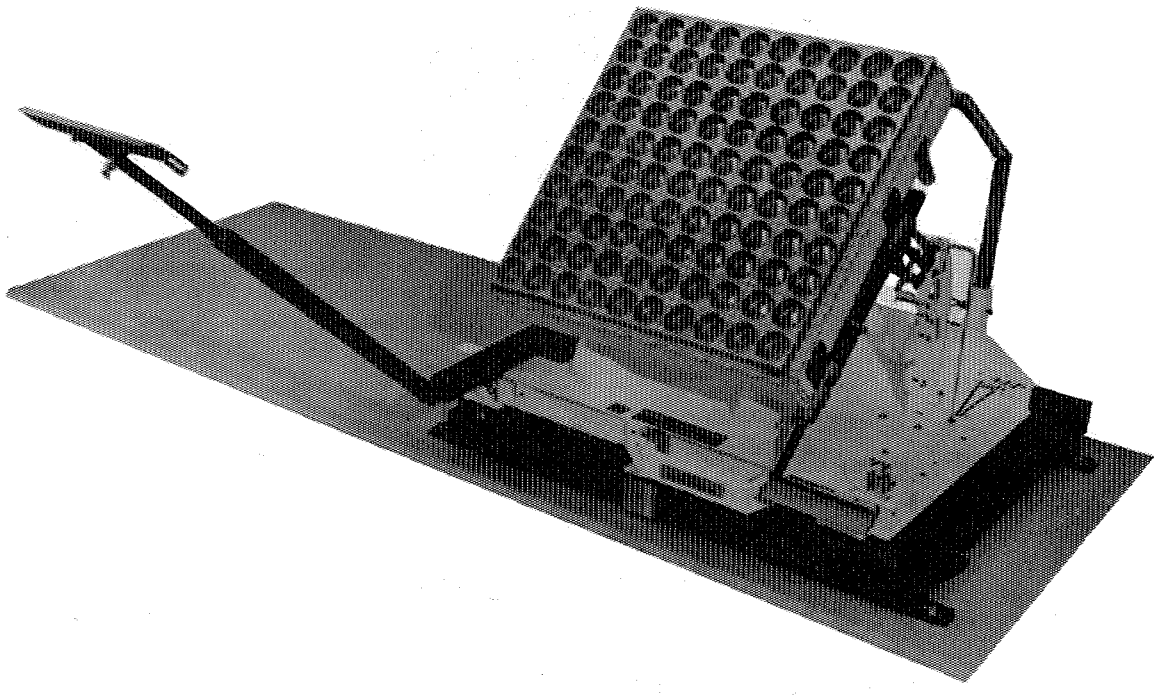

**FIGURE 1 EASEP LRRR EXPERIMENT LUNAR EQUIPMENT**

The scientific responsibility for this experiment rests with an Investigator Group headed by Professor C.O. Alley of the University of Maryland. A complete discussion of the laser ranging technique including design considerations and testing of retro-reflectors in a simulated lunar environment is included in their reports. [1,2]*

## B. LRRR EXPERIMENT EQUIPMENT

The principal components of the EASEP LRRR Lunar Equipment are the Laser Ranging Retro-Reflector (LRRR) Array, the aiming mechanism, and the pallet (Figure 2). The LRRR Array consists of 100 retro-reflectors mounted in a square aluminum panel with 100 cylindrical cavities, giving it a honeycomb-like appearance. Each retro-reflector prism is about 1½ inches (3.8 centimeters) in diameter, corner-cut from a perfect cube of highly homogeneous fused silica. Bendix Systems Division, the prime contractor, fabricated the pallet and aiming mechanism and was responsible for experiment integration and astronaut activities. The retro-reflectors were supplied by Perkin-Elmer Corporation. The LRRR Array structure was designed, fabricated, assembled, and tested by Arthur D. Little, Inc.

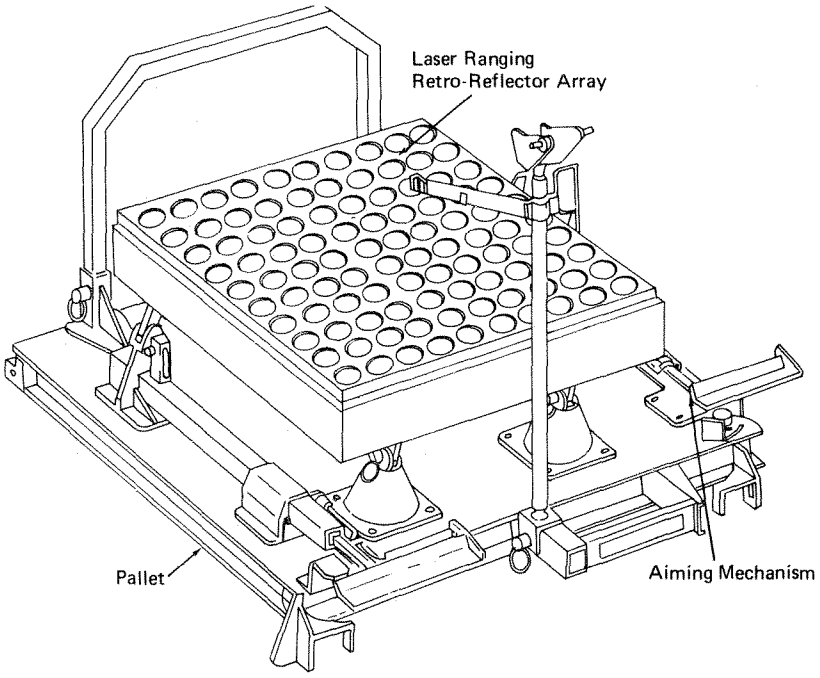


**FIGURE 2 PRINCIPAL COMPONENTS OF THE LUNAR EQUIPMENT**

*Superscript numerals refer to references listed at the end of this report.

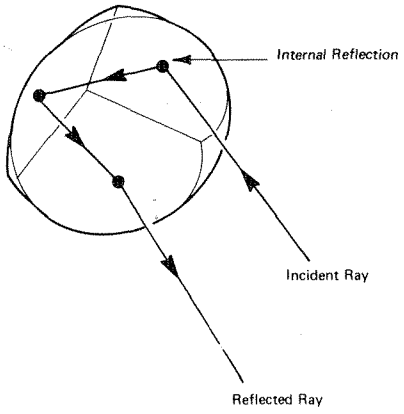


**FIGURE 3 TYPICAL LASER RAY PATH IN RETRO-REFLECTOR**

In addition to supporting and aligning the retro-reflectors and providing mechanical protection during the Apollo flight, the array structure had to provide thermal control on the moon. As illustrated in Figure 3, a light beam incident to the retro-reflectors is internally reflected in sequence from the three back faces of each retro-reflector and then returns in a path parallel to the incident beam. The parallelism between reflected and incident beam ensures that the reflected laser pulse will return to the vicinity of its origin on the earth. In order to maintain a high degree of parallelism and to ensure that enough energy returns to earth to be detected, the retro-reflectors had to be fabricated with extreme precision from very homogeneous material. Since index of refraction varies with temperature, for good optical performance the retro-reflectors had to be mounted so that they would be almost isothermal.

# II. PROGRAM APPROACH

## A. DESIGN CONSIDERATIONS

The major design requirements for the LRRR Array[3] were as follows:

- The array shall be capable of withstanding the Apollo mechanical environment. (The specific levels of vibration, acceleration, and shock are discussed in Section VI.)

- When deployed in the lunar environment, the array must provide passive thermal control to minimize temperature gradients in the retro-reflectors and thereby ensure satisfactory optical performance.

- The array must align the individual retro-reflectors such that the pointing direction of each is within ± 2° of the mean array pointing direction.

- The total weight of the array, including the 100 retro-reflectors (each weighs 0.077 pound), must not exceed 34 pounds.

- The array must be fabricated of space-approved materials, and, as a design goal, should have a ten-year life in the lunar environment.

The interface with the Bendix pallet and aiming mechanism[4] required, in addition to exact fit between mating brackets, that:

- The mean array pointing direction of the array mounted on the pallet must be within ± 1/4° of the nominal pallet pointing direction.

- The array thermal design must provide for the conductive and radiative heat transfer between the array and the pallet.

The array design also had to be compatible with the retro-reflectors,[5] for example:

- The retro-reflector mounting must be compatible with the mounting tab configuration and manufacturing tolerances of the fused-silica retro-reflectors.

- The retro-reflectors must be handled, prior to assembly in the array and during handling and shipping of the assembled arrays, in such a manner as to prevent contamination or damage to the retro-reflectors.

## B. PROGRAM SCHEDULE

The timing of the EASEP program required that the design development, fabrication, assembly, and delivery of the retro-reflector arrays be accomplished on an extremely tight schedule – 5½ months from start of contract to delivery of flight hardware. As shown in Figure 4, the program was divided into two phases: Phase A – Engineering Design; and Phase B – Fabrication.

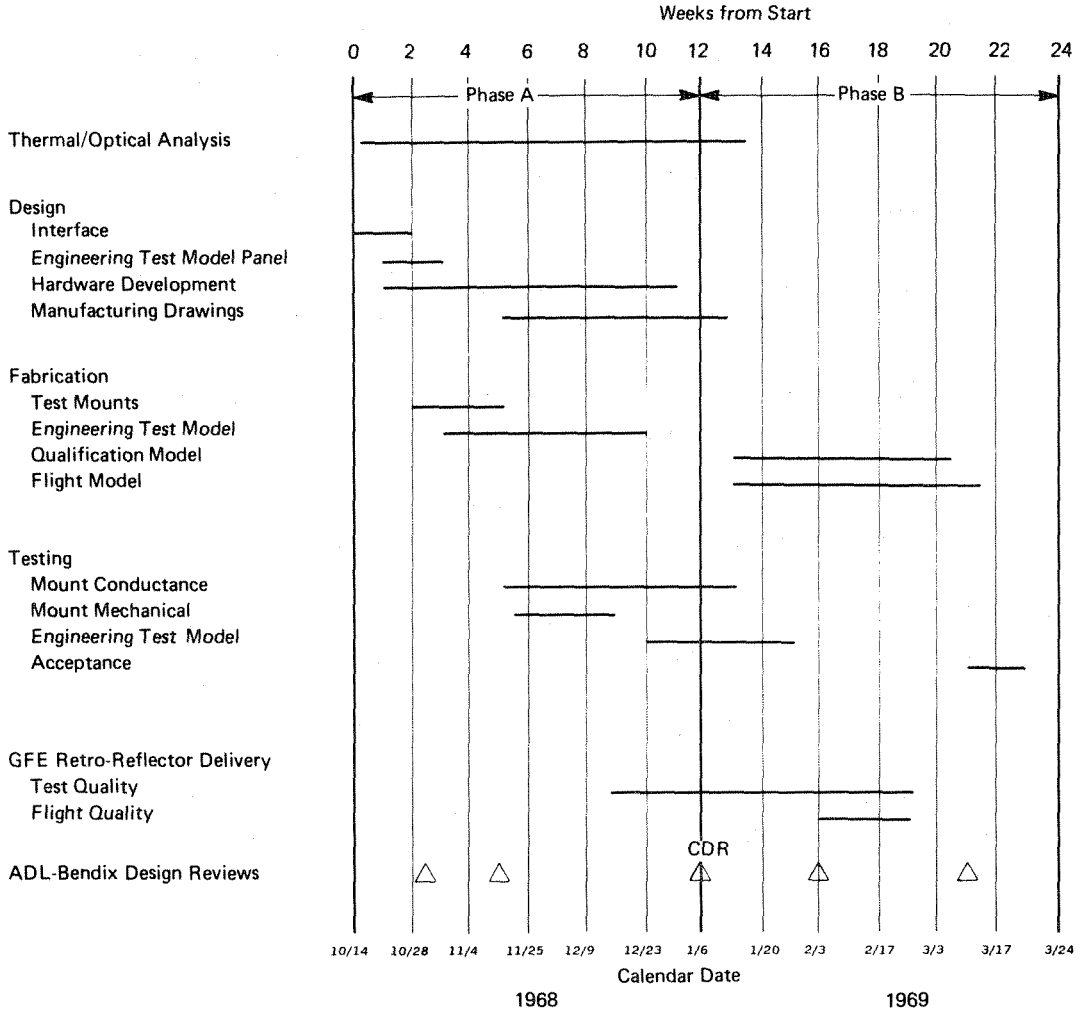


**FIGURE 4 LRRR ARRAY PROGRAM SCHEDULE**

Phase A included analysis, design, and development testing, leading to a final design configuration. The pacing item for Phase A was the design, fabrication, and testing of the engineering test model (ETM). The schedule was based on quickly establishing the mechanical interfaces and the basic panel design – in approximately three weeks – fabricating and assembling the ETM in seven weeks, and performing mechanical and initial alignment tests on the completed ETM in the final two weeks. In parallel with the ETM activity, development testing was conducted on single retro-reflector test units to assess their mechanical performance: i.e., mount thermal conductance, and mount temperature compensation. Also, preliminary mechanical tests were conducted with the ETM panel prior to installing all the retro-reflectors. During Phase A, a combined thermal and optical analysis computer program was developed and used to predict the optical return of the design configuration throughout the lunar day. We also developed manufacturing techniques and quality assurance procedures. This phase concluded in twelve weeks with a critical design review (CDR).

Phase B consisted of the fabrication, assembly, acceptance testing, and delivery of the flight and qualification arrays, in accordance with NASA quality assurance and documentation requirements. In Phase B, the pacing items were the procurement of component parts, the receipt of the retro-reflectors, final assembly, and acceptance testing. In the early part of Phase B, additional alignment tests were conducted on the ETM at extreme hot and cold temperatures to assess thermal distortion; final mount conductance tests were performed to establish the final assembly procedure; and additional thermal optical calculations with the final value of mount conductance were completed.

Phase B concluded with the delivery of the qualification and flight arrays.

# III. THERMAL/OPTICAL ANALYSIS

## A. INTRODUCTION

The success of the LRRR Experiment depends on the retro-reflector optical performance being nearly diffraction-limited. Therefore, the retro-reflectors had to be fabricated precisely from very homogeneous material. The array design also must be able to maintain the retro-reflectors at nearly isothermal conditions in the lunar environment, since small temperature differences would cause noticeable optical distortion. Furthermore, the array design had to be based on a passive thermal control concept, relying on the array geometry and surface properties, to eliminate the need for electric power for thermal control.

Temperature gradients within the fused-silica retro-reflector cause spatial variations in the index of refraction; therefore, the laser beam entering the face of the retro-reflector at different locations will be totally internally reflected and will emerge with nonuniform phase. As a result, the far-field diffraction pattern differs from the pattern one would obtain with an isothermal retro-reflector.

Temperature gradients in the fused-silica retro-reflectors are induced by (1) radiative heat transfer between the retro-reflector and the support structure, (2) the solar flux, which is volumetrically absorbed and heats the retro-reflector during the lunar day, and (3) the infrared flux emitted by the lunar surface. Conductive heat transfer between the retro-reflector and the supporting structure also contributes to the temperature gradients.

Although the heat flow within the retro-reflector is small, the temperature differences within it can be several degrees because of the low thermal conductivity of the fused silica (about 1/100 the conductivity of aluminum). Such temperature differences would appreciably change the diffraction pattern of the reflected laser beam.

In the lunar environment, the retro-reflectors dissipate the power absorbed from environmental sources and that conducted through the supports to the structure, mainly by radiation to the low-temperature space background from the front surface of the retro-reflector. At the surface, the temperature gradient within the fused silica must equal the radiated flux, in accordance with the equation:

$$-k \left.\frac{\partial T}{\partial y}\right|_{\text{surface}} = \epsilon \sigma T^4_{\text{surface}} - F \qquad (1)$$

where:

| | | |
|---|---|---|
| $k$ | = | conductivity of the fused silica |
| $\frac{\partial T}{\partial y}$ | = | temperature gradient at the surface |
| $\epsilon$ | = | total hemispherical emittance of the fused silica |
| $\sigma$ | = | Stefan Boltzman constant |
| $T$ | = | temperature |
| $F$ | = | absorbed radiation flux at the surface |

In general, the temperature at the retro-reflector surface is lower than the temperature at the vertex; and in accordance with Equation 1, the higher the average temperature level, the larger the gradient at the surface.

From this overly simplified discussion, one can see that the temperature gradients in the retro-reflectors will be largest during the 14 days when the lunar surface is in sunlight and smallest during the lunar night, when the average temperature of the lunar surface falls below 100°K.

One basic approach to reduce the temperature gradients in the retro-reflectors was to design an array structure which would minimize the average retro-reflector temperature during the lunar day by use of surface radiators that have a low solar absorptance-to-emittance ratio. The usefulness of this approach was limited by the materials available for coatings, since one of the design requirements was that their surface thermal/optical properties not degrade within a lifetime of 10 years on the lunar surface.

Another approach to minimize the temperature gradients was to support the retro-reflector in a nearly isothermal cavity. For example, by placing the retro-reflector below the surface of the aperture of a cylindrical cavity, the solar flux absorbed volumetrically within the retro-reflector could be reduced during significant portions of the lunar day. Furthermore, the walls of the cavity would radiate to the face of the retro-reflector, thereby reducing the temperature difference between the apex and face of the retro-reflector. If the cavity were of very large L/W,* the gradients in the retro-reflector would be reduced to an insignificant amount. However, the libration pattern of the moon could result in the cavity

*Cavity height-to-width ratio

partially obscuring the laser beam coming from the earth. A cavity of large L/W would provide for excellent thermal performance of the retro-reflector, but the losses associated with the obscuration of the incident laser beam would be large. However, there would be an L/W of the cavity which would maximize the optical performance of the system.

In prior work by the Investigator Group and ADL, guidelines were developed for the thermal control design. In an initial study[1] Dr. James Faller evaluated the effect of solar heating of various sizes of reflectors on the wavefront distortion of reflected laser energy. On the basis of his analysis, solid fused-silica retro-reflectors with a face diameter of 1.5 inches were selected. Under contracts to the University of Maryland, ADL evaluated several thermal control design concepts,[6,7] of which the "louver" or cavity concept proved to be the most attractive. In this concept, the retro-reflectors are recessed in cylindrical cavities below the upper surface of the retro-reflector array which partially shield the retro-reflectors from incident solar energy and tend to provide an isothermal environment for the retro-reflectors (see Figure 5). In addition to shielding the retro-reflectors from incident solar energy, the cavities restrict the view between the retro-reflectors and the low-temperature space background. Further isolation is achieved by maintaining retro-reflectors on low-conductance mounts, by minimizing the emittance of the cavity surface behind the retro-reflector, and by insulating the bottom and sides of the array structure.

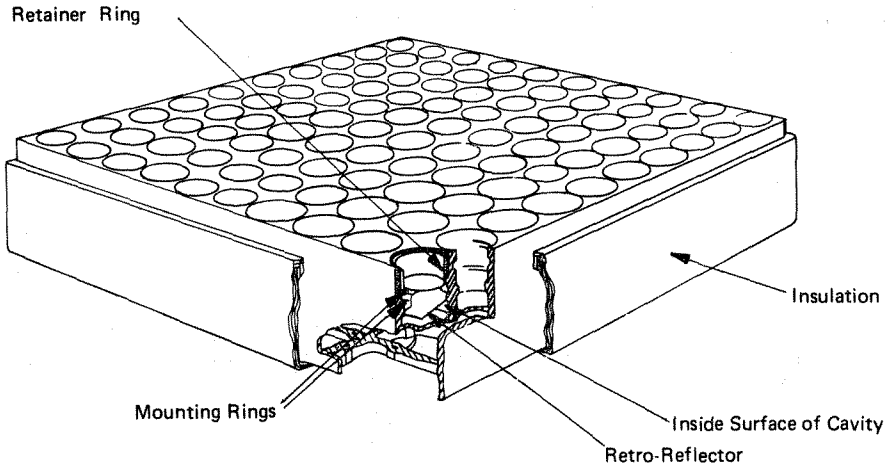


**FIGURE 5 LOUVER THERMAL CONTROL CONCEPT**

The purpose of the thermal/optical analysis was to develop an analytical method which could both guide the thermal control design and predict the optical performance of the flight array in the lunar environment. In the sections to follow, we will discuss the development of the analytical model, the use of the model in evaluating array thermal design parameters, and the prediction of the thermal optical performance of the final array design throughout the lunar day.

## B. ANALYTICAL MODEL

### 1. Overall Computational Approach

The analysis of the optical performance of the retro-reflector array in the lunar environment included descriptions of the heat transfer to and from the retro-reflectors, the temperature distributions within the retro-reflector resulting from these heat flows, and finally the optical effects resulting from the temperature distribution. As shown in Figure 6, the computational procedure involved three distinct computer programs. The thermal analysis program, which simulated the thermal coupling to the retro-reflector as well as the physical model of the retro-reflector, was used to predict temperature distributions in the retro-reflector as a function of sun angle and array design parameters. A ray trace program was used to follow a number of rays through the thermally perturbed retro-reflector and, by integrating the changes in index of refraction along each ray, develop a contour map of phase shift leaving the retro-reflector front face. The phase shift data was in turn used as input data to a Fourier Transform program, which was used to obtain the distribution of irradiance in the far-field diffraction pattern.

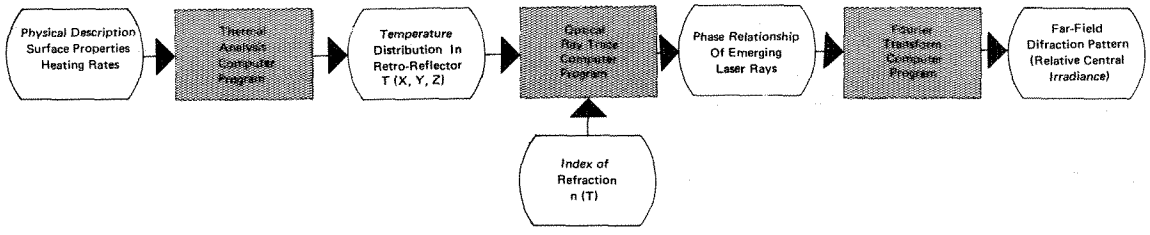


**FIGURE 6 COMPUTATIONAL PROCEDURE FOR THERMAL/OPTICAL ANALYSIS**

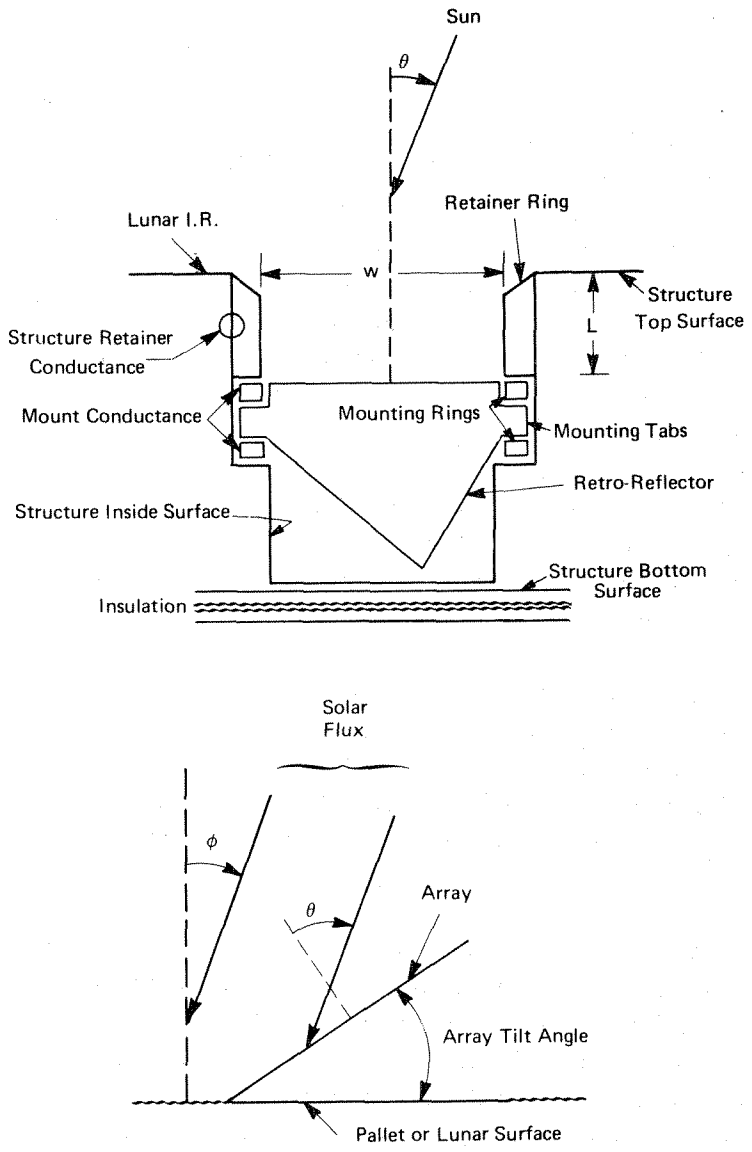


**FIGURE 7 THERMAL MODEL AND DEFINITION OF SUN ANGLES**

## 2. Description of Thermal Couplings

Figure 7 shows a schematic drawing of the computer model of a retro-reflector mounting within the structure. The retro-reflector, connected to the structure by three mounting tabs, is in thermal communication with the surrounding structure and retainer ring by radiant energy transfer in the infrared, and by conduction across the mounting tabs. The array may be tilted at some angle to the lunar surface, in which case the retro-reflector will also be in thermal communication with the lunar surface.

Incident solar energy and lunar infrared radiant energy are absorbed by the top and bottom surfaces of the structure surrounding the reflector. In addition, beyond certain angles of incidence, the solar energy is not retro-reflected but transmitted to the inside surface of the structure surrounding the retro-reflector. In this case, the inside surface acts as an absorbing cavity, and re-radiates heat to the back surfaces of the retro-reflector. To minimize the heat transfer between the cavity and the back surfaces of the retro-reflector, the emittance of the cavity should be relatively low. Emittance measurements of machined 6061 aluminum surfaces showed values of emittance between 0.021 and 0.024. The solar absorptance of the cavity surface was assumed to be 0.1, which is typical of clean, polished

aluminum surfaces. The geometry of the cavity, with its multiple reflections, increases the effective absorptance of the structure.

Since the retainer ring views the top surface of the retro-reflector, it is important for it to have a high emittance; a low solar absorptance is desirable but less important. For this surface, a clear (nondyed) unsealed sulfuric anodizing process was used to coat 1100-series aluminum. Clear anodized aluminum surfaces yield total hemispherical emittances greater than 0.7 when the aluminum oxide thickness is larger than approximately 0.3 mil,[8,9] and their emittance is stable after exposure to UV radiation and proton bombardment. Laboratory tests of aluminum samples anodized in accordance with the array process specifications showed the total hemispherical emittance of the anodized surfaces to be 0.75. Weaver's data[9] indicate that the initial absorptance is independent of coating thickness and treatment. The average initial solar absorptance was approximately 0.15 and the solar absorptance approximately doubled after an exposure to vacuum ultraviolet. Cooley's data[8] indicate initial solar absorptances in the range of 0.14 to 0.15; however, after exposure to a simulated environment for approximately 500 equivalent sun-hours, the changes in solar absorptance were of the order of 0.02 to 0.03.

The array is also in thermal communication with the pallet via conduction and radiation. This interchange is treated as a net power gain or loss to the structure. The structure is considered to lose energy by radiation from the top and bottom surfaces, and by conduction to the retainer ring, from which it is radiated to space. Absorption of solar and lunar energy on the structure bottom is minimized by the use of several layers of multilayer insulation.

Figure 8 defines the structure-retainer conductance and the total mount conductance across the three mounting tabs. Heat is conducted to the retro-reflector by two paths: from the retainer ring through the upper mounting ring and from the structure through the lower mounting ring. The conductances of these two paths is assumed to be equal – and the total mount conductance is defined as the sum of both. Because these thermal paths are difficult to define analytically we undertook a test program (Section VI) to measure the mount conductance, and the structure-to-retainer conductance for various mount configurations. Tests of initial mount configurations indicated a mount conductance of 0.023 watt/°K, which, with improvements in mount design, was finally reduced to 0.01 watt/°K. These tests also gave a value for the structure-retainer conductance of 0.018 watt/°K.

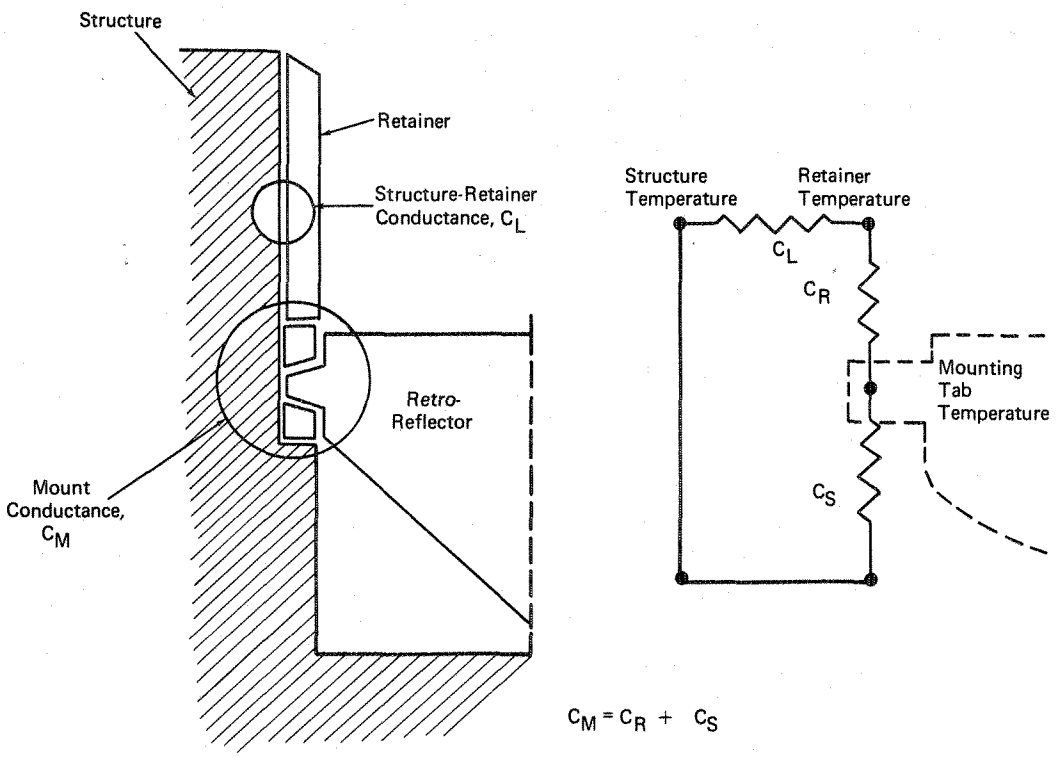


**FIGURE 8 DEFINITIONS OF STRUCTURE-RETAINER CONDUCTANCE, $C_L$, AND MOUNT CONDUCTANCE, $C_M$**

In addition to the thermal couplings, partial absorption of incident solar energy within the retro-reflector represents another important contribution to the total energy transport to the retro-reflector. The model treats the local volumetric heat generation attendant with solar absorption as uniform. Although the local absorption of the solar energy is not exactly uniform, computer studies have shown that temperature gradients in the retro-reflector are relatively independent of the distribution of the generated heat.

## 3. Thermal Model of Retro-Reflector

The heat flow within the reflector and the heat fluxes at its surfaces were determined using the Method of Zones.[7] In earlier studies[7] a tetrahedron was used to represent the geometry of the retro-reflector. However, in the present study, to more accurately represent the physical shape and dimensions of an actual reflector, the tetrahedron model was modified to a seven-sided prism formed by passing three planes perpendicular to the front surface of the tetrahedron in such a manner that the upper surface of the prism was hexagonal in shape.

Figure 9 shows the tetrahedron and the seven-sided prism thermal models. In both cases, the upper surface was divided into four sections. However, the upper surface of the seven-sided prism was more nearly circular than that of the tetrahedron. In addition, for the same altitude the upper surface area was within 9% of the actual retro-reflector area; for the tetrahedron, the surface area error was 60%. The seven-sided prism also allowed a more accurate representation of the mounting tabs. Figure 9 illustrates the method of accounting for heat flow across a single mounting tab for both models. With the tetrahedron, conductive heat flow into the reflector was effectively uniform along the perimenter of the reflector. With the seven-sided prism, heat flow across the mounting tabs was applied over three distinct locations with physical dimensions more nearly matching those of the actual mounting tabs.

When tested under equal boundary conditions, the temperature distributions predicted by the seven-sided prism differed significantly from, and were more realistic than, those predicted by the tetrahedron.

Subdivision of the seven-sided prism into five elemental zones resulted in a set of 26 simultaneous equations describing the heat flows within the interior and at the surfaces of the prism. These equations, which define the 26 mean zone and surface temperatures, were solved by use of a digital computer program. From these computed mean temperatures, local temperature distributions were calculated and utilized in the optical ray trace program.

Finite difference heat balance equations were similarly written for the structure, retainer ring, and insulation system. The equations for the radiant interchange between the

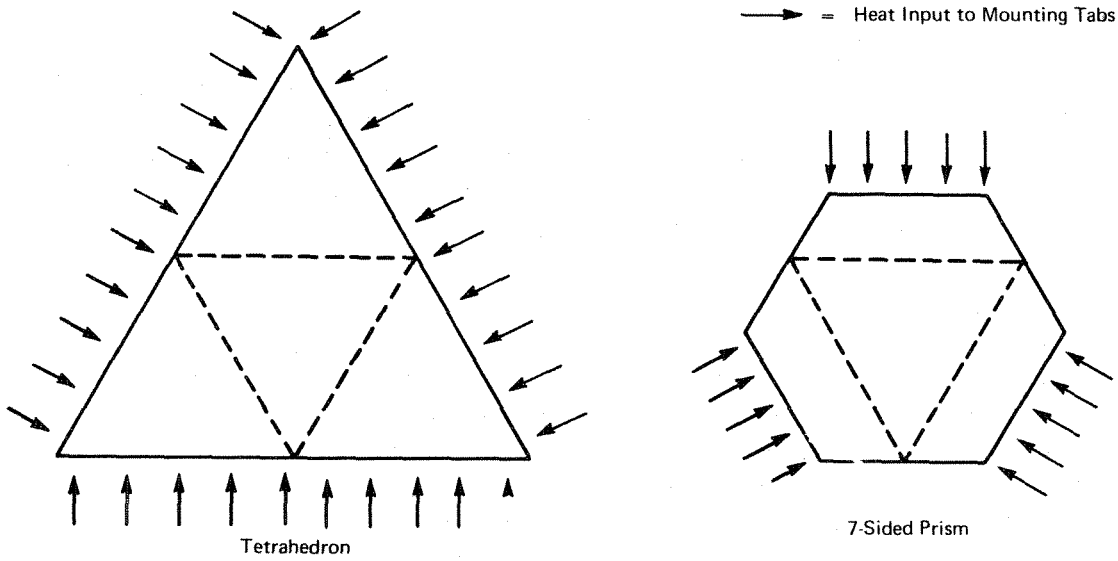


**FIGURE 9 TETRAHEDRON AND 7-SIDED-PRISM THERMAL MODELS OF RETRO-REFLECTOR**

retainer ring and retro-reflector surfaces were based on the use of the (Oppenheim) network analogy method for diffusely reflecting surfaces.

The resulting matrix of 30 simultaneous nonlinear equations was solved on a CDC 6400 computer using the ADL Transient Thermal Analysis (ADLTTA) program.

## 4. Prediction of Optical Performance

Retro-reflector optical performance was computed for selected sets of temperature distributions using an ADL ray trace program and the Itek Corporation Fast Fourier Transform computer program.[10] The temperature distributions were obtained using the thermal model.

Phase data for each retro-reflector temperature distribution case is generated using the ADL Ray Trace Program written for the purpose. This program sets up 441 rays normally incident on the retro-reflector front face. Each ray is individually advanced in 1-millimeter-long path increments through the silica. As a particular ray is advanced through the retro-reflector, a subprogram computes the local temperatures from the zone temperatures determined by the Method of Zones. From the local temperature and using the functional dependence of the refractive index with temperature, the increment in phase change is calculated. The ray trace accumulates 50 such phase-change increments, resulting in a net phase change for the exiting ray at the retro-reflector front face. The output of this program is a table of optical phases as seen at one plane in space. In this case the phase data is registered in a plane just outside of, and parallel with, the front face of the retro-reflector.

The phase shift data serves as input to the Fourier Transform Program, which predicts optical performance in the form of a three-dimensional plot and printout of the distribution of irradiance in the far-field diffraction pattern. The diffraction pattern is representative of the distribution of returned irradiance from one retro-reflector as seen at the earth. A convenient single number from these calculations which characterizes optical performance is the relative central irradiance (W/Wo) in the diffraction pattern. This quantity is the central irradiance normalized to the central irradiance for an isothermal, perfect reflector of the same geometry with normally entering and exiting laser beam. The computed results for optical performance are given in terms of this figure of merit.

The constants used in computing phases and relative central irradiance were: refractive index 1.4555; temperature coefficient of refractive index, $1.00 \times 10^{\circ}K^{-5}$; and optical wavelength, $0.6943 \times 10^{-4}$ cm.

## 5. Verification of Analytical Model

The timing and scope of the EASEP LRRR Array Program did not allow for complete experimental verification of predicted array thermal/optical performance in a simulated lunar environment. However, it was possible to make use of experimental data obtained in

mount conductance tests to check temperature differences predicted by the thermal analysis. In addition, the computer-calculations of central irradiance were tested against an analytic solution valid for a linear vertical temperature gradient.

a. Comparison of Predicted Retro-Reflector Temperatures with Experimental Data

As a test of the predictive method, the thermal analysis was used to predict the local temperatures within the retro-reflector for a given set of experimental conditions encountered in the mount conductance studies. For this calculation, the structure temperature maintained during the test and the experimentally determined conductances were specified input parameters.

The results of this calculation are presented in Table 1, which lists the predicted and measured values of the apex and top-center temperatures of the reflector, and a temperature near the edge of the top face of the reflector. From these local temperatures, we calculated values of vertical and radial $\Delta T$. In general, vertical $\Delta T$ is defined as the temperature difference across the reflector along a line vertical to the upper face and passing through the apex; i.e., the apex temperature minus the temperature at the center of the top face. The term "radial $\Delta T$" signifies the temperature difference between the center of the top face and the mounting tab:

$$\text{Vertical } \Delta T = T_{apex} - T_{top}$$

$$\text{Radial } \Delta T = T_{top} - T_{tab}$$

However, the radial $\Delta T$ listed in Table 1 was based on the edge temperature rather than the tab temperature, since the latter was not actually measured. The predicted and measured temperatures were very close and, therefore, enhanced our confidence in the predictive techniques.

TABLE 1

COMPARISON OF PREDICTED RETRO-REFLECTOR TEMPERATURES WITH EXPERIMENTAL DATA

| Quantity | Predicted (°K) | Measured (°K) |
|---|---|---|
| $T_{APEX}$ | 305.6 | 305.9 |
| $T_{TOP}$ | 303.9 | 303.9 |
| $T_{EDGE}$ | 304.6 | 304.8 |
| $\Delta T_{VERT}$ | 1.7 | 2.0 |
| $\Delta T_{RAD}$ | -0.7 | −0.9 |

Note: Calculated results based on measured values of:

*Structure Temperature* – 351.3°K
Mount Conductance – 0.00435 Watt/°K
Retainer-Structure Conductance – 0.0066 Watt/°K

b. Comparison of Computer Predictions of Central Irradiance with Analytic Solution for a Vertical Linear Gradient

In prior work,[7] we developed an analytic solution for predicting central irradiance as a function of temperature difference for a retro-reflector with a vertical temperature gradient. For the case where the vertical temperature distribution was linear, a closed-form solution was obtained. As an initial verification of the ADL Ray Trace program in conjunction with the Itek Fourier Transform program, a number of arbitrary test cases which resulted in linear vertical temperature distributions were used as input data. The resulting values of central irradiance predicted from the computer program are compared with the analytic solution in Figure 10 – and shown to be in good agreement.

## C. PARAMETRIC STUDIES

Several parametric studies were conducted to establish array thermal design criteria. The influences of various physical parameters on retro-reflector thermal performance were determined by computer studies similar to those conducted in a previous study.[7] Although the general trends remained unchanged, significant changes in predicted thermal performance were brought about by refining the model of the retro-reflector from the tetrahedron used in previous calculations to a more representative seven-sided prism.

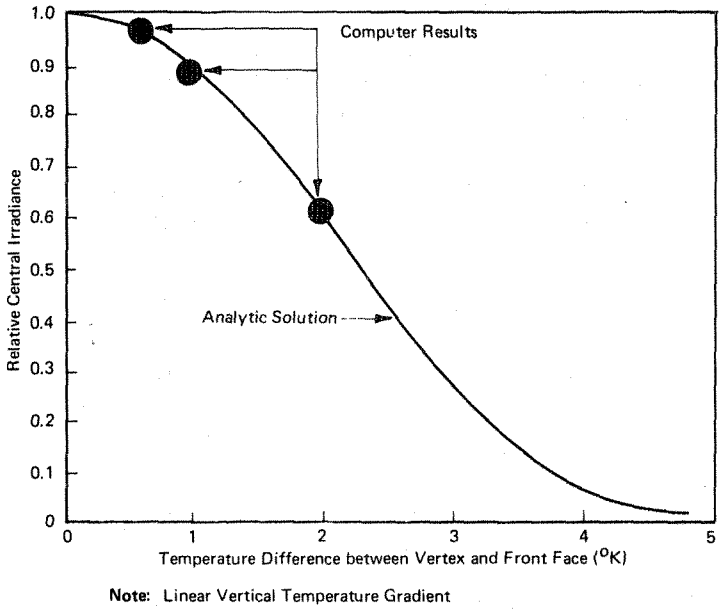


**FIGURE 10 COMPARISON OF ANALYTIC SOLUTION AND RELATIVE CENTRAL IRRADIANCE PREDICTED BY COMPUTER PROGRAMS**

The results of the parametric studies are summarized in Table 2, where the predicted values of vertical $\Delta T$ and radial $\Delta T$ are given for a base case, and then the changes in these quantities are listed for specified parametric changes. The base case is characterized by a retainer height-to-width ratio of 0.3, the array is assumed to be parallel to the lunar surface, and various surface properties are as listed. Furthermore, the reflectors are considered to be aligned such that at a given sun angle all reflectors simultaneously allow a portion of the solar energy to pass through their back faces, in which case the maximum $\Delta T$ occurs when the sun angle is near 16° from the normal. The base case was not intended to represent the design configuration. The parameters are, however, close to those expected. For this base case, the predicted values of vertical $\Delta T$ and radial $\Delta T$ are, 2.6°K and -4.6°K, respectively.

As shown in Table 2, the radial $\Delta T$ could theoretically be reduced by a factor of two – thus substantially improving thermal performance – if the mount conductance were reduced by a factor of 10. However, it does not appear possible to reduce the mount conductance by this large a factor.

Thermal performance could also be improved by increasing the retainer-structure conductance from 0.0042 to 0.1 watt/°K. The higher conductance would permit more of the solar energy absorbed by the structure to be conducted to the retainer ring, from which it would radiate into space or towards the upper surface of the retro-reflector. The resulting decrease in the structure temperature would thus decrease the thermal gradients within the retro-reflector.

Thermal performance could also be improved by radiatively decoupling the top surface of the array, thus reducing the structure temperature. In the base case, both the solar absorptance and the infrared emittance of the top of the array were assumed to be 0.2 (representative of a grit-blasted aluminum surface). The reduction in solar energy absorbed by the structure, obtained by radiatively decoupling the top surface, more than offset the reduction in infrared radiating surface area of the structure. Calculations performed for

## TABLE 2

## EFFECT OF ARRAY DESIGN PARAMETERS ON RETRO-REFLECTOR TEMPERATURE DIFFERENCES

| Parameter | Base Case Value | Value Change | △T Change (°K) Vertical | △T Change (°K) Radial |
|---|---|---|---|---|
| Mount Conductance (watt/°K) | 0.0114 | Decrease to 0.00114 | -0.4 | +2.9 |
| Retainer Structure Conductance (watt/°K) | 0.0042 | Increase to 0.1 | -0.2 | +0.5 |
| Array Absorptance | 0.2 | Decrease to 0 | -0.1 | +0.1 |
| Array Emittance | 0.2 | | | |
| Array-Moon Coupling | Radiative | Decouple | -0.1 | +0.1 |
| Cavity Height-To-Width Ratio | 0.3 | Increase to 0.5 | -0.5 | +0.9 |
| Retro-Reflector Alignment | Unidirectional | Bi-directional | -0.5 | +1.1 |
| Array Tilt Angle (degrees) | 0 | Increase to 4.0 | +0.5 | -0.8 |
| Retainer Absorptance | 0.32 | Increase to 1.0 | +0.6 | -1.2 |
| Retainer Emittance | 0.78 | Not varied | | |
| Sun Angle Relative to Array Normal (degrees) | 20 | | | |

**Note:** For base case values, $\Delta T_{vertical} = 2.6^{\circ}K$

$\Delta T_{radial} = -4.6^{\circ}K$

another case indicated that thermal performance would significantly improve if the surface emittance could be made high while the solar absorptance was kept low.

Thermal communication between the moon and the array will be controlled by several layers of insulation with an effective emittance and absorptance of 0.01. As Table 2 shows, only a small improvement in performance could be obtained by reducing these quantities to zero.

On the other hand, a significant improvement in thermal performance could be obtained by increasing the retainer height-to-width ratio to 0.5, since increasing the retainer height would increase the energy radiated away from the structure. In addition, the lengthened retainer would present a more isothermal environment to the retro-reflector. A retainer height-to-width ratio (L/W) of 0.5 was subsequently used in the final design.

We also performed a set of calculations for a special (bi-directional) arrangement of the retro-reflectors wihin the array. We assumed that the retro-reflectors were aligned such that at a 16° sun angle a portion of the incident solar flux would be transmitted through half of them and at angles beyond 45° solar flux would also be transmitted through the remainder. Table 2 indicates the change in performance at a 20° sun angle. At this angle, the temperature gradients obviously are smaller than those appropriate to the base case, since less energy is transmitted through the retro-reflectors and absorbed by the structure. However, the temperature gradients are significantly increased at other sun angles (e.g., at -20°). This new arrangement of retro-reflectors would allow a portion of incident solar energy to be transmitted through half the reflectors over a range of sun angles between -45° to -16° and +16° to +45°. In the base case, where the retro-reflectors are all aligned in the same direction, solar energy is partially transmitted through all of the reflectors at angles between +16° and +45° but through none of the reflectors at sun angles between -45° and -16°. Over an entire lunar cycle the arrangement where all of the retro-reflectors are aligned in the same direction (unidirectional) would yield a better thermal performance than the alternative arrangement.

Table 2 also lists some possible degradations in thermal performance. Tilting the array would increase the radiative coupling between the array and the lunar surface. At sun angles where the temperature gradients are largest, the temperature of the lunar surface would be higher than that of the array. Hence, the radiative interchange would result in a net increase in energy input to the array. However, with the array tilted from the horizontal position, solar energy would be directly incident on the top of the array over a smaller portion of the lunar day. Over a lunar cycle, the result might be a net improvement in thermal performance.

The final parametric variation listed in Table 2 is a change in retainer solar absorptance from 0.32 to 1. Since the increased absorptance would result in a greater energy input to the structure, the temperature gradients within the retro-reflectors would be larger.

Table 2 reveals, therefore, that the most influential parameter on thermal performance is the mount conductance. The results of a more detailed examination of this parameter, including its optical effects, are presented in Table 3. Reducing the mount conductance by a factor of 2 increased the optical return from 0.51 to 0.72. Reduction by a factor of 3 increased the return from 0.51 to 0.85.

**TABLE 3**

**INFLUENCE OF MOUNT CONDUCTANCE ON THERMAL/OPTICAL PERFORMANCE**

| Mount Conductance (Watt/°K) | Vertical ΔT (°K) | Radial ΔT (°K) | Central Irradiance |
|---|---|---|---|
| 0.0114 | 1.801 | -3.067 | 0.507 |
| 0.0057 | 1.638 | -2.336 | 0.719 |
| 0.0038 | 1.524 | -1.818 | 0.845 |
| 0.00114 | 1.343 | -1.003 | 0.949 |

**ARRAY PARAMETERS**

| | |
|---|---|
| Cavity Height-To-Width Ratio | = 0.5 |
| Retainer Absorptance | = 0.32 |
| Retainer Emittance | 0.78 |
| Array Top Absorptance | = 0.2 |
| Array Top Emittance | 0.2 |
| Array Tilt Angle | = 0 |
| Retainer-Structure Conductance | = 0.1 Watt/°K |

## D. ARRAY THERMAL/OPTICAL PERFORMANCE

The analytical methods described in Section B were applied to the final array design to compute temperature, temperature distribution, and optical performance for the entire lunar cycle. Complete performance calculations are presented using the best design data available at the time of the Critical Design Review (CDR). In addition, the performance changes resulting from final design iteration immediately after the CDR are also discussed.

All calculations were performed assuming quasi-steady heat transfer. An earlier study revealed only a slight difference between a transient and quasi-steady analysis of thermal performance.[7]

### 1. Initial Studies

The initial studies performed for the CDR were based on the best values of mount and structure-retainer conductance available at that time, 0.023 watt/°K and 0.005 watt/°K, respectively. The emittance and solar absorptance applied to the top of the array were 0.025 and 0.06, respectively, which are representative of a polished aluminum surface. The clear anodized retainer ring was assigned an emittance of 0.78 and a solar absorptance of 0.32. The emittance of the cavity walls behind the retro-reflectors was taken as 0.025; their absorptance, as 0.1. The array insulation was described by an effective emissivity of 0.01. In addition, since values of the net heat input from or to the pallet were not available, the initial calculations neglected the influence of the pallet on array performance. In the calculations, the reflectors are all aligned the same way and in a direction such that they are retro-reflecting between sun angles relative to the array normal of -16° and +45°.

Computed values of the vertical $\Delta T$, the radial $\Delta T$, and the structure temperature are illustrated in Figures 11A, B, and C, respectively. The results are plotted versus two sun angles, $\phi$ and $\theta$. As previously defined in Figure 7, sun angle $\phi$ is referenced to the normal projecting from the lunar surface; angle $\theta$ is referenced to a normal to the array. For this study, the two angles differ by 34°, which represents a nominal angle at which the array would be tilted when deployed at the target site.

The highest temperatures are reached during lunar day at a sun angle $\theta = -16°$, where the retro-reflectors become partially transmitting to the incident solar flux. Here, the predicted vertical and radial $\Delta T$'s are 2.1°K and -3.9°K, respectively. During the period of the day when the retro-reflectors do not transmit any solar energy to the structure, the maximum values of the vertical and radial $\Delta T$'s are 1.5°K and -2.7°K, respectively. The maximum structure temperature attained during this period is 340°K.

When the sun is incident normally on the array, the $\Delta T$'s are greatly reduced. At this instant, the only solar input to the structure is the energy absorbed by the top surface of the array, in which case the predicted structure temperature drops considerably and the radial $\Delta T$ becomes positive. However, because of the thermal mass of the array, the structure temperature will not undergo such a rapid decrease near $\theta = 0°$ but will be closer to the values predicted near $\theta = \pm\ 10°$.[7]

During lunar night (sun angle $\phi$ less than -90° or greater than +90°), the $\Delta T$'s are effectively zero. The structure temperature attained during lunar night is not shown in these figures. However, with quasi-steady heat transfer, the lowest temperature it can attain is of the order of 50°K. A calculation of the actual time/temperature history would require consideration of the thermal mass of the reflector array.

Figure 11D shows the predicted optical performance as measured by the relative central irradiance, assuming normal incidence of the laser beam. (The effects of off-normal incidence further decrease the optical return.)

The return is 100% during lunar nighttime and above 80% for somewhat less than half of the lunar day. However, it is less than 80% for the period during which the retro-reflectors are partially transmitting to the incident solar flux. The slight decrease in return near sun angle $\theta = 0°$ is a consequence of the predicted positive radial $\Delta T$. Figure 11D indicates that the optical return will be 80%, or higher, over approximately 75% of an entire lunar cycle.

Figure 12 shows contour maps which illustrate the irradiance distribution in the far field diffraction pattern for an isothermal situation, closely simulated by lunar night, and for a sun angle $\phi = -64°$, at which time large gradients exist. These plots graphically demonstrate how temperature gradients reduce the height of the central spike in the diffraction pattern. Since temperature gradients also tend to spread out the central irradiance, and since the receiving station will be slightly off center, the use of central irradiance ratio as a figure of merit is slightly conservative.

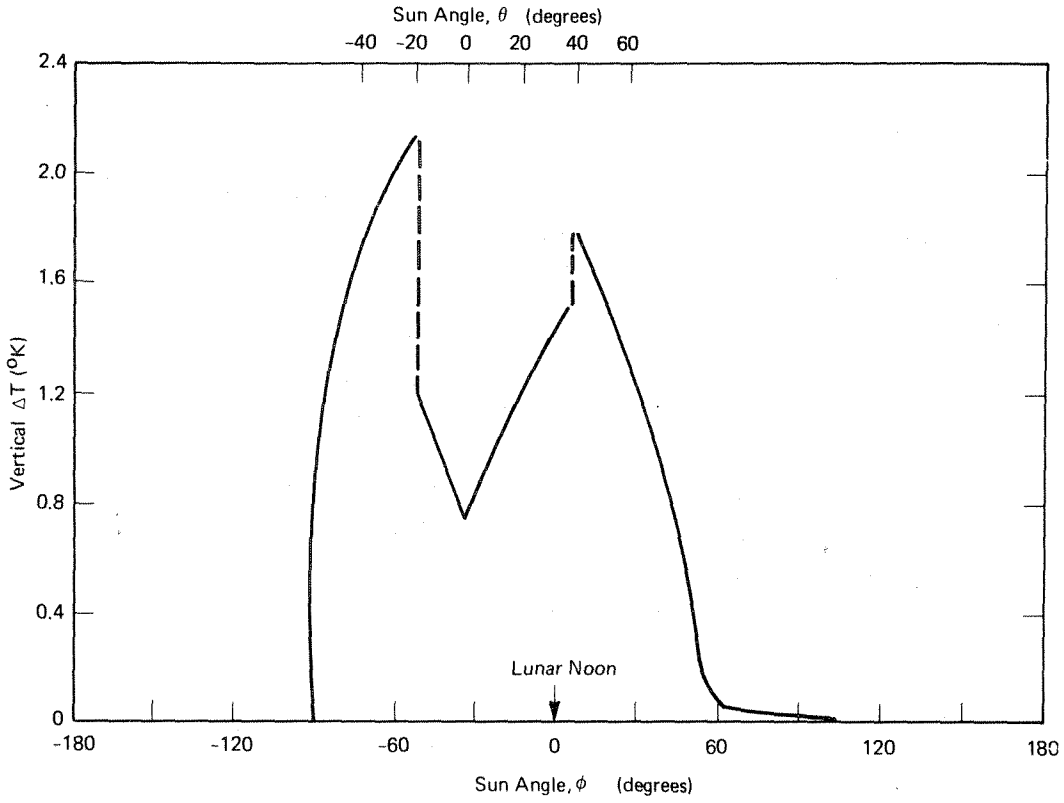


A. PREDICTED VERTICAL Δ T

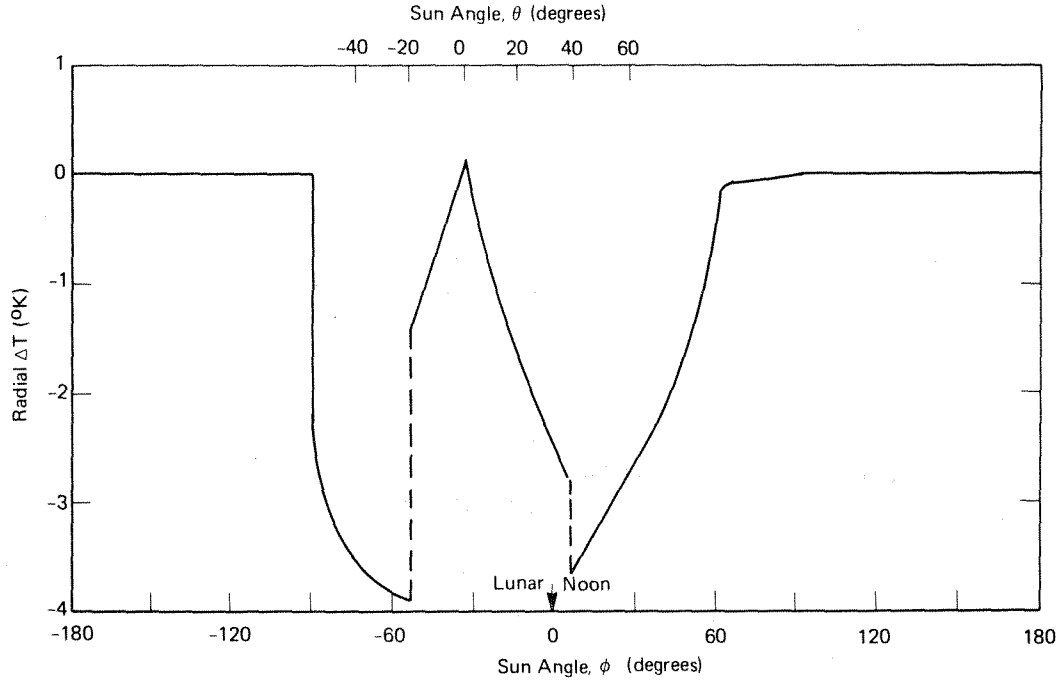


B. PREDICTED RADIAL Δ T

FIGURE 11 THERMAL-OPTICAL PERFORMANCE OF CDR CONFIGURATION

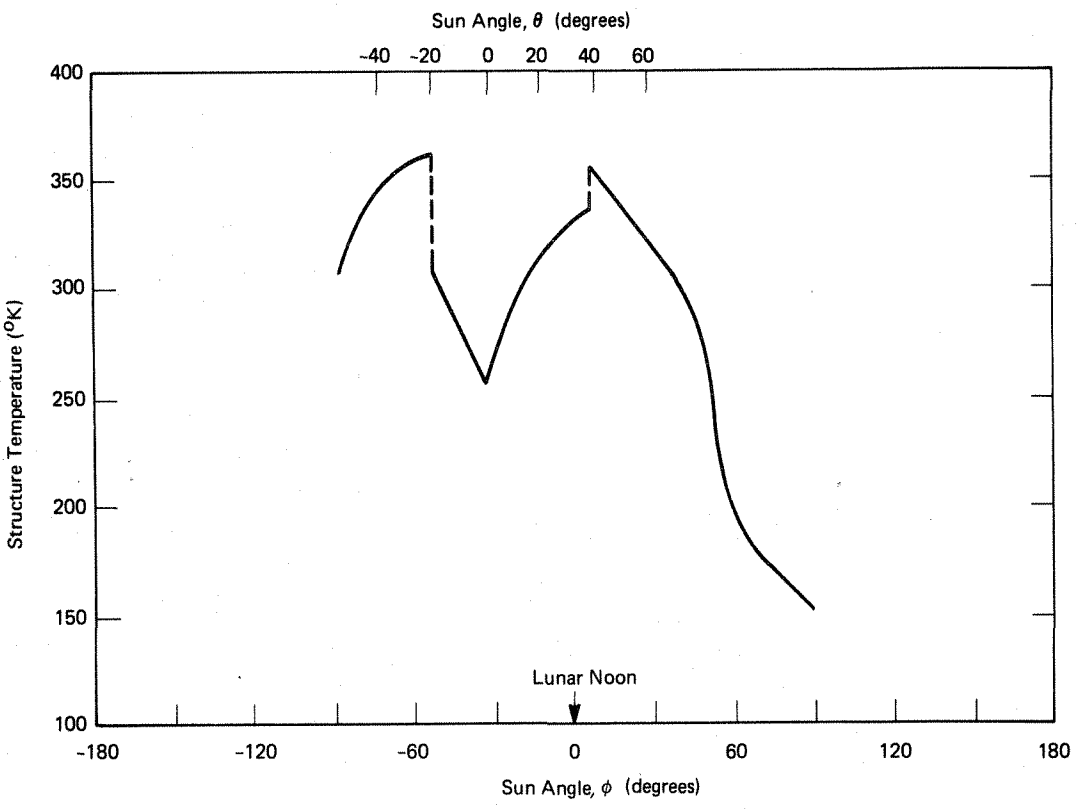


C. PREDICTED STRUCTURE TEMPERATURE

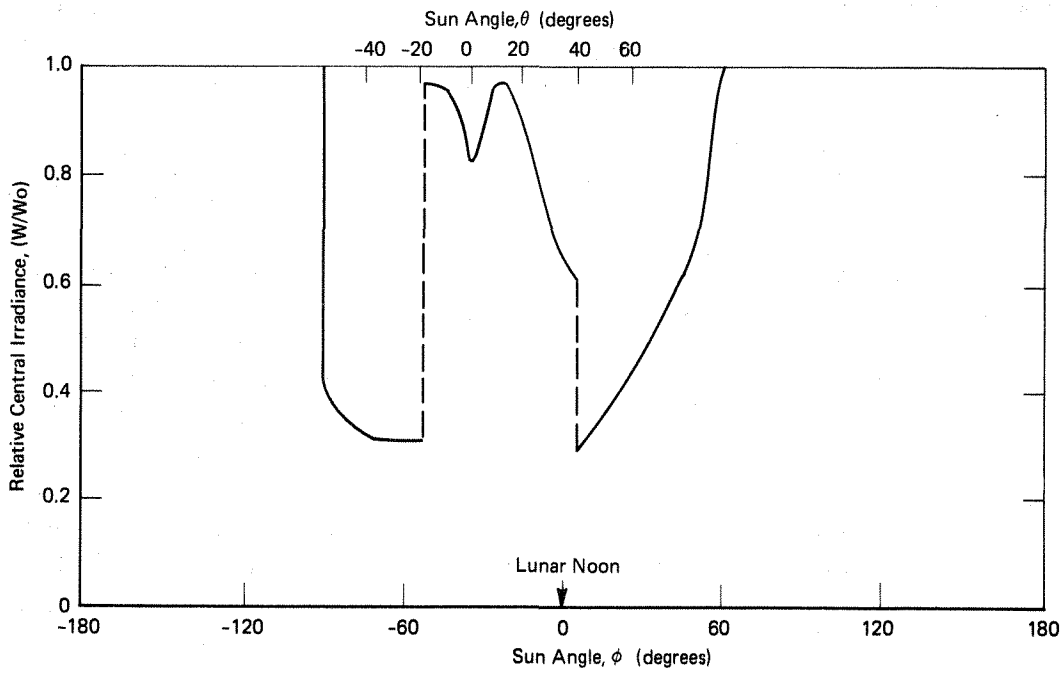


D. PREDICTED CENTRAL IRRADIANCE

FIGURE 11 THERMAL-OPTICAL PERFORMANCE OF CDR CONFIGURATION (CONTINUED)

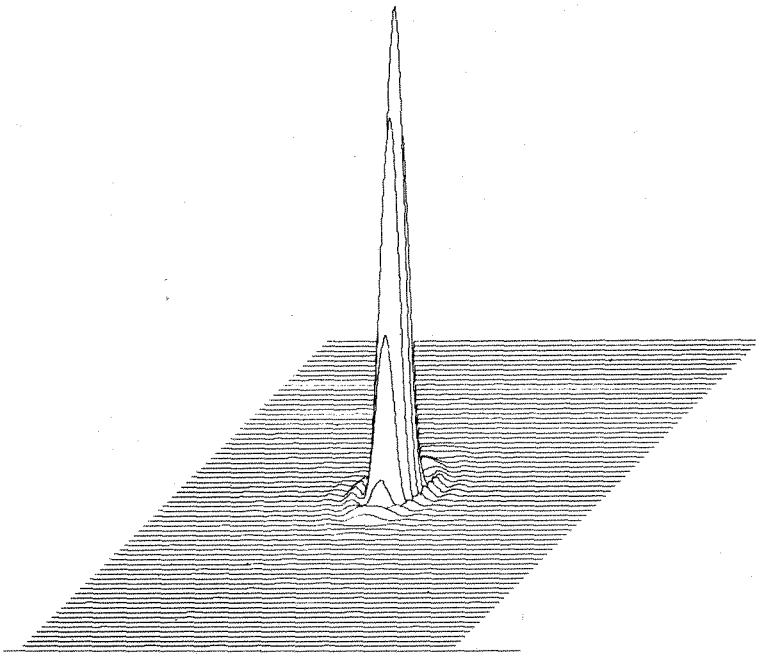

Max = 1.000 Min = 0.000
A. Isothermal Retro-Reflector

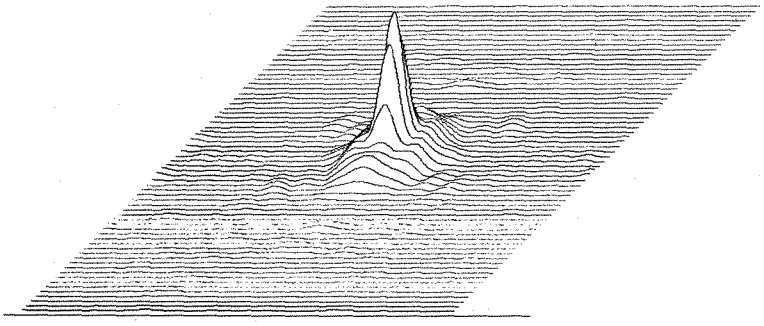

Max = 0.300 Min = 0.000
B. Maximum Gradient Condition
(Sun angle $\phi = -64^{\circ}$; $\Delta T_{vertical} = 2.0^{\circ}K$; $\Delta T_{radial} = -3.8^{\circ}K$)

**FIGURE 12 FAR FIELD (FRAUNHOFER) DIFFRACTION PATTERNS**

The influence at off-normal laser incidence on optical return can be estimated from Table 4,[7] which lists the geometrical obscuration factors – the percentage of return from a perfect isothermal retro-reflector – for angles of 0 to 20°. Results are presented, for both an isolated retro-reflector (L/W = 0) and a retro-reflector mounted within a cavity with L/W = 0.5. In the case of the isolated retro-reflector, the obscuration factors merely represent the decrease in projected area associated with off-normal incidence. However, the obscuration factors for the retro-reflector mounted in the cavity include shadowing effects and are accordingly less than those for the isolated retro-reflector.

The combined effect of off-normal incidence and thermal distortion can be estimated by simply multiplying the obscuration factor by the relative central irradiance. A more detailed analysis of the return for off-normal incidence would yield higher values of predicted return, since the largest phase shift in the reflected incident beam occurs over those portions of the retro-reflector upper face which are obscured.

TABLE 4

OBSCURATION FACTORS FOR OFF-NORMAL LASER BEAM

| Incidence Angle (Degrees) | Obscuration Factor L/W=0 | Obscuration Factor L/W=0.5 |
|---|---|---|
| 0 | 1.000 | 1.000 |
| 5 | 0.794 | 0.647 |
| 10 | 0.615 | 0.345 |
| 15 | 0.464 | 0.143 |
| 20 | 0.329 | 0.035 |

## 2. Final Design Calculations

The performance predictions of the CDR design were based on the assumption of negligible heat exchange between the pallet and array structure. In addition, the mount and structure-retainer conductances were taken to be 0.023 watt/°K and 0.005 watt/°K, respectively. Later tests showed them to be closer to 0.010 watt/°K and 0.018 watt/°K.

Figure 13 illustrates the effects of mount conductance on predicted central irradiance over a lunar cycle. A decrease in mount conductance to 0.010 watt/°K results in a significant improvement in optical return over the portions of lunar day where incident solar flux that may be partially transmitted through the fused-silica retro-reflectors will heat up the structure. The change in central irradiance is only slight over the range of sun angles -20° to +40°, where the collimated solar flux is retro-reflected.

Figure 14 shows the effect of pallet heat flow on predicted central irradiance. The magnitude of the heat flow is treated as a parameter and is considered to be positive when the net heat flow is from the pallet to the array structure. A positive heat flow of 20 watts to

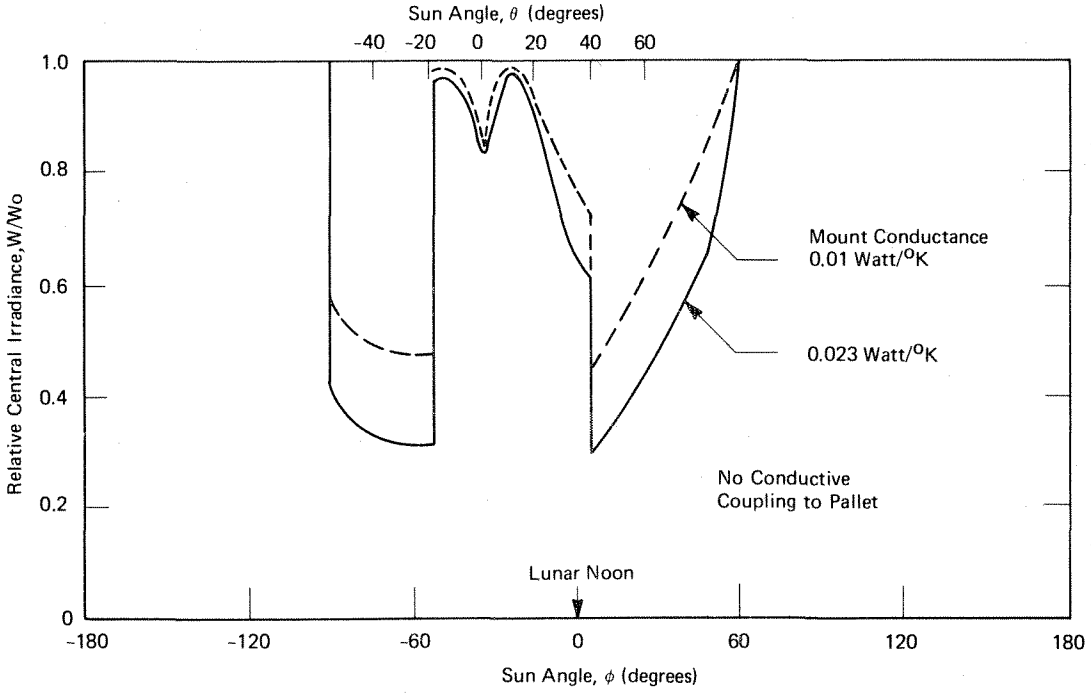


FIGURE 13 EFFECT OF MOUNT CONDUCTANCE ON CENTRAL IRRADIANCE

the array results in a substantial decrease in relative central irradiance. However, this result does not necessarily correspond to the actual heat exchange experiment, but only indicates the influence of heat input on optical performance.

The actual net heat exchange between the array and the pallet is expected to be more nearly that illustrated in Figure 15, where predicted net heat input to an array tilted at 34° from the horizontal is plotted.[11]

Over most of the lunar day the heat flow is out of – rather than in to – the array structure. In this case, we expect an improvement in optical return over that shown in Figure 14. Figure 16 shows an estimate of the relative central irradiance expected for the final array design based on the results shown in Figures 14 and 15. Coupling to the pallet improves the performance considerably. Over most of the lunar day the relative central irradiance is between 55% and 90%.

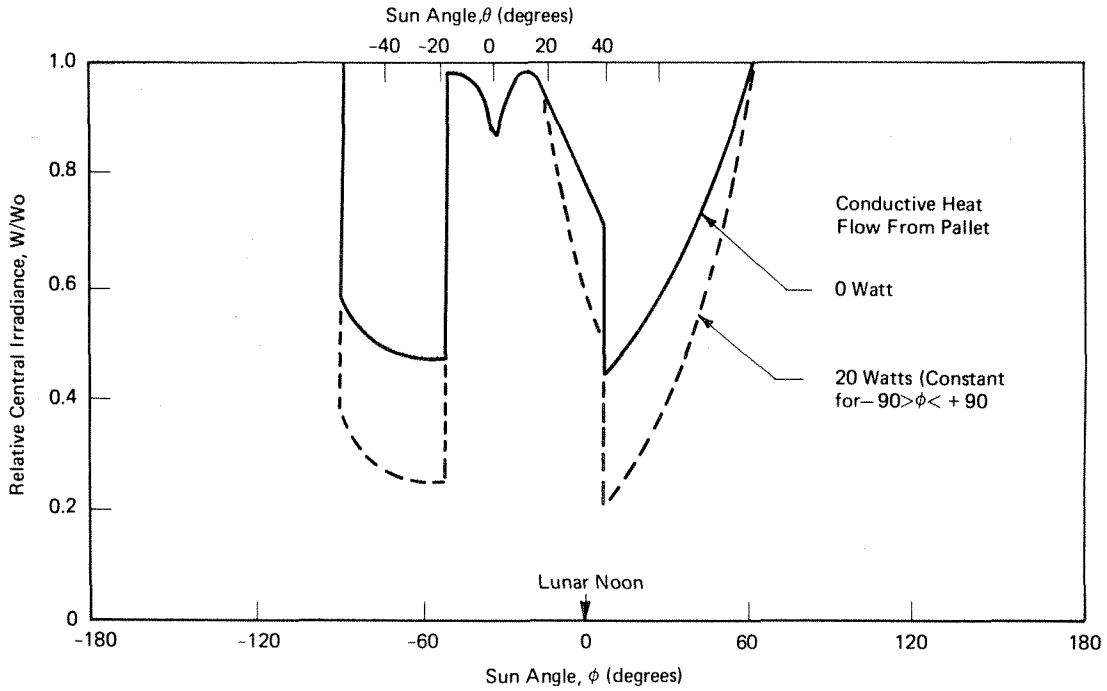


**Note:** Mount Conductance 0.01 Watt/°K

**FIGURE 14 EFFECT OF PALLET HEAT FLOW ON CENTRAL IRRADIANCE**

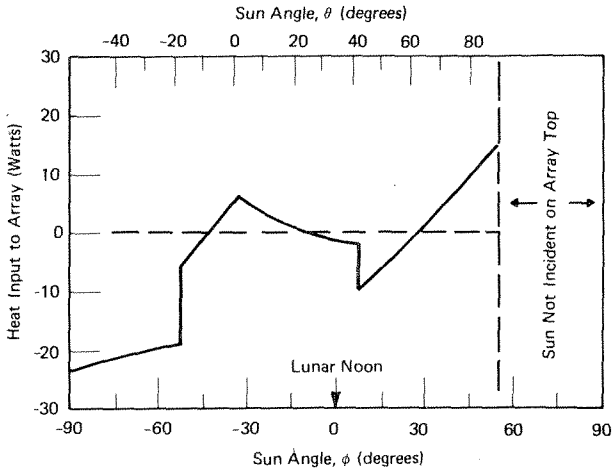


**FIGURE 15 HEAT INPUT TO ARRAY FROM PALLET FOR 34° ARRAY TILT ANGLE**

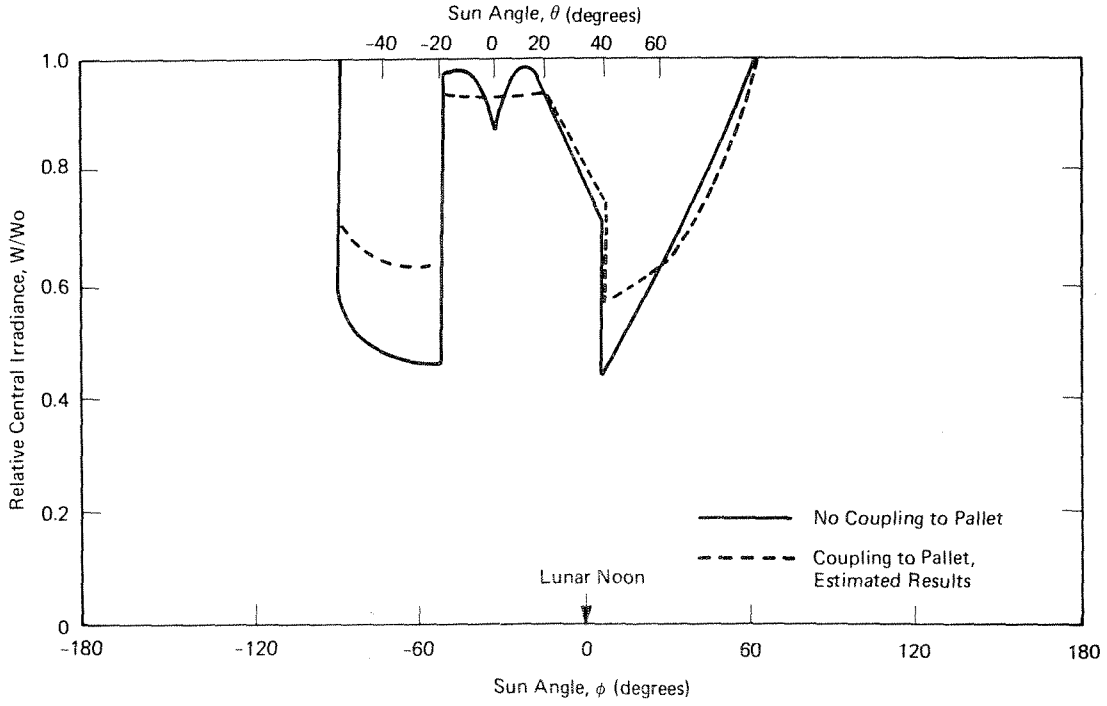


**Note:** Mount Conductance 0.01 Watt/°K

**FIGURE 16 PREDICTED CENTRAL IRRADIANCE-FINAL DESIGN CALCULATIONS**

# IV. MECHANICAL DESIGN

The array design was based on the performance and interface requirements summarized in Section II, as well as design criteria developed in the thermal analyses (Section III). The tight program schedules also had a major impact on the design process, since the design and method of construction had to be suitable for the short analysis and manufacturing time available. The schedule was especially acute for the array panel, whose basic design and interface requirements had to be established in the first three weeks of the program to permit construction and testing of the ETM. In the other major design areas – retro-reflector mounting, array insulation, and transportation cover – timing was less acute since the design process could proceed in parallel with fabrication of the ETM through most of the 12-week engineering design phase.

## A. ARRAY PANEL

The array panel was designed to accommodate 100 retro-reflectors, to be capable of withstanding the Apollo mechanical environment, and to be compatible with a method of retro-reflector mounting which would provide both thermal control and mechanical support. Very early in the program, it was decided, on the basis of the thermal analyses, that the retro-reflectors would be recessed in cavities whose height was one-half the retro-reflector face diameter.

A short design study showed that an array panel composed of orthogonal webs about 4 inches deep and spaced 3.5 inches apart would adequately support 100 retro-reflectors in groups of four between the webs (Fig. 17). In this design, a 0.05-inch-thick diaphragm would be located at mid-height in the panel to provide the necessary lateral stiffness. The continuity of the orthogonal web structure from the front to back of the array panel would provide maximum stiffness and minimize amplification of environmental mechanical inputs. The panel mounting brackets would be bolted directly to the back edge of the web members at their intersections. The webs connecting mounting bracket locations would be thick for proper load distribution and local thickening beyond this would provide the necessary mounting pad surface. The bolts that secured the mounting brackets would be high-strength shear bolts slide-fit into the line-reamed bracket-panel boss hole to eliminate amplification of any mechanical input across the mounting bracket-array panel interface. To minimize the weight of the array, we would drill out as much of the front face material as we could without reducing its strength, and bond in thin aluminum plugs.

The array panel was machined from a solid 6061-T6 aluminum block 4 inches thick and 18 inches square chosen for its homogeneity and uniform temper. Machining was chosen because it was much simpler to control than brazing, casting, or other fabrication

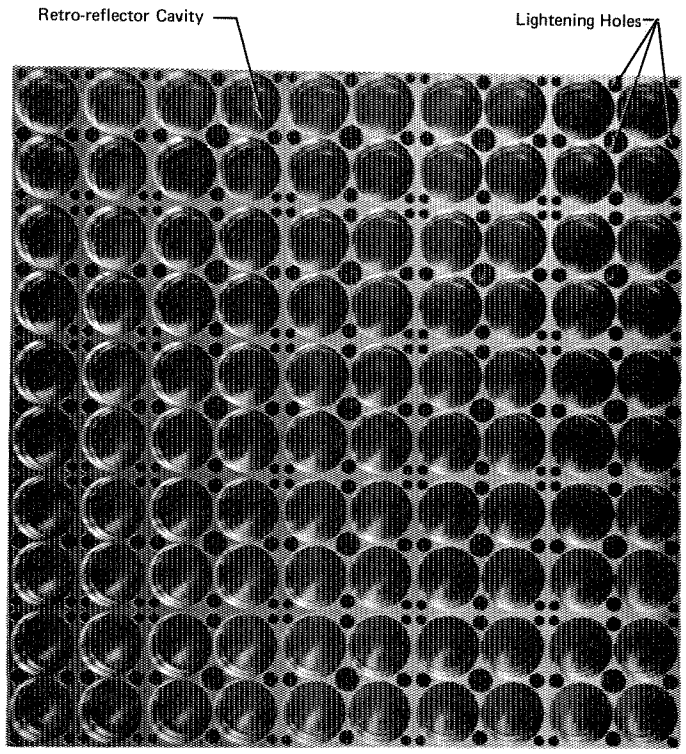


A. FRONT

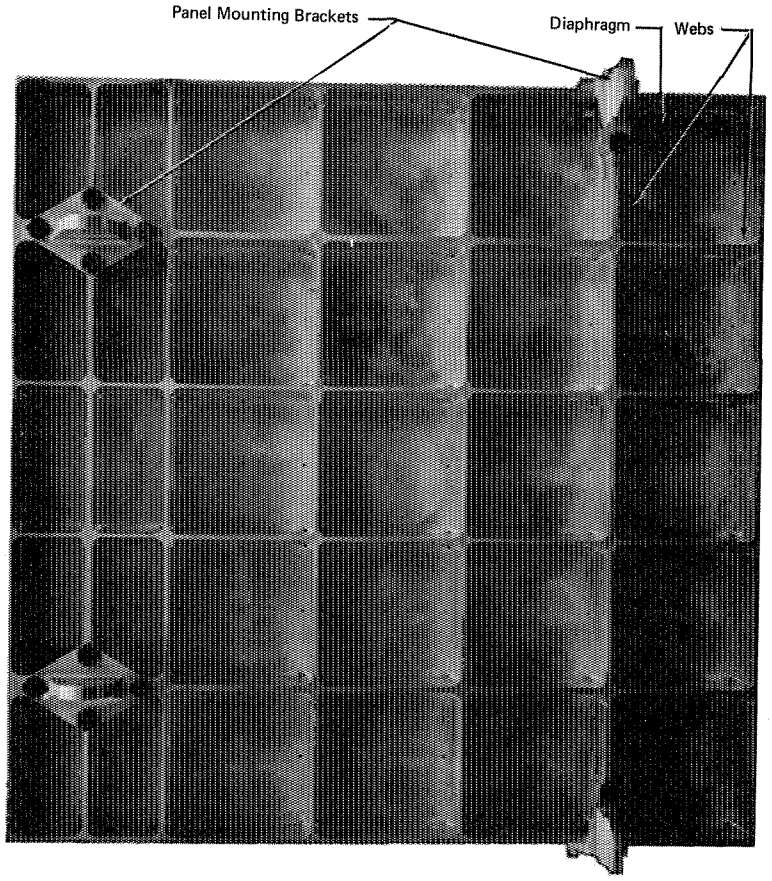


B. REAR

FIGURE 17 ARRAY PANEL STRUCTURE

procedures. The choice of material and alloy was based primarily upon availability, strength per unit weight, ease of machining, corrosion resistance, and ability to provide the correct thermal properties on the front (exposed) face. Magnesium was considered but discarded because of the extensive processes required to achieve the proper thermal/optical properties and the possibility of deterioration of coatings under high humidity.

During the panel design study, various other mounting patterns for the retro-reflectors were examined but eliminated because (a) they did not permit continuous ribs from the front to the back face of the panel and/or (b) they were incompatible with the basically orthogonal layout of the pallet mounting points. The use of isolators (i.e., a soft mounting system) was also considered as a means of permitting a less rigid, lighter weight, array. However, analysis showed that, within the limitations of time, a soft mounting system would have been heavier and less reliable than the selected design.

## B. RETRO-REFLECTOR MOUNTING

The design of the retro-reflector mounting reflects the overall array specifications, results of thermal analyses, and mechanical and space limitations associated with the panel configuration. Because of the difficulty of satisfying all the requirements, several mount concepts were investigated prior to a final design being chosen.

### 1. Mount Design Constraints

The retro-reflector mounting in the array panel had to conform to the following specifications:

- The array-mounted retro-reflector must withstand the Apollo mechanical environment without fracturing or generating debris that might contaminate the optical surfaces. The estimated amplification of the input environment by the array panel will result in maximum accelerations at the corner mounting surfaces of 250 g's.

- The individual retro-reflectors must be mounted so that they are not mechanically distorted during operation on the lunar surface.

- The mount must thermally isolate the retro-reflector from the array panel. The mount conductance must be of the same order as that for typical insulating load supports for multilayer insulation systems.

- During operation, the reflectors will be subjected to temperatures ranging from +250°F to -300°F.

- The normal to the front face of each mounted retro-reflector must be within ± 2°of the mean array pointing direction.

- The allowable radial thickness for the retro-reflector mount is 0.095 inch. (An increase in this thickness causes a twentyfold increase in array panel width, which increases array weight and lowers natural frequency.)

- The reflector mount must be appropriate for reliably mounting up to 100 retro-reflectors per array panel in a "clean room" environment.

- The retro-reflector mount must be simple enough to be designed, fabricated, assembled, tested, and qualified within 12 weeks.

- The mount must be constructed from materials on the Bendix Approved Materials List (ATM 242).

The ramifications of these specifications were quite significant but not necessarily obvious. What was required was a mount system capable of sustaining cyclic loads of about 18 pounds (the maximum acceleration multiplied by the mass of the retro-reflector). It had to be made of lightly loaded nonmetallic components (to minimize thermal conductance) that conformed precisely to the retro-reflector geometry (to minimize distortion) and would accommodate the operating temperature range without distorting the retro-reflector. Furthermore, the mount had to be simple to design, fabricate, and assemble, possess a high spring constant (to make the mount natural frequency greater than the highest mechanical environment input frequency), and be compatible with the load distribution and cleanliness of precision optical elements. These design requirements appeared to be mutually exclusive in that they required a mount with a stiff (high spring constant) high-load capacity but one that could accommodate the relative shrinkage of the panel around the retro-reflector without any significant increase in contact pressure (low spring constant).

## 2. Mount Design Concepts

### a. Spring Mounts

In the first mount concepts spring elements were used to locate the retro-reflector within the array panel cavity. A threaded retainer ring was used to confine the spring

elements and the retro-reflector and was accurately adjusted to obtain sufficient preload to prevent impacting at maximum accelerations.

The spring mount concepts, however, could not be reduced to practice, mainly because of the conflicting spring constant requirements. A high spring constant was required to keep the mount's natural frequency above the range of input frequencies, yet a low spring constant was required to accommodate differential thermal contraction between the aluminum array panel and the retro-reflector. Furthermore, a spring element with sufficient stiffness to provide a high retro-reflector mount natural frequency, when preloaded enough to prevent separation from the retro-reflector at maximum accelerations, exerted steady-state forces on the retro-reflector which would distort it beyond the allowable amount.

b. Spring-Loaded Chock Mounts

The second generation of mount concepts used chocks or wedge-shaped elements spring-loaded into place to prevent motion of the retro-reflector during shock and vibration.

During temperature cycling, the spring-loading device accommodated motion of the chocks by its differential thermal expansion and contraction between the retro-reflector and the array panel.

The many variations of this concept all required the use of high preloading forces to prevent separation of the surfaces (during maximum acceleration), which would cause impacting and the possible formation of debris. The high preload forces would have resulted in sufficient contact pressure on the retro-reflector to distort it. In addition, the high contact pressures would have led to an intolerably high thermal conductance between the retro-reflector and the array panel.

At this point in the mount evolution, a tapered tab was used on the retro-reflector to eliminate tensile stress in the retro-reflector (during differential expansion) and to minimize the spring preloading force. The tab angle was set such that its tangent was equal to the estimated coefficient of friction between the chock and the tab surface. Thus, during differential expansion, the chock would slide down the slanted tab face instead of pulling on the tab and causing tensile stress. Although the spring-loaded chock mount concepts were subsequently discarded, the tapered retro-reflector tab was retained because of its other desirable properties.

c. Controlled-Clearance Mount

The next generation of mount concepts was designed to eliminate steady-state force levels that would distort the retro-reflector. In these concepts, Teflon mounting rings contacting the retro-reflector tabs (tapered) were confined in the array panel cavity by the threaded retainer ring with controlled axial clearance. Thus, the retro-reflector and Teflon mounting ring assembly would slide freely within the confinement zone during shock, vibration, and differential thermal expansion. By controlling the axial clearance to about 0.001 inch and the radial clearance to 0.002 inch, impacting during vibration would be kept within tolerable limits.

A model of such a mount concept was constructed and tested at acceleration levels up to 40 g's (the limit of the vibration machine) with satisfactory results. The only problem with this mount was that it would be difficult and time-consuming to adjust the very precise clearances. There would always be the risk of insufficient radial clearance, and, during low-temperature cycles, the array would contract and exert excessive compressive loads on the retro-reflector and Teflon mounting ring assembly, possibly distorting the retro-reflector.

d. Temperature-Compensated Mount

While we were trying to eliminate the precise adjustment required with the controlled-clearance mount, we developed a temperature-compensated mount (Fig. 18) which also eliminated the problem of impact-loading of the retro-reflector.

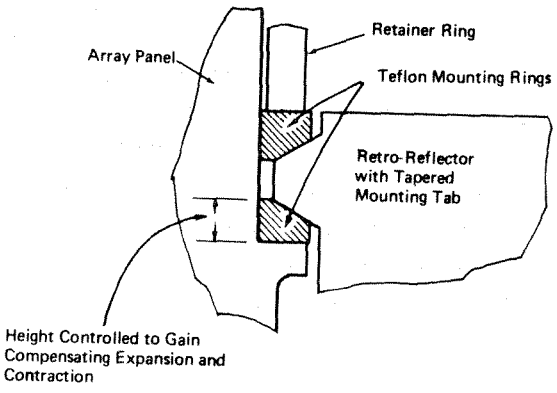


**FIGURE 18 TEMPERATURE-COMPENSATED MOUNT**

The temperature-compensating ability of the mount depended upon the very high coefficient of expansion of Teflon (five times that of aluminum) and the taper of the retro-reflector mounting tabs. For example, during a low-temperature excursion, the aluminum panel and the Teflon mounting rings would contract while the fused-silica retro-reflector would not (near zero coefficient of expansion). As the bore of the mount contracted, it would move the Teflon rings radially inward, where they would have to accommodate a greater tab thickness (because of the taper) and a reduced axial length (the panel would contract axially as well as radially). If their axial length were properly sized, the high thermal contraction (axially) of the Teflon mounting rings would exactly match the new

hardware configuration. The axial length could be easily computed after determining the coefficients of expansion of all the mount materials, their size, and the included angle of the retro-reflector tab.

We selected Teflon for the mounting rings because of its favorable combination of properties: i.e., high coefficient of expansion, inertness to lunar environment, low coefficient of friction, and ability to creep and conform to the retro-reflector mounting tab surfaces.

### 3. Retainer Ring Design

During the retro-reflector mount design evolution, the retainer ring design was finalized. Two general retainer ring concepts were considered: a threaded retainer and a split spring collar (internal snap ring). The characteristics of these two types of retainers were compared as follows:

| | Threaded Retainer | Split Collar |
|---|---|---|
| (a) | Can be assembled and disassembled any number of times before final assembly and subsequent lockup. | Should be assembled only once – otherwise, reference edges will become worn or damaged. |
| (b) | Prior to final lockup, disassembly is readily accomplished with a simple tool. | Disassembly requires probable destruction of the split collar. The fused-silica retro-reflector is liable to damage during this operation because of the high force levels required. |
| (c) | Final preload level can be set or changed at last minute to suit dynamic behavior of complete system – the preload is adjustable at any time prior to final lockup. | Preload level adjustments cannot be made except at initial assembly – the preload is fixed thereafter. |
| (d) | Stress levels in component parts are easily computed; therefore, short design time. | Stress level in split collar not readily determined because of large deflections needed for insertion and uncertainty about exact final configuration; therefore, longer design time required. |

| | | |
|---|---|---|
| (e) | Does not require extreme precision in retro-reflector cavity dimensions – final tolerance buildup can be taken care of with thread adjustment. | Tolerance buildup in mounting groove size would require custom fitting each retainer. |
| (f) | No undercut required – cavity progresses from large to small bore. | Accurate undercut required for mounting collar. |
| (g) | Requires a positive lock. | Needs no final lock. |

Because of the predominant advantage of the threaded retainer ring, we chose it for use in the array panel. It would be machined from 1100 aluminum and anodized to provide the proper thermal control surfaces adjacent to the retro-reflector and an anti-galling surface on the threads. Originally it was to have been made from 6061 aluminum, anodized on the bore and Teflon-coated on the threads, but for this application the thermal optical properties of anodized 6061 were inferior to those of anodized 1100.

### 4. Final Mount Design

The final mount design (Fig. 19) which evolved from analysis and testing of mechanical and thermal performance levels consists of two Teflon mounting rings, one above and one below the tapered mounting tabs of the fused-silica retro-reflector. The lower Teflon mounting ring has an indexing tab on its top face which fits against one of the back retro-reflector faces so that it can be used to position the retro-reflector. This ring is indexed in the array panel by a slot which fits over a pin in the mounting cavity shoulder. This assembly is confined in the array panel structure by a threaded aluminum retainer ring.

The retainer ring assembly of the retro-reflector mount has a finite axial clearance in the order of 0.002-0.003 inch to minimize thermal conductance to the retro-reflector from the surrounding hardware. The correct axial clearance is achieved by (1) torquing the retainer ring to 80 in.-oz, (2) backing off one complete turn, (3) re-torquing to 16 in.-oz, and (4) backing off 36°. This clearance allows a finite movement of the retro-reflector; however, since the retro-reflector is contacted by Teflon surfaces only, no damage occurs. The axial length of the Teflon mounting rings is such that as the mount assembly experiences temperature excursions, the differential thermal expansions (radial as well as

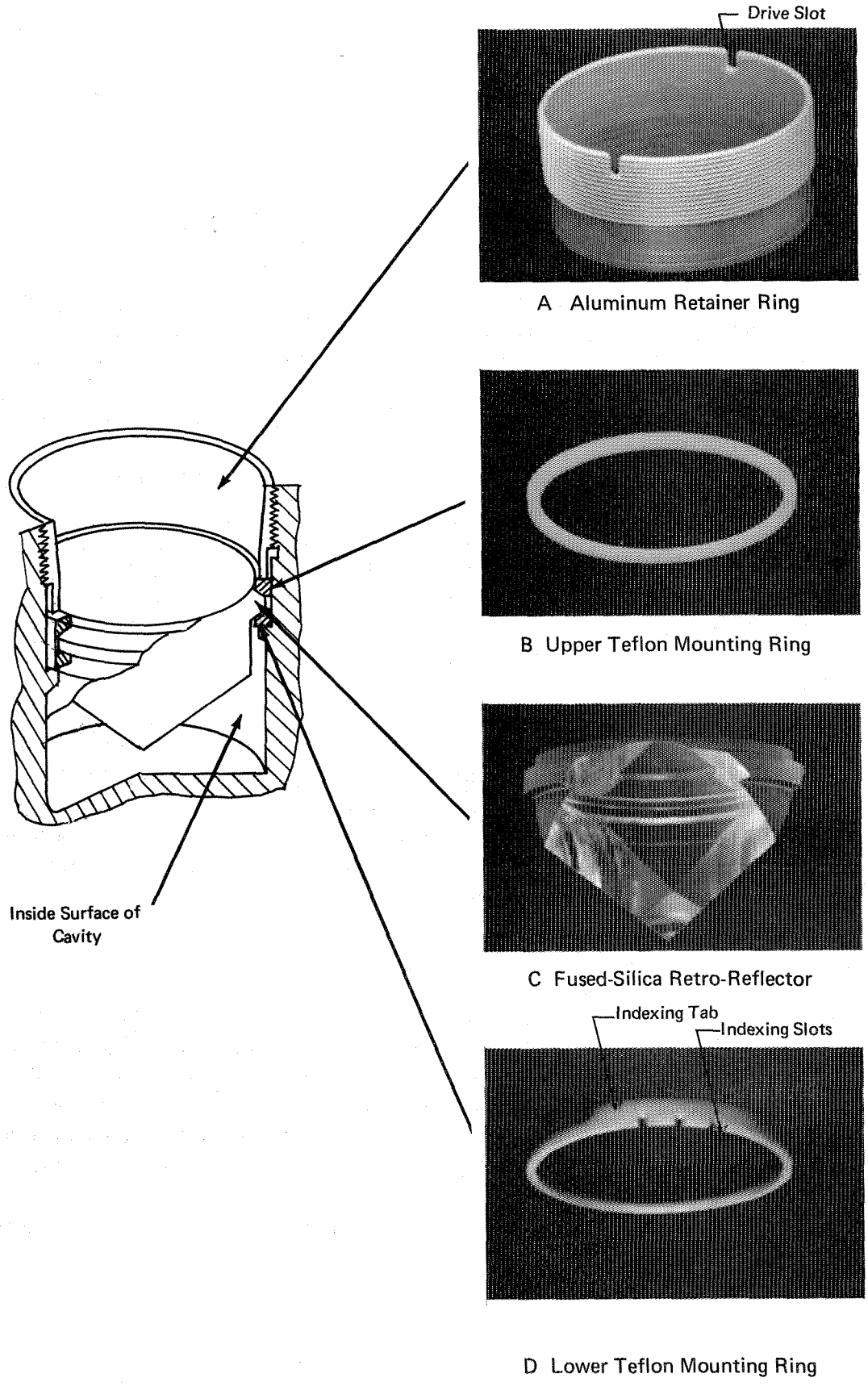


**FIGURE 19 RETRO-REFLECTOR MOUNTING**

axial) between the retro-reflector, the mounting rings, and the panel are complementary; thus, they do not result in large changes in the retro-reflector mount clearance.

The retainer ring is locked in place by deforming threads in the array panel with a special tool. Initially this was accomplished by deforming two threads in the structure by staking through one of the two drive slots in the retainer ring. However, during the testing of the Qualification Array a few of the retainer rings rotated slightly from their staked position. (In the ETM testing a slightly thicker retainer ring fabricated of 6061-T6 had successfully passed qualification level vibration with no evidence of movement.) Consequently, we initiated an experimental program with a single retro-reflector mount to determine how to prevent rotation, which led to a more positive staking technique. The final retainer ring back-off of 36° was stopped at 25° and the array structure threads were upset at two points by staking through both drive slots. Then the retainer ring was backed off the additional 11° and was staked through its wall into the previously upset structure threads. After this modification, no further rotation occurred during any vibration tests.

## C. ARRAY-PALLET INTERFACE

The array assembly is secured to the Bendix pallet at the four mounting bracket locations (Fig. 17). The array brackets terminate in tangs which fit into clevises on the pallet mounting posts, and are secured with close-fitting pins. To guarantee proper fit, a pallet simulator (for ADL) and an array simulator (for Bendix) were constructed by Bendix to simulate the hardware on either side of this interface. In both cases the simulators were combination inspection-machining fixtures.

## D. ARRAY INSULATION

The thermal performance requirements for the insulation system were established during the thermal analysis. Insulation was required on the bottom and the sides of the array to isolate the array from sunlight and from radiation from the lunar surface. Isolation required that the effective emittance of the insulation be approximately 0.05 or less. Other primary constraints were the design goal of a ten-year life on the moon, light weight, and installation on the array after the mounting, latching, and handle brackets were attached.

To meet those requirements we designed a multilayer insulation blanket consisting of the following materials (Fig. 20):

- A white Dacron cloth cover
- Three alternating layers of double-aluminized Mylar film and double thicknesses of Dacron netting
- Velcro hook tape attachments at the edges, adjacent to bracket holes, and near the center of the bottom of the array.

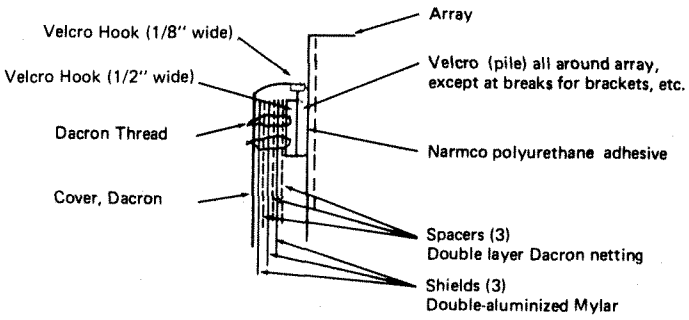


**FIGURE 20 MULTILAYER INSULATION BLANKET CROSS-SECTION**

Since there would be an unavoidable loss of effectiveness due to attachments, penetration, corner joints, etc., and the shields were a small portion of the weight of the insulation, we decided to use the three-shield system which would provide a theoretical safety factor of 10 to 12 with respect to the required 0.05 effective emittance. Tests of similar insulation assemblies for the Heat Flow Experiment and the Active Seismic Experiment showed degradation factors of approximately four from calculated to measured effectiveness.

# V. FABRICATION AND ASSEMBLY

Fabrication of the system qualification and flight models of the Laser Ranging Retro-Reflector Array was performed in accordance with the manufacturing/quality flow diagram shown in Figure 21.

## A. COMPONENT FABRICATION

Our basic philosophy for fabrication of the components was to provide a minimum of 50% spares to ensure that it would be possible for us to meet the established delivery schedule. Accordingly, we completely machined three array structures; a fourth structure was rough machined. The machining was done on manually controlled rather than on numerically controlled milling machines to save the time required to prepare tapes and because the number of structures did not justify the use of tape-controlled equipment.

The mounting rings were machined from heat-treated Teflon, with additional heat treating of the Teflon after partial machining. In the development program, final machining was accomplished immediately after heat treating. This procedure resulted in fairly stable dimensions and these rings successfully passed the qualification level of mechanical testing. However, for the qualification and flight models, an additional stabilization period of 48 hours was allowed between heat treating and final machining to ensure stable dimensions.

During the development program, aluminum retainer rings machined from 6061 aluminum had successfully passed the qualification testing. However, since 1100 series aluminum would provide a more acceptable thermal control surface on their inner diameter, the flight model retainer rings were machined from 1100 half-hard aluminum; after cleaning, the rings were soft-anodized. To prevent the soft retainer rings from rotating from their fixed position, we staked them. Thus, the clearance between the lower surface of the retainer rings and the Teflon mounting rings could neither decrease nor increase beyond the minimum or maximum tolerances.

On receipt, the retro-reflectors furnished to ADL were carefully inspected and cleaned to remove small areas of vapor-deposited aluminum on the optical surfaces and bits of wax remaining in the fillets between the mounting tabs and the main body of the retro-reflectors. Some retro-reflectors were returned for rework since their mounting tabs did not have sufficient radius to prevent them from cutting the Teflon mounting rings.

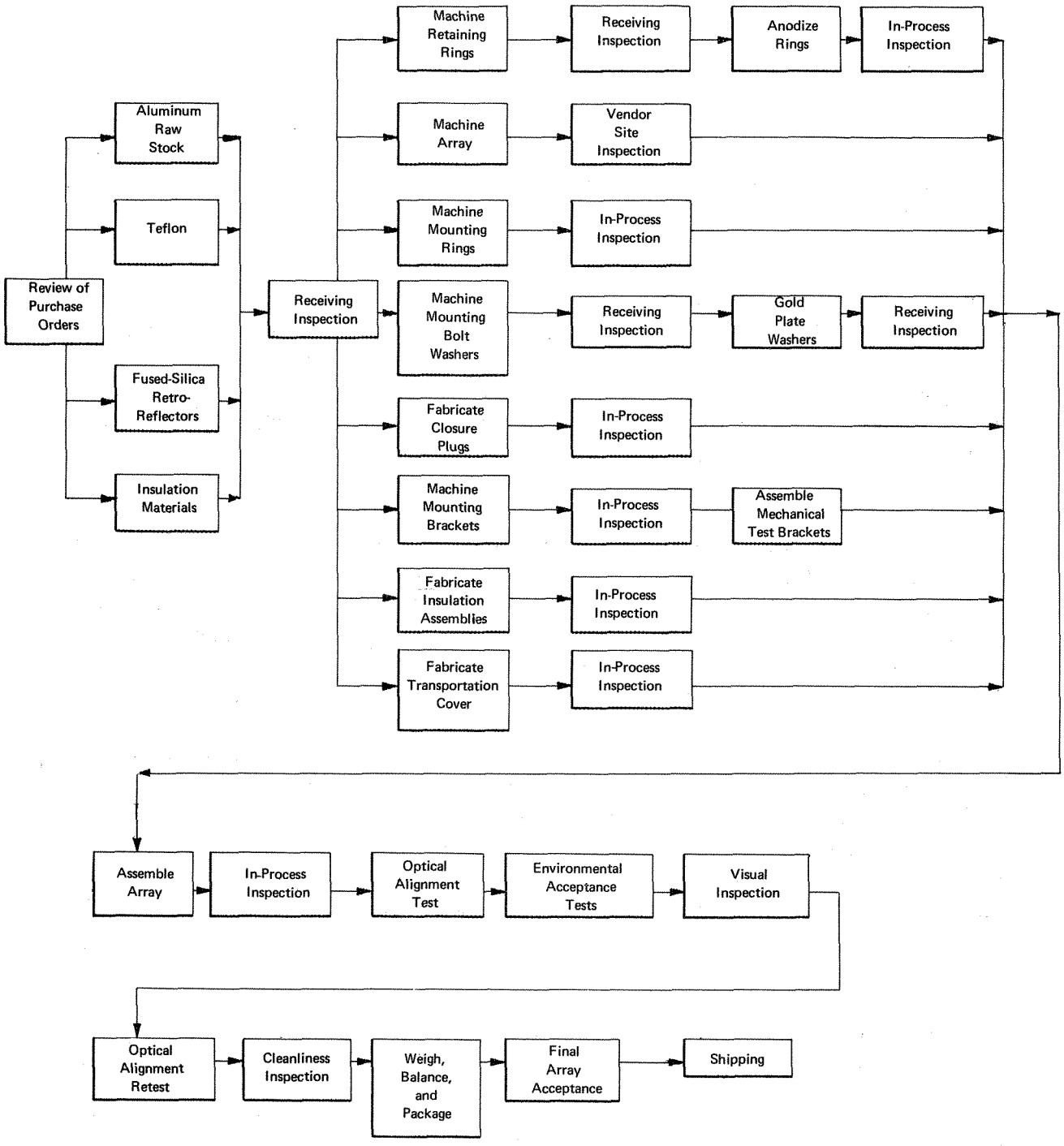


**FIGURE 21 MANUFACTURING/QUALITY ASSURANCE FLOW DIAGRAM–SYSTEM QUALIFICATION AND FLIGHT MODELS**

## B. FINAL ASSEMBLY

The mounting brackets for the array were installed on the panel structure as follows: The rough machined brackets were bolted to the rear surface of the array. The hinge brackets were then located within the Bendix drill jig and the release brackets machined to fit into their proper location on the jig. When all brackets properly fitted within the Bendix drill jig, the hinge pin holes and the release bracket holes were drilled and reamed to match this jig.

The insulation for the lower surface of the array was assembled in a separate clean area to reduce the possibility of introducing dust and/or lint into the final assembly area. Each component of the insulation was vacuum cleaned prior to its assembly into an insulation system.

After all components of the array had been prepared, and the lower mounting ring locating pins installed, the structure was ultrasonically cleaned and the Velcro straps and pads were epoxied to the array structure. From this point on, assembly took place within a pressurized "clean" area. At no time were the structures or components removed from this clean area unless they were adequately protected against contamination. The Teflon mounting rings were ultrasonically cleaned; and the retro-reflectors were installed at a laminar flow clean bench located within the assembly area in the sequence and as shown in steps 1 through 7 of Figure 22.

After the 100 retro-reflectors had been installed, a sheet of clear Mylar was fastened over the top surface of the array. The array was removed from the assembly area, installed in the Bendix drill jig and placed in the optical alignment test range. The array pointing angle was measured to ensure that all retro-reflectors had been properly installed. The array was then returned to the clean area and the aluminum retainer rings staked into position (Fig. 22, Step 8). The pointing angle of the array (9, Fig. 22) was checked, and, if acceptable, the alignment tool mounting bracket, furnished by Bendix, was installed on the array. After this, holes for the mounting and the handle brackets were cut into the multilayer insulation blanket and it was fastened onto the array with Velcro mounting strips (Fig. 23). The array was then mounted on the vibration test base plate and sealed in a heavy-gauge polyethylene bag and released to the test group.

On return from mechanical testing, the array was mounted in the Bendix drill jig and the pointing angle rechecked. In no case did the acceptance level testing cause a significant deviation of the pointing angle from that measured prior to testing.

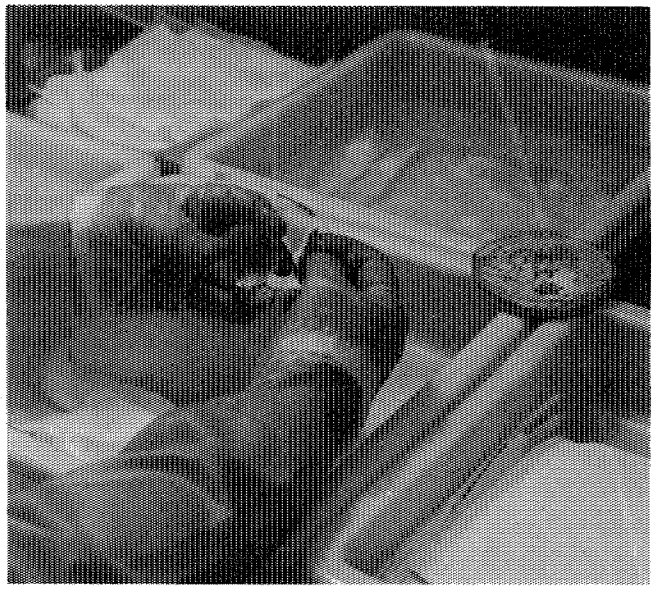

1. Clean Retro-reflector

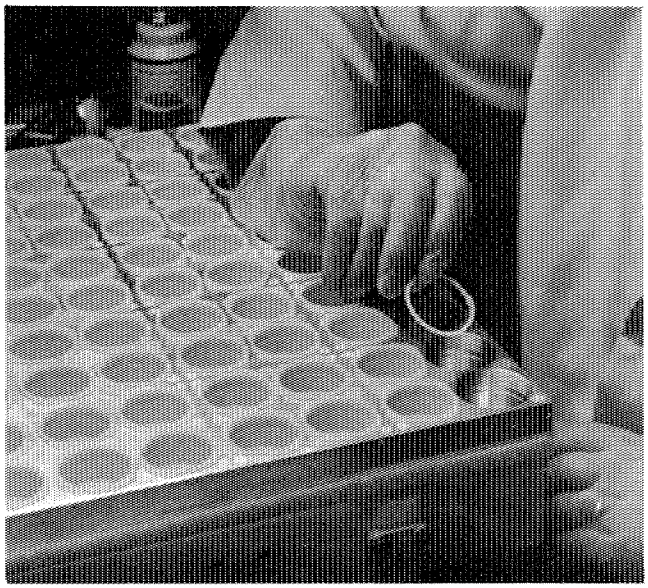

2. Install Lower Mounting Ring

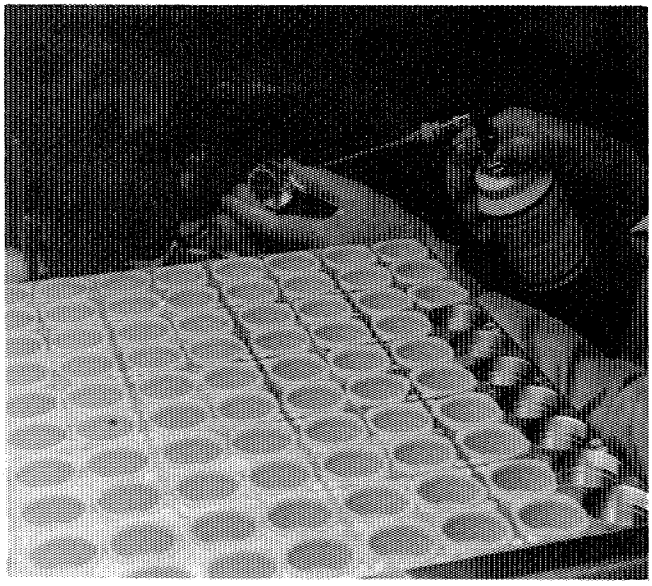

3. Final Clean Retro-reflector

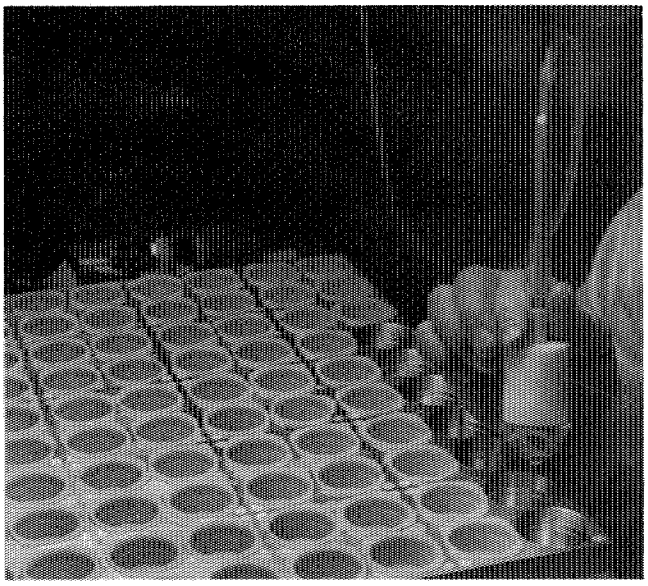

4. Install Retro-reflector

**FIGURE 22 RETRO-REFLECTOR INSTALLATION SEQUENCE**

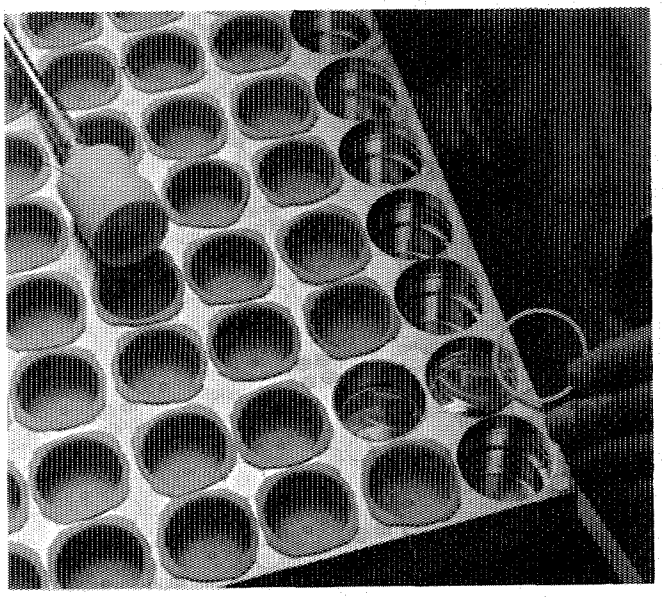

5. Install Upper Mounting Ring

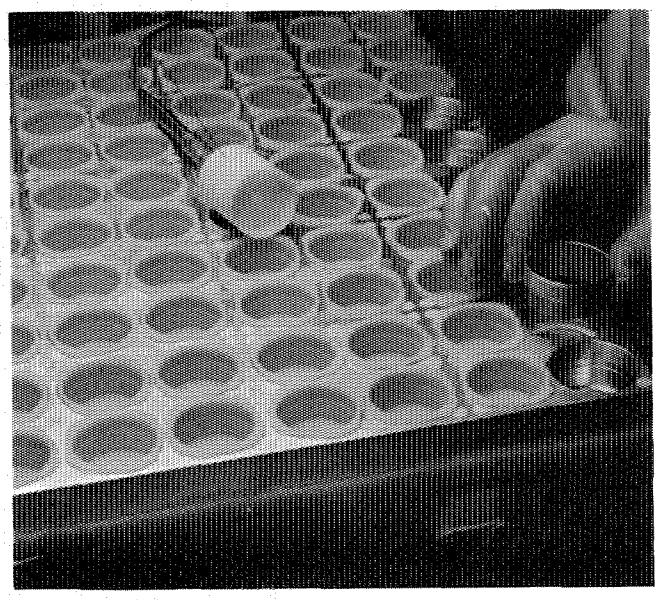

6. Install Retainer Ring

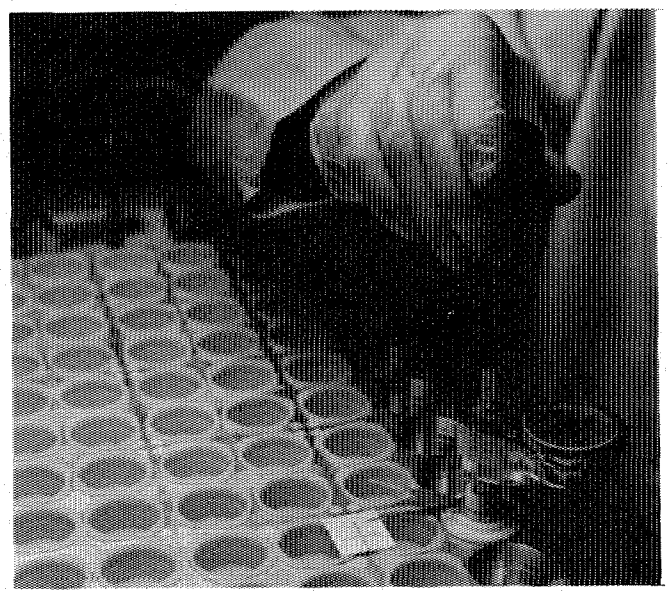

7. Torque Retainer Ring

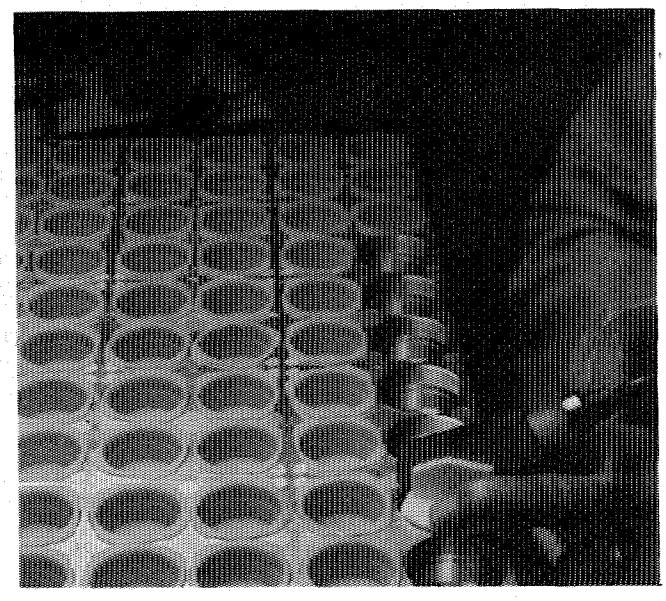

8. Stake Retainer Ring

**FIGURE 22 RETRO-REFLECTOR INSTALLATION SEQUENCE (Continued)**

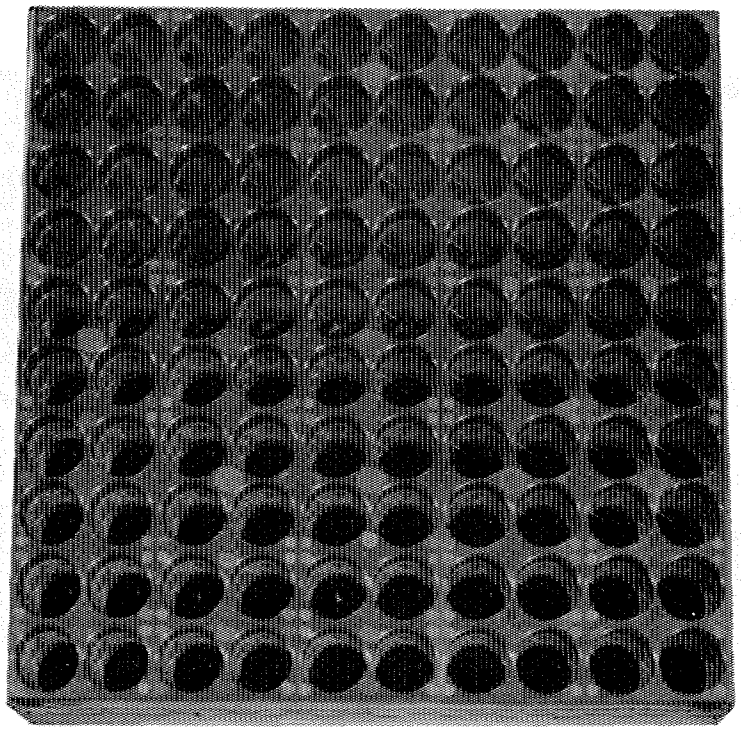

9. Completed Installation

**FIGURE 22 RETRO-REFLECTOR INSTALLATION SEQUENCE (Continued)**

To protect the retro-reflectors against falling dust or debris the array was covered with a transportation cover (Fig. 24) made of rip-stop Nylon coated with aluminized Mylar on both sides and held onto the array by cloth straps fastened to two adjacent sides. The straps extended underneath the array panel assembly and were Velcro-secured on the sides opposite the fastenings. To exclude contamination the cover fit snugly over the sides of the array.

For delivery to Bendix, the array, after all testing and optical alignment had been completed, was mounted on an aluminum handling plate. A heavy-gauge polyethylene bag was installed around the array for additional protection during shipment, and the aluminum handling plate installed into a standard, pressed metal case, as shown in Figure 25. The case was then sealed, and dry nitrogen gas was used to pressurize the shipping case. The unit then was ready for delivery.

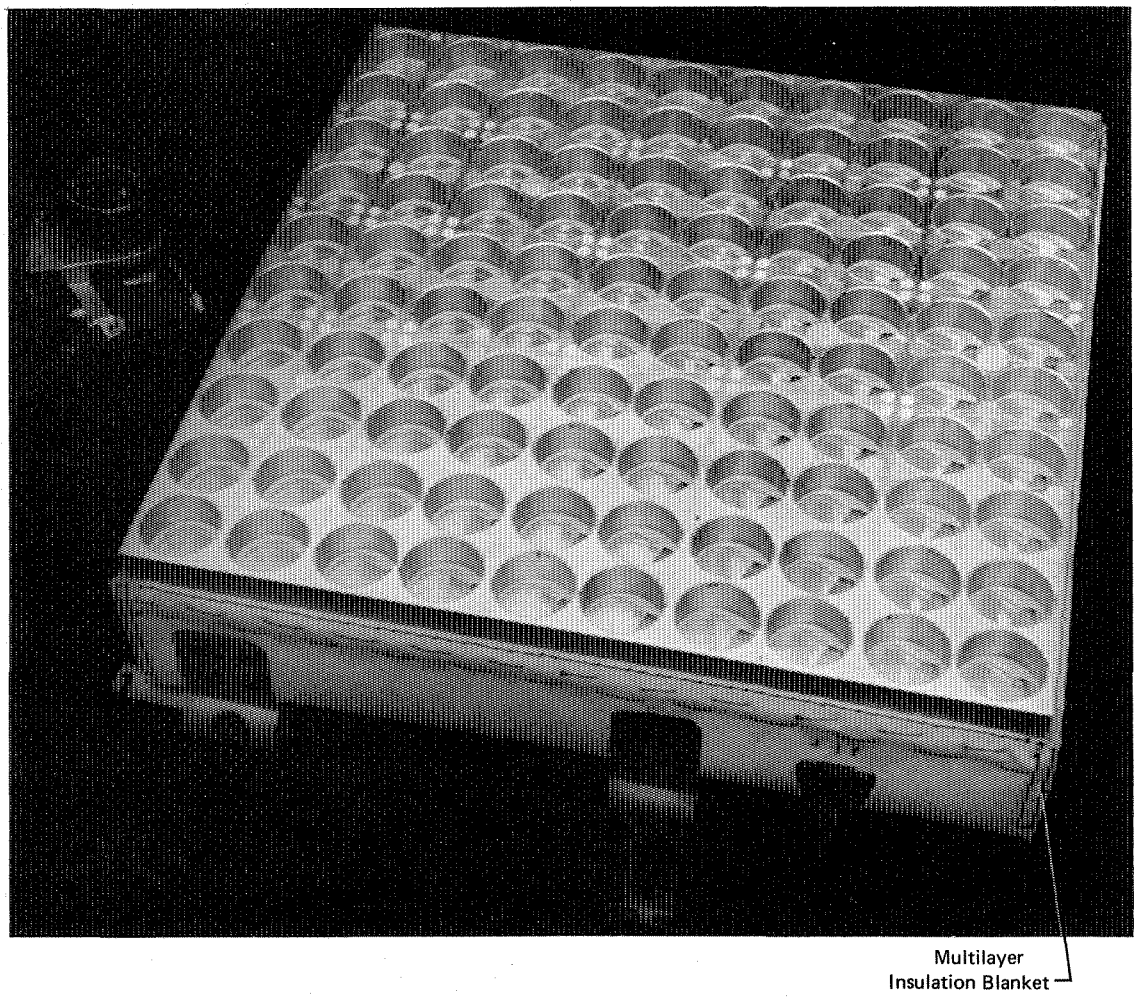


**FIGURE 23 ARRAY WITH MULTILAYER INSULATION BLANKET**

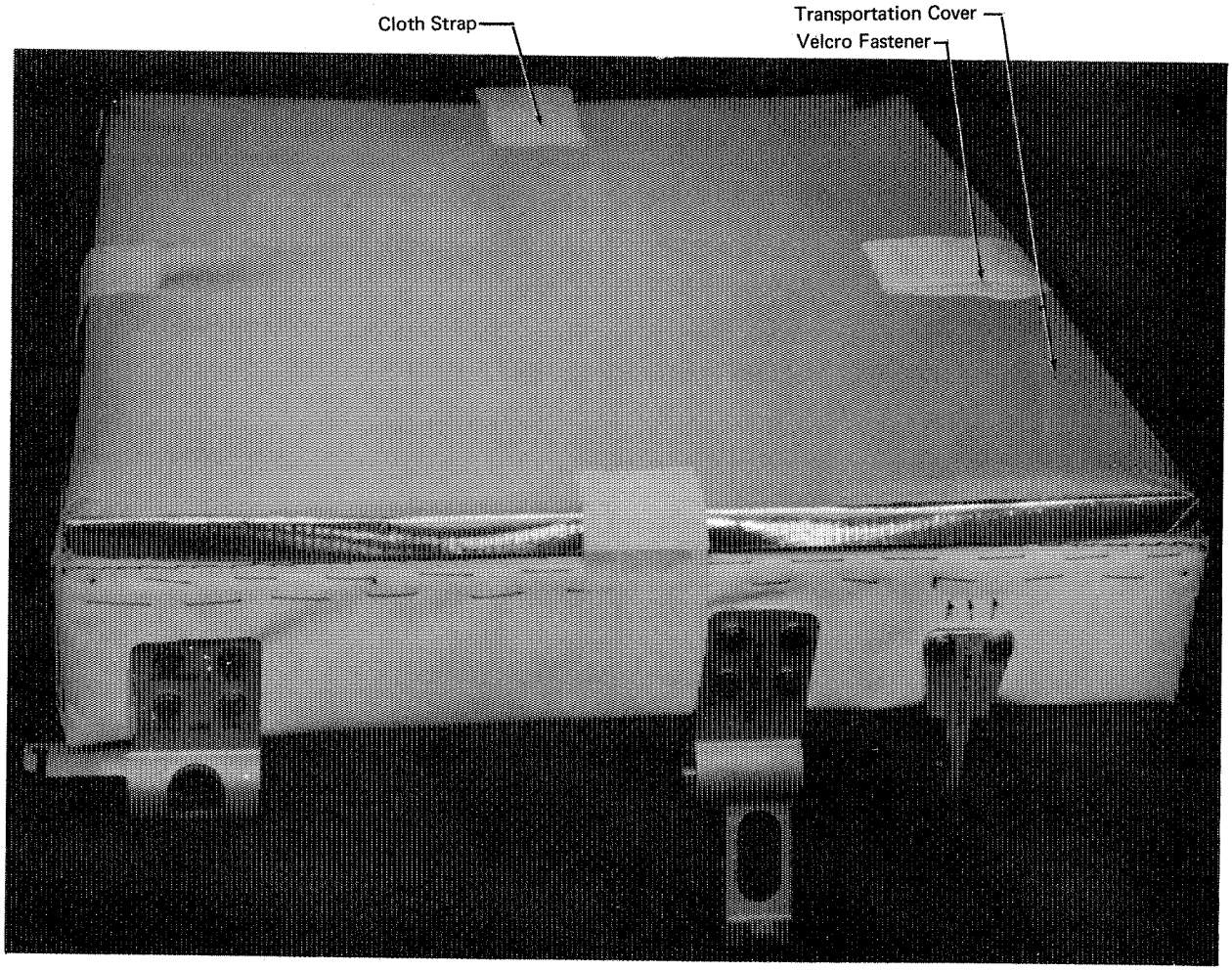


FIGURE 24 ARRAY WITH TRANSPORTATION COVER

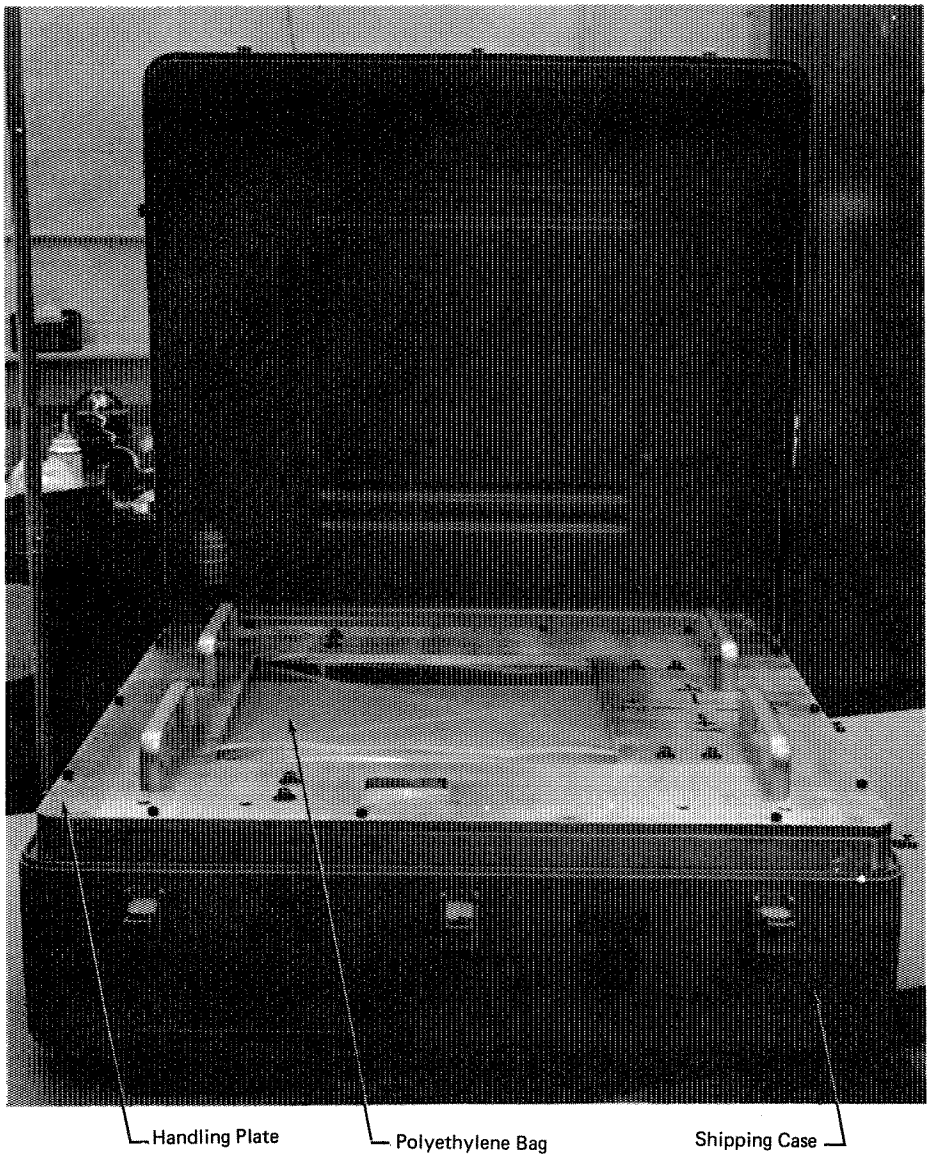


**FIGURE 25 ARRAY IN SHIPPING CASE**

# VI. TEST PROGRAM

The test program for the Laser Ranging Retro-Reflector Array consisted of development tests and acceptance tests: (1) to provide information for the successful design of the array, (2) to establish the mechanical and thermal performance characteristics of the array and the retro-reflectors, and the pointing direction of the array, and (3) to ensure that the retro-reflector array met the required performance specifications. These tests were divided into three categories: mechanical; thermal; and optical alignment.

Mechanical tests were conducted on the engineering test model (ETM) and the qualification and flight units. Thermal distortion tests were conducted on the engineering test model, and optical alignment tests on the engineering test model, the qualification model, and the flight model. Mount conductance and mount temperature compensation tests were conducted on sectional development models of the array to guide the development of the flight models.

## A. MECHANICAL TESTS

The mechanical tests were of two general types: engineering and development tests on the entire array and on components; qualification and acceptance tests on the completed array.

Engineering and development tests were performed to verify theoretical estimates, supply information on the behavior of individual components, or provide proof of the adequacy of the design of the array and components. Qualification and acceptance tests were performed in conjunction with before-and-after optical alignment tests to demonstrate that the array would function properly within the specified design goals.

### 1. Engineering and Development Tests

The mechanical test inputs consisted of random and/or sine excitation. Because of their less critical nature, we did not consider shock and steady-state acceleration inputs although Engineering Test Model No. 1 did receive the shock pulse exposure. The environmental specification is shown in Table 5.

The first series of tests consisted of sinusoidal testing of single retro-reflectors in a five-inch aluminum cube, which could be bolted directly to the shaker head in all six orthogonal directions.

Initially, we used simulated retro-reflectors made of aluminum, instrumented with small accelerometers, and machined to duplicate both the weight and the center of gravity

TABLE 5

MECHANICAL ENVIRONMENT

| FREQUENCY (HZ) | ACCEPTANCE LEVEL | QUALIFICATION LEVEL |
|---|---|---|
| **I. SINUSOIDAL** | | |
| 5 – 20 | 0.30 IN. D.A. | 0.35 IN. D.A. |
| 20 – 100 | 5.4g | 7.0g (zero to peak) |
| Sweep: 3/4 oct/min | 5 – 100 Hz | 5 – 100 – 5 Hz |
| Tolerance: ± 10% | | |
| Directions: X, Y, Z | | |
| **II. RANDOM** | | |
| Tolerance: PSD, ± 3 db; g, rms, ± 10% | | |
| Directions: X, Y, Z | | |
| A. LAUNCH AND BOOST, DURATION: 2-1/2 MIN | | |
| 10 – 30 | 9 db/oct rise | 9 db/oct rise |
| 30 – 1250 | $0.06g^2$/Hz | $0.10g^2$/Hz |
| 1250 – 1500 | 12 db/oct rise | 12 db/oct rise |
| 1500 – 2000 | $0.12g^2$/Hz | $0.20g^2$/Hz |
| g, rms | 12.4 | 16.1 |
| B. LUNAR DESCENT, DURATION: 12-1/2 MIN | | |
| 10 – 25 | 9 db/oct rise | 9 db/oct rise |
| 25 – 1150 | $0.03g^2$/Hz | $0.05g^2$/Hz |
| 1150 – 1500 | 12 db/oct rise | 12 db/oct rise |
| 1500 – 2000 | $0.09g^2$/Hz | $0.15g^2$/Hz |
| g, rms | 9.8 | 12.8 |
| **III. SHOCK (ENGINEERING TESTS ONLY)** | | |
| 10 ms rise, 1 ms fall | | |
| Sawtooth | 15.4 g | 20.0 g |
| Tolerance : MIL–STD 810 B | | |
| Directions: +X, ± Y, ± Z | | |

of a fused-silica retro-reflector. The test cavity for the retro-reflector was identical to a cavity of the array.

We made sine sweep tests from 5 Hz to 2,500 Hz at input levels up to 40g in three axes. Shaker and cube resonances made it possible for us to intentionally expose the cavity and retro-reflector to levels up to 150g (zero to peak). The results showed that transmissibility across the mounting rings was essentially unity. Thus, the retro-reflectors would experience the same levels as the array cavity walls. A final test with an unfinished fused-silica retro-reflector showed that the retro-reflector could withstand this severe environment. With a transmissibility of unity, we assumed that the 100 retro-reflectors were a mass load, rigidly attached to the array structure, with an unknown amount of frictional damping provided by the Teflon interfaces.

During the tests, severe rotation of the retro-reflectors (with small clamping forces) indicated the need for fixing their rotational positions in the cavities.

The next series of tests was conducted on ETM-1*under various conditions. A test fixture (Fig. 26), consisting of a 1½ inch magnesium plate 20 inches square, was prepared for all of the mechanical environmental tests on a completed array. In the first three tests, the array was mounted to the fixture by stiff pads whose contact area with the array was identical to that contemplated for the brackets. The pads were rigidly mounted to the fixture, and the fixture, in turn, was mounted to the shaker. The pad-to-array bolting was almost identical to that proposed for the final bracket-to-array bolting.

Under low-level (2g) sinusoidal input, the array showed no natural frequencies up to 300 Hz. At the qualification level (7g) sinusoidal input, the array was rigid up to and probably beyond 100 Hz.

In the first three qualification-level random exposures, the array was filled with 5, 61, and finally, the full complement of 100 retro-reflectors as they became available (in some instances, aluminum retro-reflectors were used when fused-silica retro-reflectors were not available).

In the fourth and last random exposure, the final bracket configurations were used. They were bolted to the array in the proposed berth flight array manner while the lower ends were held rigidly in new pads bolted to the magnesium fixture. The response of the array was measured with an accelerometer in each of the three directions: near the center cavity in the pointing direction, and in the middle of the sides of the array in the other two lateral directions.

* To assure that test schedules were met, we constructed two engineering test models: ETM-1 was used for all mechanical tests and most of the optical alignment tests; ETM-2 was only used for some optical alignment tests.

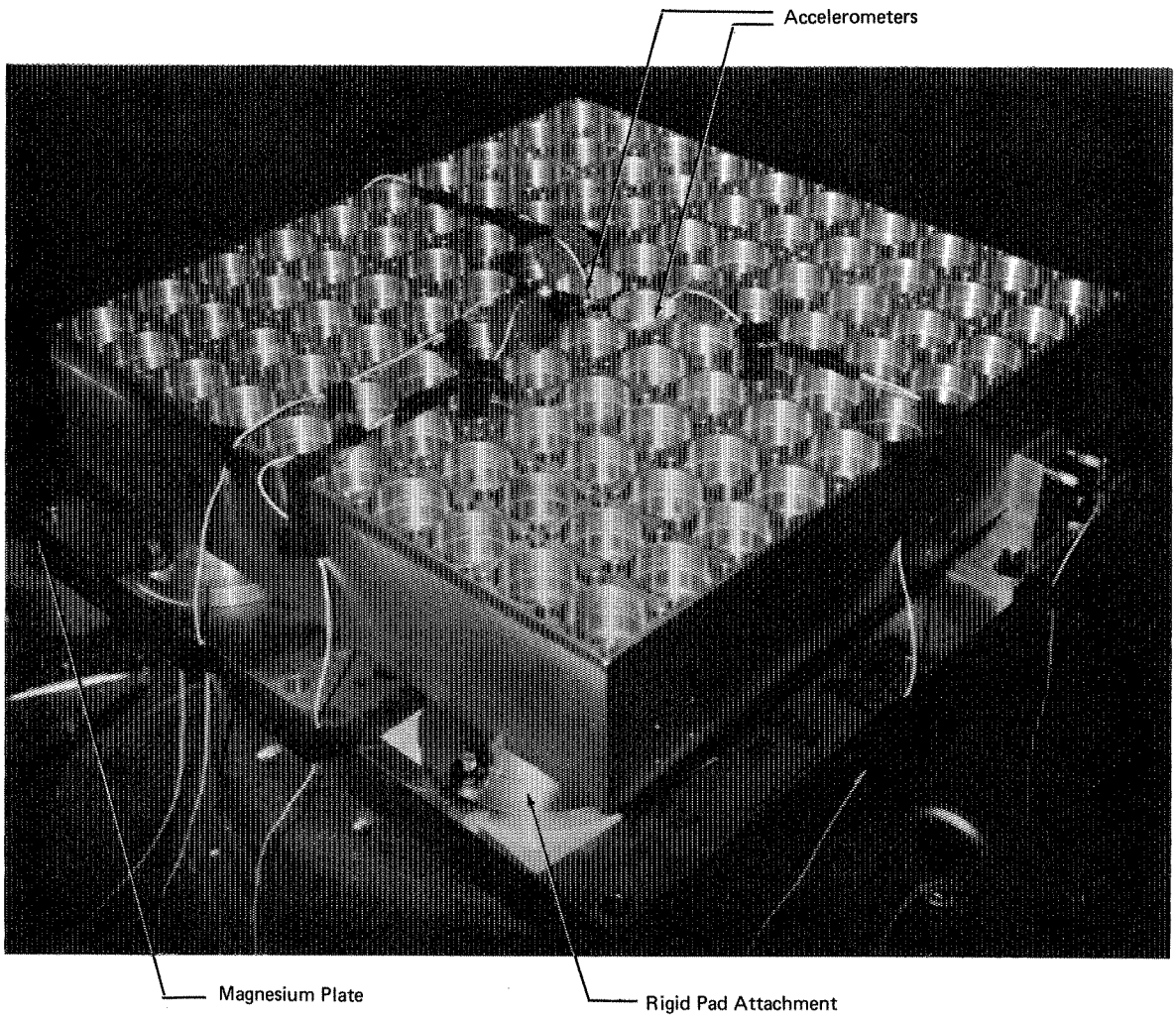


**FIGURE 26 ETM ON MECHANICAL TEST FIXTURE**

The results (Table 6) indicated that the X-response was less than that predicted, probably because the damping characteristics of the array were greater than those indicated in the design analysis. The response in the Y-direction with brackets was quite high, as could be expected because of the high flexibility of the brackets.

**TABLE 6**

**ARRAY RESPONSE TO 16.1g (RMS) RANDOM INPUT**

**Conditions:**

| **Mounting** | | **Rigid Pad** | | **Brackets** |
|---|---|---|---|---|
| No. of Retro-Reflectors | 5 | 61 | 100 | 100 |
| **Array Response (g, rms)** | | | | |
| X (Pointing) | 65.0 | 34.0 | 40.0 | 48.0 |
| Y (Parallel to Hinge) | – | 23.0 | – | 60.0 |
| Z | 32.0 | 24.0 | 22.5 | 45.0 |

There were no indications of any failures in any location of the array or bracket structure. With the exception of the Y-direction, the ETM-1 array received the random qualification level (launch, 16.1g, rms; descent, 12.8g, rms) and the sinusoidal of 7g, a total of four times.

The shock tests on ETM-1 showed that the array with brackets responded as expected, one-to-one.

Because the titanium bolts and nuts and the "preload indicating washers" were critical structural components, we examined torque-tension relationship of these fasteners in the array. The preload indicating washers were not available early enough in the program to be included in the development tests. Therefore, the breaking torque, the prevailing torque, and the back-off torque of the nut and bolt assembly (with mating materials and dimensions identical to the array installation) were determined. After all the random tests, we carefully recorded the back-off torque to ensure that no loosening occurred and that consistent set-up torques had been maintained during assembly.

As a result of these tests, set-up torque was used as a check on proper tensioning when the preload washers were used in the qualification and flight model arrays. Calculations showed that the preload in the bolts would increase by about 25,000 psi because of the high temperature that would be encountered on the lunar surface. Although the assembly was designed for operation at high temperature, we tested a sample assembly to 300°F (40° above the expected temperature) for 12 hours. After the temperature returned to room temperature, back-off torque and inspection of the assembly indicated that no failure had taken place.

### 2. Acceptance Tests

Mechanical vibration tests at acceptance level and alignment tests before and after vibration were performed on the qualification and flight model arrays. The vibration and alignment tests after vibration constituted the acceptance tests on these units. The mechanical tests were performed in accordance with test procedure TP4:0511-E1-15.[12]

The first acceptance level vibration testing on the qualification model array consisted only of X-axis inputs. At the completion of tests on this axis, inspection of the array showed that several retainer rings had rotated. Consequently, a new method of staking the retainer was devised. An assembly using the new staking method was then tested on the five-inch single mount test fixture and compared with an assembly staked in the original manner.

These single mount vibration tests were carried out at sinusoidal sweep levels of 30 and 40g and by dwelling at 300 and 1,000 Hz for ten minutes each. Post-test inspection revealed that the retainer ring staked by the old method rotated whereas the one with the new staking method was still permanently fixed to the cavity thread.

The qualification model was then restaked and retested at the acceptance levels. Laboratory inspection confirmed the fact that none of the retainer rings had moved.

The flight model was also exposed to the acceptance vibration levels and, similarly, no motion occurred.

Post-test inspection of both models after vibration tests revealed no damage to or physical changes in the arrays.

## B. OPTICAL ALIGNMENT AND THERMAL DISTORTION TESTS

A series of tests was conducted on the arrays to measure the degree of alignment of each retro-reflector within the array with respect to the array pointing direction, and to measure the array pointing direction with respect to a fixed reference. Development tests were conducted on the engineering test models of the array: (1) before and after subjecting the array to a mechanical test environment, to determine the alignment stability of the retro-reflectors; and (2) before, during, and after subjecting the array to thermal cycling from -300°F to +250°F, to establish the effects of thermal distortion on the array alignment.

The qualification and flight models of the array were: (1) aligned with the Bendix drill and alignment fixture[13] before the holes were drilled in the array brackets; (2) checked for alignment of all reflectors in the array after assembly and before mechanical vibration; (3) checked after mechanical vibration to determine the pointing direction of the array and the pointing direction of each reflector in the array.

An optical alignment test range and a thermal distortion test fixture were designed and fabricated for these tests. Calibration, test, and data reduction procedures[14, 15, 16] were prepared and submitted to Bendix as a part of the acceptance data packages.

### 1. Test Equipment

#### a. Design

The principal components of the optical alignment test range apparatus (Fig. 27) are a moveable test bed, collimated light source, measurement grid, recording camera, and support structure. The thermal distortion test fixture consists of a thermally installed liquid-nitrogen-cooled container, electrically heated plates, and the legs which support the array on the moveable test bed. The moveable test bed is designed so that the array can be maintained horizontal and moved in two directions so that each retro-reflector can be located beneath the light beam. Two electric heaters are wrapped on the edges of the array and held in place by metal strips. The heaters are thermostatically controlled by thermocouple sensors located on the edges of the array. A beaded polystyrene insulating container is placed underneath and adjacent to the array. Thin sheets of aluminum foil and aluminized Mylar are placed within the container to form a liquid seal and provide additional insulation. The electric heaters are used to raise the array temperature to 250°F; liquid nitrogen poured into the polystyrene container is used to lower the array temperature to -320°F. The container, heaters, and test bed are designed so that the array need not be moved between low-, room-, and high-temperature tests. Thermocouples are used to measure temperatures at various locations on the array.

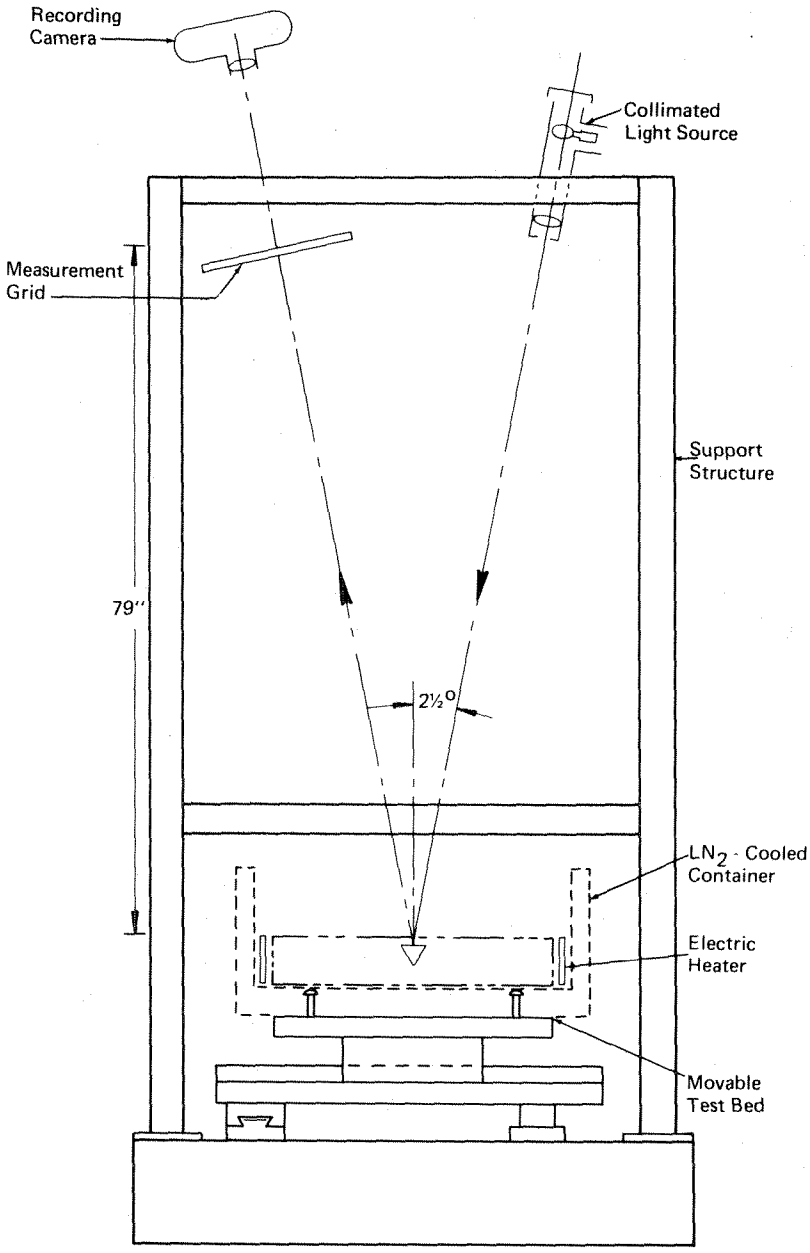


FIGURE 27 OPTICAL ALIGNMENT TEST RANGE APPARATUS

b. Fabrication

The test equipment was fabricated and assembled and tests were made to align the source, grid, and test bed and to ensure that the components were performing satisfactorily. Checkout measurements indicated that the reproducibility of the angular measurements on a single retro-reflector would be approximately 0.01°.

After ETM tests were completed, we made minor modifications to the test range to ensure more precise positioning and alignment of the light source, grid, and moveable test bed. A front surface mirror calibration fixture was modified for use with the Bendix drill and alignment fixture. The mirror and the Bendix fixture were used to align the optical test range and the array during subsequent tests. We calibrated the optical alignment test range prior to each test of a qualification or flight model array.

2. Tests

In the optical alignment test range, a collimated light beam was directed onto the

front surface of each retro-reflector at an angle of incidence of approximately 2.5°. The light beam was specularly reflected from the front surface of each retro-reflector onto the measurement grid. The pointing direction of the retro-reflector was then calculated from the sum of the vectors that represented the incident and reflected light beams.

The coordinates of the intersection of the reflected beam and the coordinate grid were a measure of the angular excursion of the reflected beam from an ideal reflected beam (i.e., that beam which would be reflected from a retro-reflector whose front surface was parallel to the reference surface of the array; the grid was oriented so that an ideal reflected beam intersected the grid at a predetermined location). The experimentally determined locations of the reflected beams were transformed (by means of a data reduction computer program) from intersections of a plane (the measurement grid) to positions in three-dimensional space. These positions, the fixed position of the incident beam, and the known dimensions of the system were related to the location of the pointing direction of the retro-reflector in space. The computer, keeping track of the pointing vector (direction) of each retro-reflector in the array, calculated the resultant array pointing vector (the vector sum of all the individual pointing vectors) of all the individual retro-reflectors and the angle between this resultant and each pointing vector. The computer also calculated the angle between the pointing vector of each retro-reflector and the vertical and that between the resultant pointing vector and the vertical.

Because the reference surface of the array structure was initially adjusted to be horizontal, the normal to the array structure was parallel to the vertical. Thus, we determined: (1) the angular deviation of the pointing direction of each retro-reflector in the array and the resultant pointing direction of all the retro-reflectors (the array pointing direction) from the normal to the array structure, and (2) the angular deviation of the pointing direction of each retro-reflector from the array pointing direction.

The test procedure[15] was prepared and submitted to Bendix before qualification or flight models of the array were tested.

Table 7 lists all tests performed in the optical alignment test range during the program. Tests A through III were performed during Phase A of the program.

Figure 28 shows typical locations of the beams reflected from the front surfaces of the retro-reflectors. The numbers in the circles identify each retro-reflector. The circles show the magnitude of angular deviation of 0.1, 0.2, and 0.3° from the resultant reflected beam.

TABLE 7

OPTICAL ALIGNMENT TEST PROGRAM

| Test | Array Model | Number of Retro-Reflectors | Condition |
|---|---|---|---|
| A | ETM-1 | 3 | Before vibration |
| B | ETM-1 | 3 | After vibration |
| I | ETM-1 | 65 | Before vibration |
| II | ETM-1 | 65 | After vibration |
| III | ETM-1 | 96 | After vibration |
| IV | ETM-1 | 96 | Room temperature |
| V | ETM-1 | 96 | -300°F |
| VI | ETM-1 | 96 | Room temperature |
| VII | ETM-1 | 96 | +250°F |
| VIII | ETM-1 | 96 | Room temperature |
| IX | ETM-2 | 20 | Array 0.090" too high |
| X | ETM-2 | 20 | Normal height, before drilling |
| XI | ETM-2 | 20 | After drilling |
| XII | Qualification | 20 | Before drilling |
| XIII | Qualification | 20 | After drilling |
| XIV | Flight | 20 | Before drilling |
| XV | Flight | 20 | After drilling |
| XVI | Qualification | 100 | Before vibration |
| XVII | Qualification | 100 | After staking of mounting ring |
| XVIII | Qualification | 100 | Acceptance |
| XIX | Flight | 100 | Before vibration |
| XX | Flight | 100 | Acceptance |

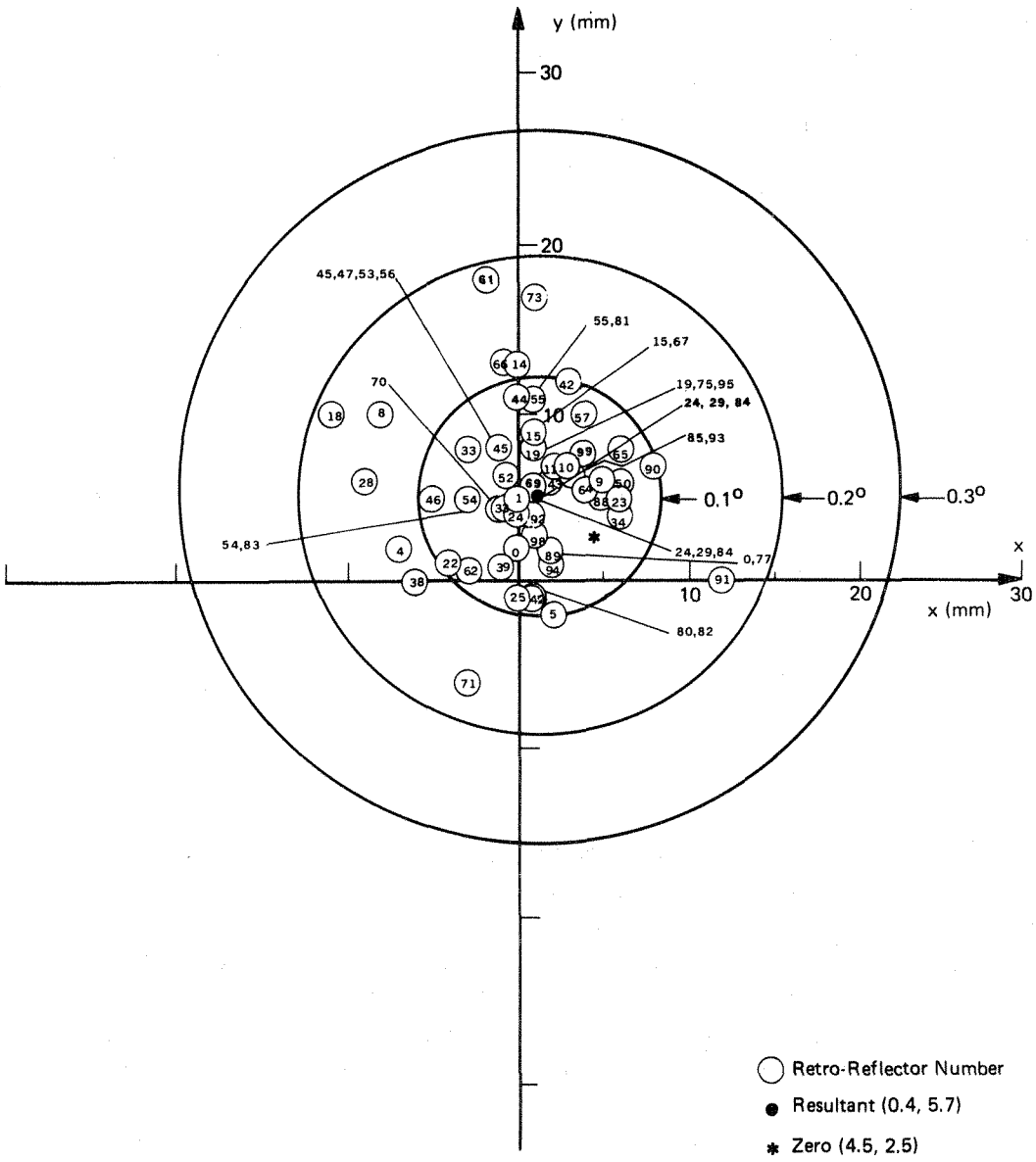


**FIGURE 28 TYPICAL LOCATIONS OF REFLECTED BEAMS ON MEASUREMENT GRID**

Preliminary tests with three retro-reflectors (Tests A and B) in the ETM-1 array showed that, before vibration, the maximum angular deviation of the pointing direction of any retro-reflector from the array pointing direction was 0.10° and the array pointing direction was 0.09° from the normal to the array front surface. After vibration, the maximum angular deviation of the pointing direction of any retro-reflector from the array pointing direction was 0.10° and the array pointing direction was 0.10° from the normal to the array front surface.

The results of the same array tested with 65 and then 96 retro-reflectors (Tests I-III) are shown in Table 8.

**TABLE 8**

**ETM OPTICAL ALIGNMENT RESULTS BEFORE AND AFTER VIBRATION TESTS**

| Test No. | Maximum Deviation of Individual Retro-Reflectors From Array Pointing Direction | Deviation of Array Point Direction From Array Normal |
|---|---|---|
| I | 0.18° | 0.07° |
| II | 0.29° | 0.08° |
| III | 0.21° | 0.06° |

The angular deviation of the pointing direction of each retro-reflector from the array pointing direction, and the angular deviation of the array pointing direction and the array normal were well within the limits of ±2° and 0.25°, respectively, as defined by the array performance and interface specifications. Vibration tests, conducted at the qualification level, had no significant effect on the total alignment of the retro-reflector. Several retro-reflectors shifted position slightly, resulting in a new array pointing direction and different deviations of individual retro-reflectors from the array pointing direction.

Tests IV through VIII were performed on the ETM-1 array to see if the array would be distorted by extreme environmental temperatures. The results of the tests are presented in Table 9.

TABLE 9

ETM OPTICAL ALIGNMENT RESULTS BEFORE, DURING, AND AFTER THERMAL DISTORTION TESTS

| Test No. | Maximum Deviation of Individual Retro-Reflectors From Array Pointing Direction | Deviation of Array Pointing Direction From Array Normal |
|---|---|---|
| IV | 0.27° | 0.03° |
| V | 0.19° | 0.02° |
| VI | 0.23° | 0.02° |
| VII | 0.22° | 0.02° |
| VIII | 0.22° | 0.02° |
| Allowable Range | ±2° | ±.25° |

During the thermal distortion tests, 13 copper-constantan thermocouples were located on the array: three were attached to the retro-reflectors, two to the retainer rings, and eight to the array structure. In the low-temperature tests, temperatures at various locations of the array were approximately -314°F to -320°F and the temperatures of three retro-reflectors varied from -308°F to -311°F. In the high-temperature tests, temperatures at various locations on the array were approximately 241°F to 258°F and the temperatures of three representative retro-reflectors varied from 236°F to 240°F.

The pointing direction of the array did not change significantly as a result of thermal distortion. Specific retro-reflectors changed by up to 0.13°; however, this change was insignificant, since the array specification called for an accuracy of ±2°.

Tests IX and X were performed on ETM-2 array with 20 test retro-reflectors installed, 4 in each corner of the array (cavity Nos. 00, 01, 10, and 11; 08, 09, 18, and 19; 80, 81, 90, and 91; and 88, 89, 98, and 99; see Figure 29 for cavity locations), and 4 in the center (Nos. 44, 45, 54, and 55).

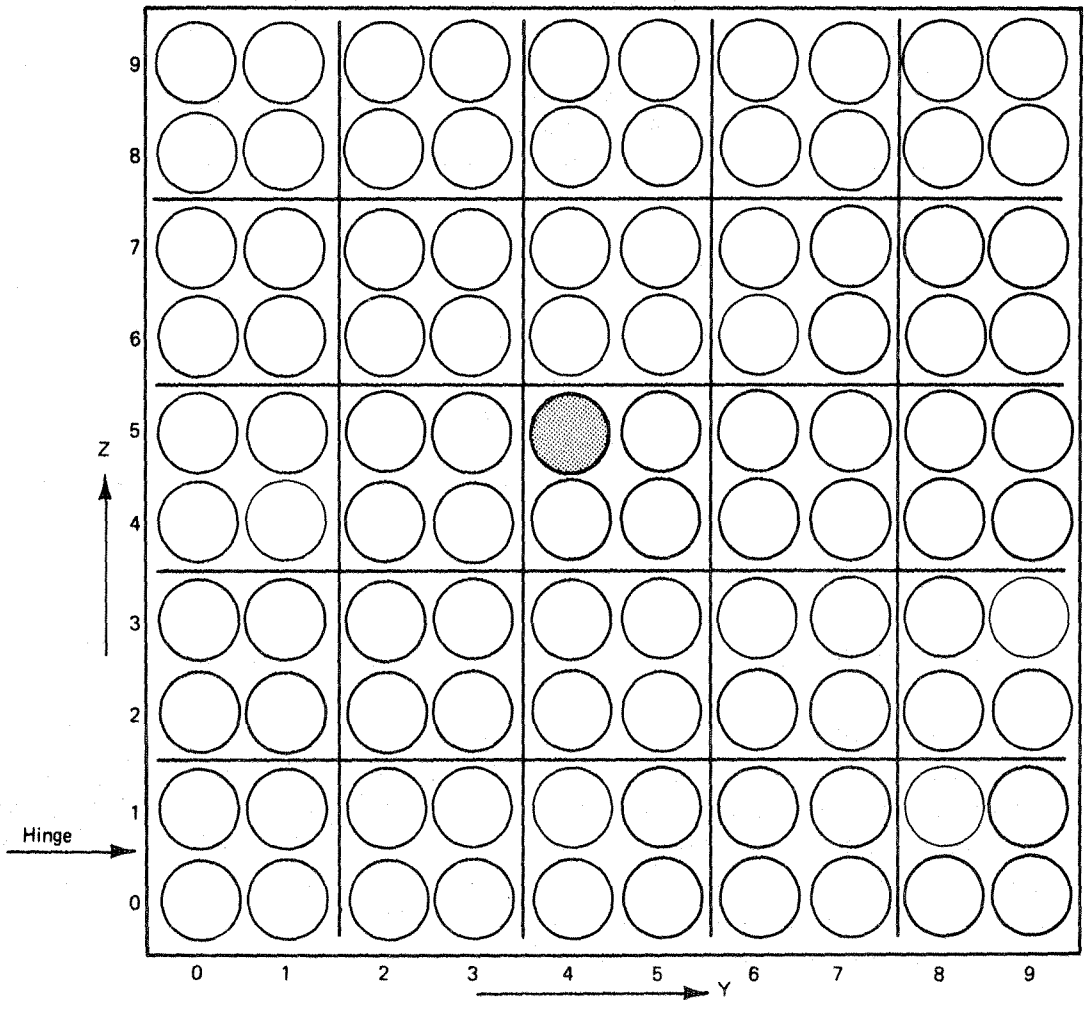


**Note:** Shaded Reflector is Number 54.

**FIGURE 29 RETRO-REFLECTOR CAVITY NUMBERS AND LOCATIONS**

In test IX, 0.088" thick blocks were placed between the feet of the Bendix drill and alignment fixture and the moveable test bed of the optical alignment test range, elevating the front surface of the retro-reflectors 0.088" above the level of the reflectors in test X, when the blocks were removed. The measurement grid readings for the two tests were within 0.5 mm of each other for all reflectors, indicating that small differences among levels of the individual retro-reflectors would not be translated by the test range into angular deviation (0.5 mm on the grid corresponds to an angular deviation of less than 0.01°).

Test X also served another purpose. As a part of the manufacturing procedure, holes had to be drilled and reamed in the brackets of the array. The holes had to be transferred from the Bendix drill and alignment fixture into the brackets; however, during the drilling and reaming operations, the array had to be positioned in relation to the Bendix fixture and held in this position.

In test X, the ETM-2 array was placed over the Bendix drill and alignment fixture, which in turn was placed over the moveable test bed of the optical alignment range. The pointing direction of the array was found as a function of the 20 retro-reflectors placed into the array cavities. The pointing direction of the array was adjusted until it was less than 0.1° from the vertical by moving the array. The array was clamped to the fixture and the pointing direction was checked again.

The holes in the brackets were drilled and reamed using the Bendix fixture as the drill guide.

After the drilling and reaming operation, test XI was conducted with pins passing through the newly drilled holes. The clamps were removed and only pins held the array on the Bendix fixture. The test showed that the clamping of the array to the Bendix fixture was adequate to perform drilling and reaming operations without distorting the array. This procedure was adopted as a part of the manufacturing procedure for the qualification and flight arrays.

The same 20 retro-reflectors were installed into qualification and then into flight models. In test XII, the qualification model was aligned and clamped before drilling; in test XIII, it was checked after drilling. Similarly, tests XIV and XV were conducted on the flight model.

Table 10 shows the test results for the qualification and flight models. Clamps did not distort the array structure to any appreciable extent.

TABLE 10

OPTICAL ALIGNMENT RESULTS ON QUALIFICATION AND FLIGHT ARRAYS BEFORE AND AFTER DRILLING

| Test No. | Array Model | Condition | Deviation of Array Pointing Direction From Normal | Maximum Deviation of Individual Retro-Reflector from Array Pointing Direction |
|---|---|---|---|---|
| XII | Qualification | Before Drilling | 0.02° | 0.21° |
| XIII | Qualification | After Drilling | 0.02° | 0.21° |
| XIV | Flight | Before Drilling | 0.01° | 0.26° |
| XV | Flight | After Drilling | 0.01° | 0.27° |

Tests XVI through XX were performed on completely assembled arrays in accordance with the optical alignment test procedure. Tests XVI, XVII, and XVIII were performed on the qualification model: First, before vibration of the model with the retainer ring staked by the original method; second, before vibration of the model staked according to the revised technique; and third, the acceptance test after vibration. Tests XIX and XX were performed on the flight model before and after vibration. As shown in Table 11, the alignment was well within allowable limits in all of these tests.

## C. MOUNT CONDUCTANCE TESTS

There are a number of paths through which heat can flow from the array structure and retainer ring to the retro-reflectors. Because these thermal paths were too difficult to define by analytic techniques, we measured the mount conductance, since it was significant to the array design.

TABLE 11

OPTICAL ALIGNMENT RESULTS ON QUALIFICATION AND FLIGHT ARRAYS BEFORE AND AFTER VIBRATION

| Test No. | Array Model | Condition | Deviation of Array Point Direction from Normal | Maximum Deviation of Individual Retro-Reflector from Array Pointing Direction |
|---|---|---|---|---|
| XVI | Qualification | Before Vibration | 0.01° | 0.18° |
| XVII | Qualification | After Vibration | 0.01° | 0.20° |
| XVIII | Qualification | After Vibration | 0.02° | 0.18° |
| XIX | Flight | Before Vibration | 0.04° | 0.17° |
| XX | Flight | After Vibration | 0.02° | 0.15° |

1. Test Equipment

Figure 30 shows the experimental apparatus used to measure the mount conductance of a retro-reflector. The test instrumentation is shown in Figure 31. The structure was heated in a small vacuum chamber to a fixed temperature. The retro-reflector and retainer ring radiated to a "black" $LN_2$-cooled heat sink. The temperatures within the structure, the fused-silica retro-reflector, and the retainer ring were measured with calibrated copper-constantan thermocouples.

The rate of heat flow from the retro-reflector to the $LN_2$ sink was determined from the radiating area, the emittance, and the measured temperature of the retro-reflector. The mounting conductance was calculated by subtracting the radiant heat transfer from the retainer ring and structure to the retro-reflector from the total heat flow. From the structure and retainer ring temperature measurements, and using the view area of the retainer ring to the $LN_2$ sink, a heat balance was written for the retainer, and the structure-retainer conductance calculated. The major source of probable error in mount conductance was the temperature measurements. Random errors of +0.5°K in the temperature measurements (the calibrations show an error of about ±0.2°K) cause uncertainties in the computed mount conductance of less than 10%.

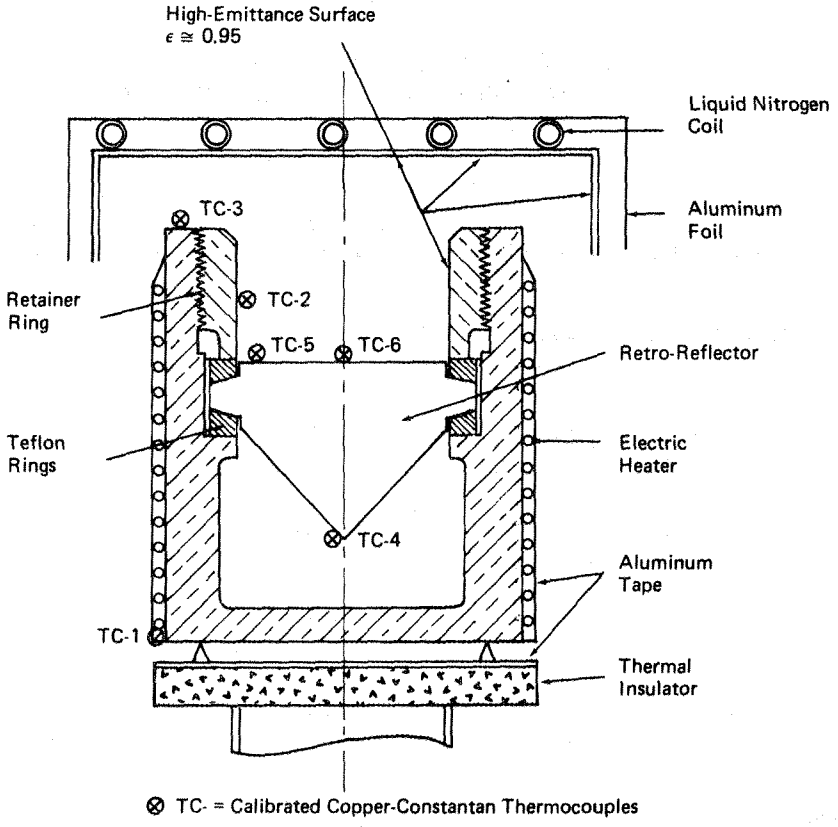


**FIGURE 30 MOUNT CONDUCTANCE TEST EQUIPMENT**

## 2. Tests

One of the main objectives of this test program was to determine a thermally acceptable assembly procedure for the retro-reflector. The thermal conductance of the mounting assembly was influenced by the amount of axial clearance. The initial axial clearance was controlled by the axial position of the threaded retainer ring during assembly. For retro-reflectors which initially had a positive clearance, the axial clearance increased during vibration testing (by approximately 30% or more). In addition, the thermal conductance was influenced to a lesser degree by the diametral clearance between the outside diameter of the Teflon retaining rings and the inside diameter of the aluminum housing.

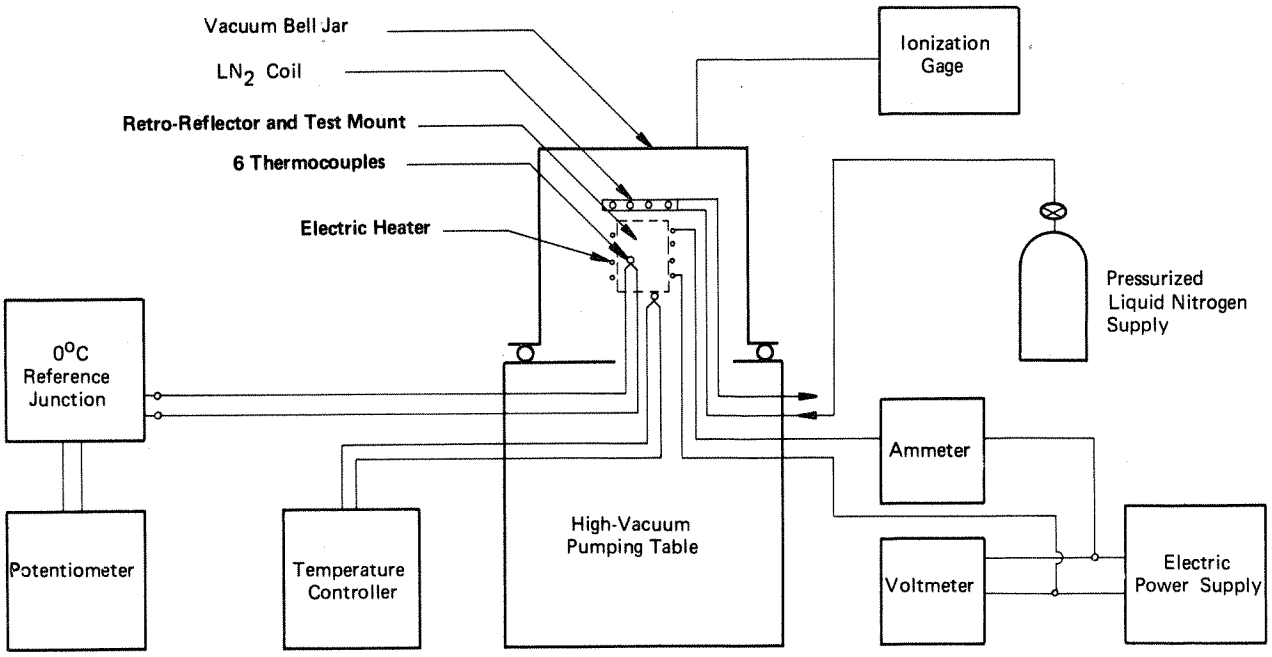


**FIGURE 31 MOUNT CONDUCTANCE TEST INSTRUMENTATION**

Figure 32 shows the results of the thermal tests; the measured mount conductance (watts/°K) was plotted versus the axial clearance in the assembly. Figure 32 also shows a series of test points relating the measured mount conductance before and after vibration tests. Increasing the axial clearance beyond +0.003" did not appear to further reduce the mount conductance.

The two points labeled "31B" and "35A" correspond to measured conductances before and after vibration for the following assembly procedure:

(1) Torque retainer ring to 80 in.-oz.

(2) Back off retainer one turn.

(3) Re-torque to 16 in.-oz.

(4) Back off retainer 36° of rotation (36° corresponds to approximately 0.003" of axial movement of the retainer).

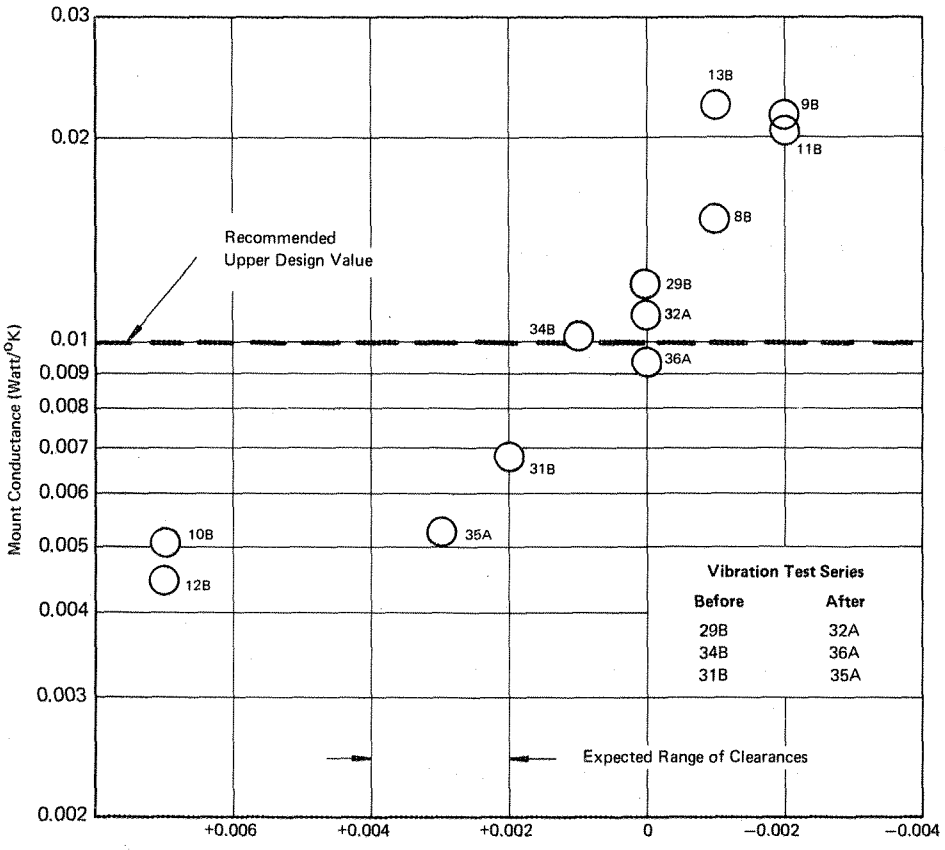


**FIGURE 32 EFFECT OF AXIAL CLEARANCE ON MOUNT CONDUCTANCE**

This assembly procedure yielded, after vibration which corresponded to the acceptance levels for random vibration input, mount conductances of approximately 0.0053 watt/°K.

Two tests were conducted at the same axial clearance with Teflon rings of selected dimensions to determine the influence of diametral clearance on mount conductance. The results were as follows:

| | Test | |
|---|---|---|
| | 31B | 37B |
| Axial Clearance (in.) | 0.002 – 0.003 | 0.0025 – 0.003 |
| Diametral clearance (in.) | 0.006 – 0.008 | 0.001 – 0.002 |
| Mount conductance (watt/°K) | 0.0067 | 0.0090 |

The range of axial clearances used in these tests correspond to the range of diametral clearances that could exist in the manufactured parts.

From a thermal standpoint, a 36° back-off of the retainer ring (i.e., an axial clearance of 0.002 – 0.003 in.) would yield near minimum mount conductance values. Because of the statistical nature of tolerance combinations and their effect on diametral clearance, the mount conductance would vary from retro-reflector to retro-reflector. For the worst case conditions (i.e., minimum diametral clearance between the Teflon rings and structure), the mount conductance would be 0.009 – 0.010 watt/°K before vibration. Our tests indicated that the effect of vibration was to increase axial clearance and thereby decrease mount conductance. Therefore, in the final thermal analysis of the array we used a mount conductance value of 0.01 watt/°K.

In conjunction with the mount conductance tests, we also measured the thermal conductance between the structure and the retainer ring – a parameter of small importance to the thermal gradients in the retro-reflector and therefore to the optical return. For example, as illustrated by the computer thermal studies, a change in the structure-retainer conductance by a factor of 25 changed the $\Delta T$ in the retro-reflector by only 7%. Thermally short-circuiting the retainer to the structure (i.e., making the conductance infinite – if it were physically possible) would change the vertical $\Delta T$ in the retro-reflector by 0.2°K, which would result in an insignificant change in the optical performance.

The optical performance calculations (Section III) were based on a structure-retainer conductance of 0.005 watt/°K. Higher structure-retainer conductances tended to reduce the thermal gradients in the retro-reflector and improve the optical return. Tests of the final hardware design showed that the structure-retainer conductance did not change after vibration testing.

## D. MOUNT TEMPERATURE-COMPENSATION TESTS

To verify the results of the calculations to size the Teflon mounting rings and to demonstrate the action of the mounting rings at the operating temperature extremes, we conducted a series of mount temperature-compensation tests.

### 1. Test Equipment

An expansion-contraction measuring apparatus was constructed by modifying a single retro-reflector mounting cavity so that a special, unthreaded, retainer ring was free to slide axially within it (the normal retainer ring threads were removed). When the retro-reflector, the mounting rings, and the special retainer ring were assembled and weighed with a nominal one-pound weight, changes in the axial length of the assembly would result in relative motion between the special retainer ring and the cavity body, thereby indicating a lack of temperature compensation in the mount.

Mechanical motion amplifiers were used at three points around the circumference to magnify the axial motion of the retainer relative to the cavity. These devices consisted of long pointers attached to two-legged bases: one leg stood on the top of the cavity; the other, on the top of the retainer ring. Relative axial motion tilted the pointer base and produced large horizontal displacements of the pointer tips. Three horizontal scales 120 degrees apart registered the horizontal displacement of the three pointers. The amplifiers were calibrated by moving the retainer ring with a micrometer and noting the scale readings. A motion amplification factor of 70 was achieved (i.e., a 0.005-inch relative motion between the retainer and cavity body produced a 0.350-inch displacement of the pointers). With a microscope, one could observe a pointer displacement as small as 0.010 inch.

To check out the apparatus, we placed an aluminum ring (the same height as the retro-reflector mounting ring assembly) in the apparatus, and temperature-cycled it between 195°F and -216°F. As expected, no significant motion of the pointers was observed during this temperature excursion.

### 2. Tests

To verify the data used in the mount sizing calculations, we replaced the retro-reflector mounting ring assembly with a Teflon ring made from the stock which was used for making the flight mounting rings. We compared the measured linear thermal expansion with manufacturer's (du Pont) data and found that, within the spread of the data, the agreement was good. Therefore, use of the du Pont data in the mounting ring sizing calculations was justified.

A number of tests were performed using both the expansion-contraction apparatus and a simpler, more qualitative, device in which clearances were measured with a thickness gauge. These tests led to a better understanding of the action of the mounting rings during temperature excursions, and substantiated the description to be presented in the following paragraphs.

Figure 33 shows cross-sectional views through the mounting ring design as well as a portion of the retro-reflector tab and surrounding hardware. These views are representative of the geometry at the retro-reflector mounting tabs at three locations around the mount circumference. Figure 33A shows the position of the mounting rings confined without clearance (a nominal load exerted by the retainer ring). This configuration would not change during temperature excursions and the nominal load would not vary significantly if the axial height of the rings were sized properly for the expansion-contraction characteristics of the material.

However, the situation was more complicated when clearance was provided during mount set-up. In the standard assembly procedure, a torque of 16 in.-oz on the retainer produced the configuration shown in Figure 33A. Backing off the retainer 36 degrees (Figure 33B) resulted in some radial clearance (the amount depending upon the free diameter of the ring and the cavity bore diameter) as well as some axial clearance (0.003 inch minus the axial "growth" of the ring due to radial movement inwards). If the retro-reflector was moved upwards, it would flex the ring outwards, due to the slanted tab faces, requiring about 0.24 lb-ft per 0.001 inch of motion until the rings are firmly seated against the confining hardware. The array assembly procedure provides for a total axial excursion of 0.002 to 0.003 inch before the mounting rings contact the cavity walls.

During mechanical environment inputs, the clearances around the mounting rings would expand and contract, depending upon the motion of the reflector, and the friction would damp relative motion between the reflector and the hardware.

Figure 33C shows the mount at +250°F (the maximum temperature limit), where the equivalent of the operational mount clearance would appear between the mounting ring and the retro-reflector slant face, since the diametrical expansion of the ring would hold it against the cavity bore. (Teflon expands and contracts more than aluminum.) If the retro-reflector were moved axially, it would have the original excursion of 0.002 to 0.003 inch before contacting the mounting rings.

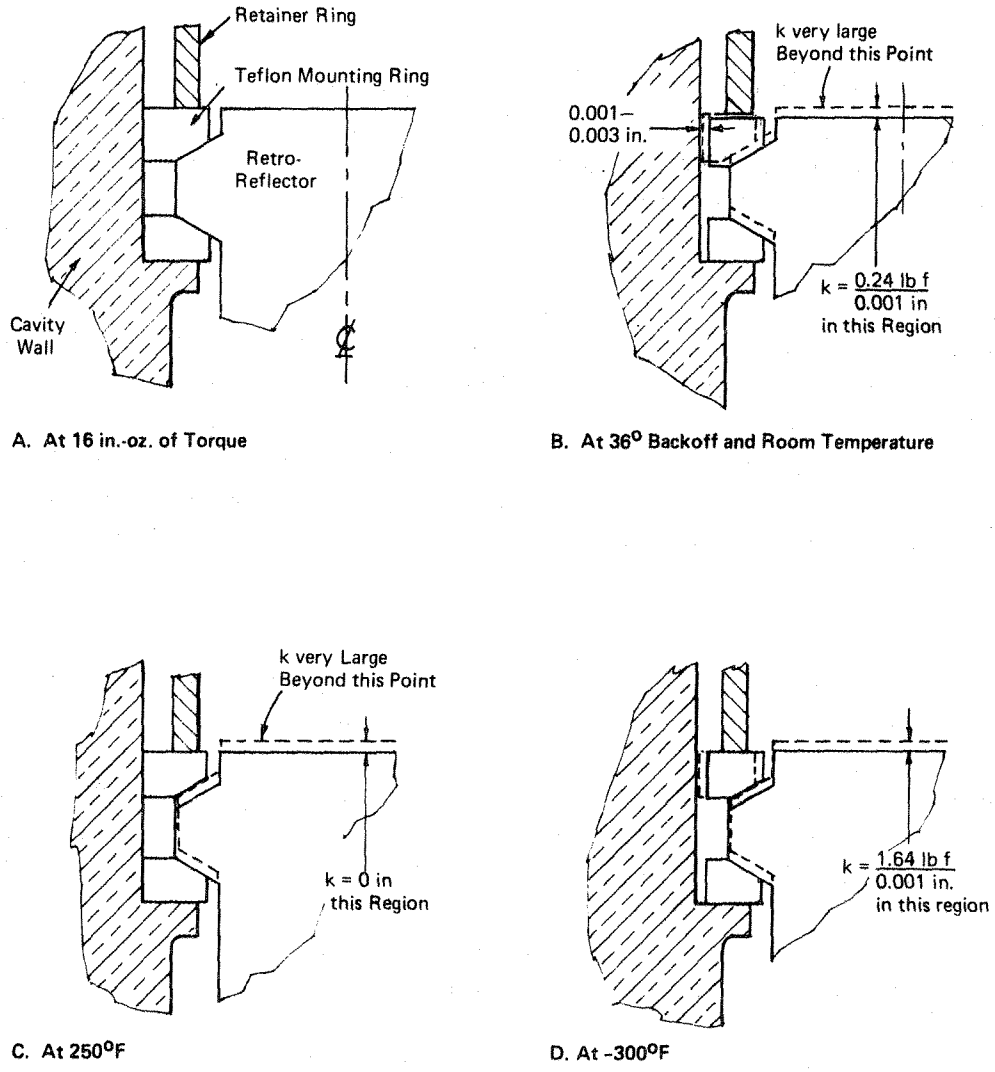


**FIGURE 33 MOUNTING RING ACTION**

Figure 33D shows the mount at -300°F (the minimum temperature limit), where the equivalent of the original mount clearance would appear between the mounting ring outer diameter and the cavity bore because the ring diameter contracted. If the retro-reflector were moved axially, it would have the original excursion of 0.002 to 0.003 inch before the mounting rings move outward and contact the cavity bore. To cause this excursion, the force would have to be larger than at room temperature because of the increase in modulus of elasticity for Teflon with decreasing temperature.

The compressive force exerted on the retro-reflector by the Teflon ring would be very limited because of the weakness of the ring, due to its small cross-section and the tendency towards cold flow which would prevent the maintenance of high loads.

The action of the present Teflon mounting rings during temperature excursions will conform to the model used for sizing the rings in all cases except near the low temperature limit. At this point, the mounting ring will contract radially inward to assume a three-lobed shape instead of remaining against the cavity bore as assumed for the model. Calculations showed that the consequences of this deviation should not be significant. Unfortunately, there was no simple conclusive test which would demonstrate that the retro-reflector would be undistorted at any temperature within the specified extremes. It would be very valuable to examine a retro-reflector, mounted in the standard manner, with an interferometer while it is subjected to a temperature-time condition which it will be subjected to on the moon. This test would give a true indication of the reflector distortion (if any) to be expected with temperature changes.

For the present mounting rings to conform exactly to the sizing model at the lowest temperatures, they should be weakened circumferentially so that they have no significant hoop continuity. Radial sawcuts on either side of the tab contact areas would fulfill this requirement. However, if this were done, the upper mounting ring would have to be oriented relative to the retro-reflector (as the lower mounting ring is now oriented) and both rings would be so fragile (because of the sawcuts) that size measurements would be questionable; manufacture would be very complicated and time-consuming.

On the basis of these tests, we concluded that the temperature compensation mount design was satisfactory and no further modifications were merited.

# VII. QUALITY ASSURANCE AND RELIABILITY

## A. QUALITY ASSURANCE PROGRAM

The Laser Ranging Retro-Reflector Quality Assurance Program was controlled by NASA Quality Publication NPC-200-3[17] as defined in the Arthur D. Little, Inc., Quality Assurance Program Plans submitted to Bendix. The program was designed to control hardware quality at a level consistent with mission objectives. Because of the endless combination of products, customers, and quality levels required to meet these mission objectives, this program was unique and not a part of a divisional or corporate system. This ability to tailor the quality program to specific requirements, while considering the skills of engineers, scientists and technicians, provided:

(1) Positive control of product quality at required mission levels;

(2) Closed loop interface between all elements of the project and the quality activities;

(3) Minimum expenditure of resources to achieve the required quality level;

(4) Exploitation of technology and skills within the project to achieve high quality.

During the Engineering Design Phase (Phase A), a modified Quality Program[18] was instituted with the distinct purpose of maintaining enough control to provide a smooth transition from experimental to flight hardware. Purchase orders were reviewed to establish the degree of quality input necessary to obtain a quality product. All materials were received through Quality Assurance receiving inspection, logged, and delivered to the engineering laboratories. Flight hardware material was logged, identified for traceability, and stored in a segregated area. Evaluations were made of our key suppliers, especially those who machined the array, the Teflon mounting ring, and the retainer rings. Special processes, such as anodizing of the retainer rings, were evaluated to ensure compliance with quality requirements.

Much time was spent with the design and test groups to solve development problems. The involvement of Quality Assurance kept all abreast of all changes and facilitated the writing of assembly and test procedures for flight hardware.

During the Fabrication Phase (Phase B), a complete quality control program, including an up-to-date inspection plan, was instituted.[19] Prior to issuance, all deliverable hardware drawings and their revisions were reviewed for their conformance to quality requirements. A continuous audit was carried out. All purchase orders were reviewed for quality requirements throughout the program. We also continued our inspections of our key vendors.

Retro-reflectors received special handling and were visually inspected for damage at receiving inspection. A complete set of records, including inspection, traceability, and completeness of shipment are on file for future reference.

All materials were identified for traceability. Material was delivered to project stores when necessary to maintain smooth flow and control.

Raw material stock was certified by the manufacturer by physical and chemical analysis; aluminum plates were x-rayed to verify absence of inclusions.

Compliance to process procedures[20] was assured by inspection travelers with step-by-step sign-offs at key stations.

A Mechanical Environmental Exposure Test Procedure and Optical Alignment Test Procedure were submitted to Bendix for approval. Support procedures ("Assembly Process Specification, Data Reduction, Alignment Apparatus Calibration and Handling Procedures") were submitted to Bendix for information only.

Acceptance, Mechanical, Environmental, and Alignment tests were witnessed by Bendix and ADL Quality Assurance representatives, and the local DCASR. Complete documentation for the qualification and flight models was provided in the Acceptance Data Packages[21] shipped with these units.

## B. RELIABILITY PROGRAM

We established a reliability program[22] to assure an inherently reliable design and the mechanization of that design into reliable space hardware. In accordance with our program plan, we emphasized a qualitative design-oriented approach rather than quantitative numerical predictions. During Phase A of this program, we were assisted by Avco/Space Systems Division.

During this program, reliability maintained cognizance of the design developments. A failure modes, effects, and criticality analysis was conducted to identify potentially critical problem areas in the design. The results were discussed with engineering personnel at an

internal design review prior to the CDR. A material list for the array was prepared. All parts materials were found to be acceptable per ATM 242 with the exception of a urethane foam used in the insulation for which we requested and received approval.

We reviewed test data from all tests from a reliability standpoint. The only failure in the program occurred when the retainer rings in the qualification unit rotated during vibration testing. This condition was corrected by an improved staking technique and the qualification model successfully retested. No failures occurred in any of the tests of the flight model. Three discrepant-material reports were issued for the qualification model and two for the flight model. None of these corrected discrepancies had any effect on the reliability of the array.

In our reliability assessment reports on the qualification model[2 3] and the flight model[2 4] we noted that all of the normal development procedures implicit in insuring a highly reliable product have been complied with. The basic structure (panel) is extremely strong when measured in terms of maximum developed stress levels, no non-standard parts or materials are required, and the manufacturing and assembly processes are well-controlled. The results of the alignment tests demonstrate the integrity of the array structure and mounting design (both mean element-to-element deviation and mean pointing direction error after vibration testing are less than 10% of allowable tolerance). We conclude that the reliability of the Laser Ranging Retro-Reflector Array is very high.

## LIST OF REFERENCES

1. *Laser Ranging to Optical Retro-Reflectors on the Moon;* University of Maryland proposal to NASA, December 13, 1965 (Revised February 11, 1966);
   a. Supplement dated June 30, 1966
   b. Second Supplement, dated January 9, 1967

2. *Confirmation of Predicted Performance of Solid Fused-Silica Optical Corner Reflectors in Simulated Lunar Environment;* University of Maryland progress report to NASA, October 10, 1966.

3. Bendix Aerospace Systems Division Sub-Contract SC511, Effective Date October 14, 1968, and Amendment No. 1, January 14, 1969.

4. Retro-Reflector Array/Support Structure and Alignment Mechanism, Bendix 1CD Drawing 2342000, Rev. A, March 3, 1969.

5. Retro-Reflector (University of Maryland), Bendix 1CD Drawing 2342001, Rev. B, January 16, 1969.

6. *Thermal Analysis and Preliminary Mechanical Design of Retro-Reflector Array* – Arthur D. Little, Inc., Final Report to the University of Maryland, Purchase Order No. 186162, August 1967.

7. *Analysis of Thermal Control Designs for Retro-Reflector Array* – Final Report to the University of Maryland – Purchase Order No. 210900 – December 1968.

8. Cooley, J. A. "Evaluation of Thermal Control Coating in the Space Environment," AFML-TR-67-158, December 1967.

9. Weaver, J. H., "Effects of Vacuum U.V. on Optical Properties of Anodized Aluminum Temperature Control Coatings," AFML-TR-67-421, May 1968.

10. Lehrman, S.H., "Application of the Fast Fourier Transform to the Optical Transfer Function," Itek Corp., Lexington, Mass., February 1968.

11. Thermal Presentation on LRRR at Bendix CDR on January 15, 1969. Included in BxA Document EATM 61, February 28, 1969.

12. Mechanical Environmental Exposure Test Procedures, Arthur D. Little, Inc., Test Procedure No. TP4:0511-E1-15, Rev. D, March 4, 1969.

13. Drill and Alignment Fixture – LRRR Array Interface, Bendix Drawing TD-2342071-01, Rev. A, January 28, 1969.

14. Procedures for Calibrating Test Apparatus Used for Optical Alignment Tests. Arthur D. Little, Inc., Calibration Procedure No. TEE-1:0511-E1-26, February 14, 1969.

15. Optical Alignment Test Procedures, Arthur D. Little, Inc., Test Procedure No. TP5: 0511-E1-15, February 13, 1969.

16. Procedures for Reduction of Data Obtained from Optical Alignment Tests, Arthur D. Little, Inc., Data Procedure No. TEE-2:0511-E1-26, February 18, 1969.

17. NPC 200-3 Inspection System Provisions for Suppliers of Space Material Parts, Components, and Services , April 1962.

18. *Arthur D. Little, Inc., Proposal "Laser Ranging Retro-Reflector Experiment for Contingency Science Package,"* L-1140, October 16, 1968.

19. Quality Assurance Program Plan (submitted to Bendix with ADL letter L215, March 11, 1969).

20. Assembly Process No. QA1:0511-E1-16, Rev. C, March 18, 1969.

21. Acceptance Data Package; a. Qualification Model; b. Flight Model.

22. Reliability Program Plan, Arthur D. Little, Inc., November 4, 1968.

23. Reliability Assessment Report – Qualification Model, Arthur D. Little, Inc., Document RA-1:0511-E1-29, April 4, 1969.

24. Reliability Assessment Report – Flight Model, Arthur D. Little, Inc., Document RA-2:0511-E1-29, April 7, 1969.

## LIST OF PRINCIPAL ADL PARTICIPANTS

A. W. Amundsen
P. Athens
L. M. Bablouzian
A. C. Behre
R. P. Berthiaume
I. A. Black
A. C. Blasenak
E. J. Boudreau
I. D. Boynton
B. Bullock
K. H. Bunker
J. C. Burke
C. R. Campbell
T. Capuzzo
B. M. Chmura
J. Cleary
D. F. Comstock
C. W. Costas
A. J. Denasavich
F. J. DePloey
C. D. DiFraia
I. W. Dingwell
R. D. Donahue
E. M. Drake
A. G. Emslie
J. Essigmann
J. Forlizzi
A. A. Fowle
F. Gabron
B. Gibbons
P. E. Glaser
K. W. Glynn
S. S. Gray
B. C. Hanley
R. B. Hinckley
H. J. King
R. M. Lucas
J. E. McCullough
N. A. Memmo
R. L. Merriam
J. Modica
D. Nathanson
E. H. Newton
G. T. Parish
E. B. Rebbello
D. L. Richardson
F. E. Ruccia
R. D. Sanborn
R. M. Sawdo
L. A. Selander
J. L. Sienczyk
P. F. Strong
R. A. Swanbon
W. G. Sylvester
T. G. Tatosian
E. F. Tilton
W. H. Varley
R. E. Vogel
A. E. Wechsler
R. L. Wells